

147

Final Technical Report
for
HYDAMP
A Joint Industry Program on Hydrodynamic Damping and Combined Motion

by

T. E. Horton
Professor of Engineering
209 St. Andrews Cr.
Oxford, MS 38655
(601)-234-3262

Jointly Sponsored by:

Agip, Milano, ITALY
Mobil R & D Corp. Dallas, TX
Minerals Management Service, Washington, D.C.
Naval Civil Engineering Lab. Port Hueneme, CA
Texaco Inc. Houston, TX

June 1991

PREFACE

In the proposal on the HYDAMP project we stated the objectives as:

1. Supply rational damping data for design.
2. Provide an understanding of the combined motion problem.
3. Demonstrate the power of the Inertial Pressure Method (IPM).

On the basis of advice from "Industry" we constrained the first objective to constant coefficient data compatible with the standard Morison based programs. The IPM would be used only as a guide in the study.

The proposed plan was to apply the IPM with the SSPA data to obtain coefficient time series and to correlate these with corresponding Morison coefficients. The Morison data would then be tested against the observed force. The result would be a Hierarchy of recommendations for improving predictions with existing Morison programs. The IPM would be used to explore modifications of the Morison equation so that its functional form and coefficients can better represent the observed perturbations arising when two motions are combined as with two periodic motions or with periodic and steady motions.

The constraints on IPM advocacy was a constant source of frustration but forced the issue of a simple, accurate, and rational means of representing hydrodynamic loading. During this study we have explored several ways of making the IPM to Morison transition. I feel that this report presents the simplest and most accurate way and has remained true to the proposed plan and objectives.

I have struggled long trying to create a clear and informative document, realizing it is permeated with "different" and as a result sometimes difficult ideas. In this document we have tried to achieve a comprehensive overview taking the point of view of the user. In some places we may have drifted into an overly detailed or obtuse discussion.

The presentation here was intended to be distinct from that of the four reports and/or presentations:

1. Minutes of the Proposal Meeting on HYDAMP (May 1988)
2. Progress Report on HYDAMP Project (February 1990)
3. May HYDAMP Meeting Minutes covering high frequency data (May 1990)
4. November HYDAMP Meeting Minutes covering influence of currents upon forces due to periodic motions (November 1990)

which occurred during the investigation. These represented a "now" view of the effort and contain some details which have not been reproduced in this document. The final Chapter of this Report attempts an explicit connections to some of these items.

Chapter 1 presents a descriptive view of the IPM, its past accomplishments, the SSPA data, and the combined motion problem.

Chapter 2 presents a detailed treatment of the IPM from derivation to the specifics of its use. A more detailed overview of the SSPA data is found in its final sections. The details on the IPM are not essential to the understanding of the rest of the report; however, the hope is, that with the demonstrated accomplishments in Chapters 3 to 5, one would be pleased to have these details on the IPM.

Chapters 3 and 4 are devoted to the combined motion problem involving a steady velocity and simple harmonic motion. Chapter 3 contains the overview of the data and the procedure used to convert the IPM coefficient pattern into a hierarchy of Morison coefficient approximations. Chapter 4 compares the Morison force predictions with the observed force.

Chapter 5 is really devoted to the combined motion problem involving two simple periodic motions. However, the approach used with the data, which turns out to be the linear approximation, needs some justification. This lengthy excursion turned into an excellent illustration of how the IPM can be used to rationalize Morison approximations.

Each Chapter has an initial section which serves as an introduction and guide; however, each Chapter does not have a section devoted to its conclusions. These have been relegated to a common collection in Chapter 6, which also contains observations and recommendations.

As in all previous investigations with the IPM, we are amazed by its new revelations.

I shall end by expressing my gratitude to the participants for their contributions and patience.

T. E. Horton

June, 1991

LIST OF SYMBOLS

A_x	Amplitude of motion in the x or in-line direction
A_o	Amplitude of low frequency motion (Table 5.1, p 66)
A'	Amplitude of high frequency motion (Table 5.1, p 66)
a	(1) Chapter 2 the radius of the cylinder; (2) Chapter 5 the coefficient determined by IPM and velocity ratios (Defined on p 59 with Eq (12b))
b	A coefficient determined by IPM and velocity ratios (Defined on p 59 with Eq (12b))
c	A coefficient determined by IPM and velocity ratios (Defined on p 59 with Eq (12b))
C_a	Inertial coefficient for Morison equation (p 15, Eq (6))
C'_a	The inertial correction coefficient for Morison equation, $C_a = 1 - C'_a$, (introduced on p 16)
C_d	The drag coefficient for Morison equation (p 15, Eq (6) and p 68, Eq(16))
C'_d	The high frequency drag coefficient (p 67, Eq (15) and Table 5.2)
$(C_f - C_r)$	The IPM coefficient
$(C_f + C_r)$	The IPM inertial coefficient
C_o	The mean value of the IPM coefficient (p 59)
C'	The amplitude of the perturbation of the IPM coefficient (p 59)
D	Cylinder diameter
DF_x	D-Force, in-line hydrodynamic force less the ideal inertial force (introduced on p 16; Eq (11) on p 19)
F_d	Drag or damping force
\bar{F}_d	Normalized drag or damping force $F_d / \rho DL$
$(\bar{F}_d)'$	High frequency component of the normalized drag or damping force (p 67, Eq (15))
$(\bar{F}_d)_o$	Low frequency component of the normalized drag or damping force (p 68, Eq (16))
F_x	Hydrodynamic force on a moving cylinder
f	Frequency of periodic motion
f'	Frequency of high frequency motion
f_o	Frequency of low frequency motion
R	Interaction force term in IPM (defined Eq (5b); discussion p 12)
T	Period of motion
t	Time
\dot{U}	Acceleration of the cylinder
U	Velocity of the cylinder
U_s	Steady motion velocity
U_p	Periodic velocity amplitude

U_o	Mean velocity of cylinder
U'	Perturbation velocity amplitude
V	Instantaneous perturbation velocity
\tilde{V}	Dimensionless instantaneous perturbation velocity, V/U_o
δ	Deviation of pressure coefficients from ideal (p 15)
θ	Angular position on the cylinder (p 10)
θ_{min}	Theta-min, position on the cylinder surface where the ideal pressure distribution is a minimum
ρ	Density of fluid
ω	Circular frequency, $2\pi f$

TABLE OF CONTENTS

CHAPTER 1 INTRODUCTION	1
DATA BASE	1
HYDRODYNAMIC LOADING	2
THE INERTIAL PRESSURE METHOD	2
FIGURE 1.1 COMPARISON OF THE MORISON EQUATION WITH THE IPM EQUATION	3
IPM CORRELATIONS	4
FIGURE 1.2 EXAMPLE OF THE THETA-MIN CORRELATION PATTERN	5
IPM WITH COMBINED MOTION	6
APPROACH AND RESULTS	6
FIGURE 1.3 THETA-MIN CORRELATION PLOTS	7
CHAPTER 2 IPM & SSPA	9
DEVELOPMENT OF THE IPM EQUATION	9
FIGURE 2.1 VERTICAL CYLINDER MOVING WITH VELOCITY U ALONG THE X-AXIS	10
USING THE IPM ALGORITHM	12
COMMENTS ON THETA-MIN	13
FIGURE 2.2 TIME SERIES REPRESENTATION FOR A MOVING CYLINDER	14
MORISON AND IPM EQUATIONS	15
D-FORCE FORM OF EQUATIONS	16
SSPA DATA	17
UNCERTAINTIES IN THE DATA	18
DATA REDUCTION	18
CHAPTER 3 ANALYSIS OF LOW FREQUENCY DATA	20
A. DATA AND NOMENCLATURE	20
TABLE 3.1 TABLE OF RUN NUMBERS	21
TABLE 3.2 TABLE OF REDUCED VELOCITIES	21
CORRELATION KC-NUMBERS	22
FIGURE 3.1 RELATIONSHIP BETWEEN PROPOSED CORRELATION KC-NUMBERS	23
IPM TIME SERIES DATA	24
IN-LINE TRANSVERSE FORCE	24
OBSERVATIONS ON IPM DATA	25
B. MORISON COEFFICIENTS FROM IPM	25
CONCEPT	25
FIGURE 3.2 COMPARISON OF IPM COEFFICIENT WITH VELOCITY AND ACCELERATION	26
LEVELS OF HIERARCHY	27

ADVANTAGES OF THE PROCEDURE	27
LEVEL II DATA	28
LEVEL III DATA	28
OBSERVATIONS ON COEFFICIENT DATA	28
FIGURE 3.3 LEVEL II COEFFICIENT DATA	29
FIGURE 3.4 LEVEL II COEFFICIENT DATA	30
FIGURE 3.5 LEVEL II COEFFICIENT DATA	31
FIGURE 3.6 LEVEL II COEFFICIENT DATA	32
TABLE 3.3 C_a VALUES FOR LEVEL III	33
CHAPTER 4 LOW FREQUENCY PREDICTIONS	35
LEVEL I PREDICTIONS	36
LEVEL II PREDICTIONS	36
FIGURE 4.1 COMPARISON OF D-FORCE OBSERVED TO PREDICTIONS WITH LEVEL I	37
FIGURE 4.2 COMPARISON OF D-FORCE OBSERVED TO PREDICTIONS WITH LEVEL I	38
FIGURE 4.3 COMPARISON OF D-FORCE OBSERVED TO PREDICTIONS WITH LEVEL I	39
FIGURE 4.4 COMPARISON OF D-FORCE OBSERVED TO PREDICTIONS WITH LEVEL I	40
TABLE 4.1 COMMENTS SUMMARY	41
TABLE 4.2 COMMENTS SUMMARY	42
TABLE 4.3 COMMENTS SUMMARY	43
OBSERVATIONS ON PREDICTIONS	44
COEFFICIENT COMPATIBILITY	44
GRADES FOR RUNS	44
MORISON "BUMP"	45
FIGURE 4.5 COMPARISON OF D-FORCE OBSERVED TO MORISON PREDICTIONS	46
CHAPTER 5 RV AND IF APPROXIMATIONS	48
RV MORISON OVERPREDICTION	49
FIGURE 5.1 COMPARISONS OF OBSERVED AND PREDICTED FORCES	49
BRIEF REVIEW OF RV, IF, AND OTHER FORMS	50
FIGURE 5.2 DAMPING FORCE AS A FUNCTION OF CYLINDER VELOCITY	51
FIGURE 5.3A RV COMBINED MOTION FORCE AS A FUNCTION OF CYLINDER VELOCITY	53
FIGURE 5.3B IF COMBINED MOTION FORCE AS A FUNCTION OF CYLINDER VELOCITY	53
FIGURE 5.4 OBSERVER DAMPING FORCE PATTERN	54
FIGURE 5.5A REALIZATION OF THE RV APPROXIMATION	55
FIGURE 5.5B REALIZATION OF THE IF APPROXIMATION	55

IPM COEFFICIENT PATTERN	56
FIGURE 5.6 HIGH FREQUENCY IPM COEFFICIENTS	57
FIGURE 5.7 COMPARISON OF IPM COEFFICIENT TIME SERIES	58
ANALYTICAL APPROXIMATION OF PATTERN	59
THE PERTURBATION PATTERN	60
APPLICABILITY PLOT	61
FIGURE 5.8 APPLICABILITY MAP	61
PERSPECTIVE	62
VALID APPROXIMATIONS FOR SSPA DATA	63
FIGURE 5.9 APPLICABILITY MAP WITH SSPA DATA	64
HIGH FREQUENCY DATA	65
TABLE 5.1 SUMMARY OF TEST CONDITIONS FOR HIGH FREQUENCY DATA	66
DAMPING FORCE ALGORITHM	67
COEFFICIENTS FOR HIGH FREQUENCY RUNS	69
TABLE 5.2 DRAG COEFFICIENTS FOR HIGH FREQUENCY DATA	69
OTHER OBSERVATIONS -- AN I-T EFFECT	70
CHAPTER 6 FINAL OBSERVATIONS AND COMMENTS	73
THE IPM DILEMMA	73
DATA REDUCTION PROCEDURES	74
LOW FREQUENCY DATA	74
HIGH FREQUENCY DATA	78
FINAL OBSERVATIONS ON THE I-T EFFECT	81
RECOMMENDATIONS FOR FUTURE STUDIES	82
REFERENCES	83
APPENDIX A	
APPENDIX B	

CHAPTER 1

INTRODUCTION

Hydrodynamic damping is a vital parameter in the dynamic analysis of deep water risers and compliant structures. Damping motion is part of a more general set of problems which are best described as combined motion problems. In their simplest form, combined motions involve the superposition of two motions, either two periodic motions or a periodic with a steady flow.

In offshore practice, hydrodynamic damping and combined motion load predictions are based on the Morison equation. Using time invariant drag and inertial coefficients, this equation achieves simplicity but limits accuracy and applicability. That such coefficients can not represent features of the loading mechanism was pointed out in the classic work of Keulegan¹(1958) and subsequent investigations by Verley & Moe², Dello Stritto & Horton³, Demirbilek et al⁴, and Teng & Nath⁵.

For damping, a common observation is that the Morison equation yields an over prediction. To produce certain combined motion loading the Morison equation requires an incredulous negative drag coefficient. To circumvent some of the problems, alternative forms of the Morison equation have been used. The Relative Velocity form (RV) and the Independent Flow fields form (IF) are the most frequently cited.

The IF and RV forms are described in several of the above references. The IF form has separate Morison drag terms for each of the combined motions. The RV form is the conventional Morison equation with the velocity represented by the combined velocity. This form has a single drag coefficient.

In this study our aim is to improve present practice by providing a rational basis for selection of Morison coefficients and of the equation's functional form. The study uses the combined motion data from the SSPA tests, Rodenbusch & Kallstrom⁶, with an alternative to the Morison equation, called the Inertial Pressure Method (IPM), which has been discussed by Horton & Feifarek⁷, Horton et al⁸, and Rish⁹. The IPM will serve as a guide in this study, but the results will be Morison based.

DATA BASE

The SSPA data were collected at the Swedish Maritime Research Center in Gotenburg through a JIP. The tests involved large scale smooth and roughened cylinders moving in a basin, simulating complex flow fields. The range and quality of these data are ideally suited to our study. The prototype scale (1 meter cylinder diameter) make these data attractive to designers.

A minimum of 22 Runs from the SSPA experiment were analyzed. These included tests of combined periodic motions and periodic motion with a current. They include a sequence of combined motion data in which high frequency motions, corresponding to KC-Numbers less than one, are combined with low frequency motion. Complementing these are low and high current tests involving low frequency periodic motions.

HYDRODYNAMIC LOADING

As an introduction to the IPM consider the concepts involved in the hydrodynamic loading of a cylinder. There are only two ways of exerting a force on a cylinder moving through a fluid. One is by pressure which is normal to the surface of the cylinder and the other is by shear which is tangent to the surface. For the high Reynolds Number flows encountered in offshore design the total integrated shear force is small compared to the pressure force. Thus the time varying force on a wave loaded cylinder is due to its pressure distribution and the familiar drag and inertial load components are derived from the integrated pressure force.

The scale of the pressure distribution is given by the Bernoulli equation for potential flow. For a cylinder, deviations from this pressure distribution are due to flow separation on the rear surface and return flow from previous wakes on the front. Pressure coefficients have long been used by aerodynamicists to account for such deviations from a potential flow.

THE INERTIAL PRESSURE METHOD

The Inertial Pressure Method (IPM) used in this study is based upon pressure coefficients applied to the potential flow pressure distribution on a moving cylinder. The integrated pressure distribution yields an IPM equation with a strong resemblance to the Morison equation.

On contrasting the IPM and the Morison equations given in Figure 1.1 the following observations are of note:

For the drag term, the IPM coefficient is the difference in the front and rear pressure coefficients. Its value and sign changes during a flow cycle with the reversal of the roles of the front and rear coefficients. Values of the IPM coefficient are observed to be between ± 1 . Corresponding instantaneous Morison drag coefficients are found by multiplying by $8/3$.

Morison Equation:

$$F_x/\rho DL = -C_a \pi D \dot{U}/4 - C_d 1/2 |U| U$$

IPM Equation:

$$F_x/\rho DL = -(C_f + C_r)/2 \pi D \dot{U}/4 + (C_f - C_r)(4/3 U^2 + R)$$

FIGURE 1.1

COMPARISON OF THE MORISON EQUATION WITH THE IPM EQUATION

For the inertial term, the IPM coefficient is the sum of the front and rear pressure coefficients. This sum yields the classic ideal value when the drag coefficient is 0 and decreases as the drag coefficient increases. This explicit coupling of the mass and drag coefficients has been implicitly noted by other authors over several decades.

IPM allows the computation of an empirical coefficient for each simultaneous observation of force and motion. Such IPM coefficient time series provide a clear detailed picture of the values and pattern required to precisely reproduce loading data.

Further details on the IPM are provided in Chapter 2.

IPM CORRELATIONS

The IPM's instantaneous coefficient time series is compatible with the Morison equation and can be interpreted in terms of the physics of the flow (separation, wake sweeping , etc). These make it attractive for this study. However, a more important feature has been the establishment of the Theta-min Correlation, which is a correlation between instantaneous values of the IPM coefficient and the kinematic quantity "Theta-min".

The quantity Theta-min is the location on a cylinder of the minimum potential flow pressure. This angular position sweeps back and forth over the cylinder surface (between 0° and 180°) during the flow cycle. It plays a key role in "turning on" the drag coefficient by determining when and where adverse pressure gradients exist on a cylinder. Adverse pressure gradients result in flow separation and build up of drag.

Figure 1.2 is an example of the Theta-min Correlation. Here the instantaneous values of the IPM coefficient and the Theta-min angle are cross plotted. This plot is for a combined motion flow involving multiharmonics. From this Figure it is clear that the drag does not "turn on" until Theta-min approaches 90°, the maximum velocity condition. The pattern in this figure shows inertial dominance early in the flow cycle where the drag is zero or slightly negative due to wake sweeping.

The persistence of this correlation pattern over a wide range of tests is central to using the IPM for predictions. With the pattern portrayed by the dashed lines in Figure 1.2, accurate force predictions have been achieved.

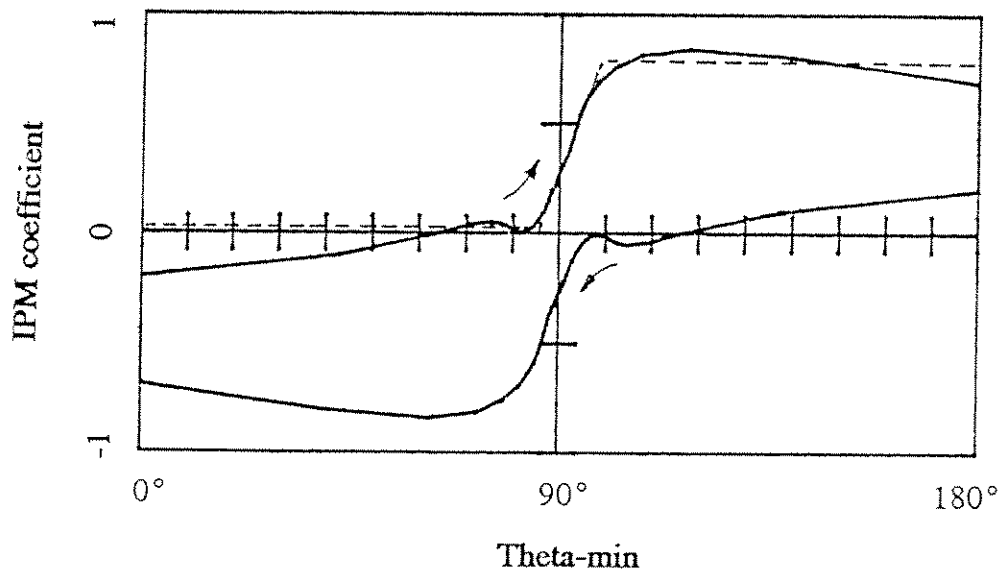


FIGURE 1.2

EXAMPLE OF THE THETA-MIN CORRELATION PATTERN

The IPM Coefficient, $(C_f - C_p)$, plotted versus Theta-min, θ_{min} , for a Combined Motion Test involving Multiharmonic Motion. The dashed line segments were effectively used to represent the pattern in force predictions. The progression around this plot is clockwise.

IPM WITH COMBINED MOTION

As a further illustration of the persistence of the Theta-min Correlation pattern, two records of SSPA data have been nearly superimposed for comparison in Figure 1.3 . These are plots of individual data points without filtering or smoothing. Both records represent the troublesome condition involving high steady currents combined with periodic motions. For such conditions no flow reversal occurs.

The level of correlation is such that the data points form the curves. For the lower plot the amplitude of motion equaled the cylinder diameter and the periodic velocity amplitude equaled the steady velocity. The upper plot is motion of half a cylinder diameter combined with a steady velocity twice the periodic velocity. The agreement is such that these plots could be interchanged.

APPROACH AND RESULTS

Our approach is to use the IPM coefficient pattern as a guide, and by paring the pattern back to forms useful with the Morison equation we can achieve: (1) improved understanding and accuracy for the Morison methodology and (2) delineation of problem areas.

Likely, the items of most interest from this study are the coefficient data. These are not presented as a single data set but as a hierarchy of approximations for use with the constant coefficient Morison equation. The coefficient hierarchy is presented in Chapter 3. Predictions based on the coefficients are presented in Chapter 4.

To this investigator, an accomplishment of greater interest is the achievement of a systematic view of the data and equations. This also serves as a good illustration of how the IPM was used as a guide. The nagging question that led to this was: how to rationalize the disparate RV and IF forms of the Morison equation and their use with low frequency high current data as well as high frequency damping data?

With the IPM such a question never arises as there is only a single IPM equation and the fluctuating coefficient pattern. The characteristic pattern is shared by both high current and damping data.

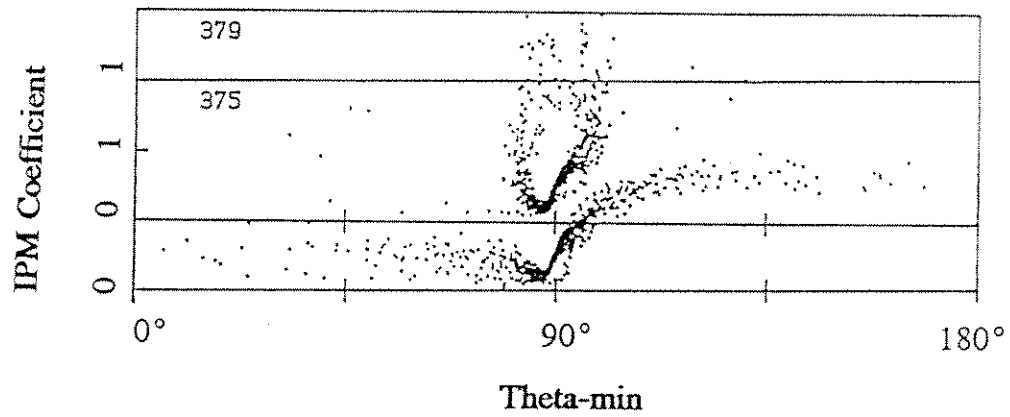


FIGURE 1.3

THETA-MIN CORRELATION PLOTS

A comparative superposition of IPM Coefficients from Two SSPA Combined Motion Runs involving large currents. For 375 the steady to periodic velocity ratio was 1 and the periodic KC-Number was 6.2 . For 379 the steady to periodic velocity ratio was 2 and the periodic KC-Number was 3.1 . For both the IPM correlation KC-Number was 27.

The IPM drag term could be characterized by the mean and the fluctuating values of both the IPM coefficient and the velocity. By an expansion of this IPM expression one sees the terms representing the various forms of the Morison equation. An order of magnitude analysis leads to a plot which delineates the range of applicability of each Morison form. The SSPA data analyzed in this study provided a validation of this plot. Chapter 5 presents these results.

CHAPTER 2

IPM & SSPA

The Inertial Pressure Method (IPM) is a rational semiempirical approach to determining wave forces. The basis of the concept is that hydrodynamic loading on a body is derived from the instantaneous pressure distribution on the surface of the body. The pressure distribution can be represented by an instantaneous ideal pressure distribution which is modified by instantaneous empirical coefficients. The ideal pressure distribution is obtained from the Bernoulli-Euler equation applied to the potential flow about the body. The pressure distribution is integrated over the surface of the body to achieve an expression for the force acting on the body. The resulting equation, the IPM equation, can be used to empirically determine the instantaneous force coefficients (IPM Coefficients), or it can be used with instantaneous coefficients to determine forces.

In this Chapter we present the development of the IPM equation following the above procedure, indicate how it is used, discuss the significance and dynamics of Theta-min, and contrast the forms of the IPM and Morison equations. The intent is to supply the reader with some of the background details of the IPM.

The SSPA data represents a unique resource as they are the product of a large scale experiment, conducted under controlled laboratory conditions for a variety of kinematic patterns. The two sets of smooth cylinder data used in this study were ideally suited to a study of combined motion. One set referred to as Low Frequency Data represents combinations of a low frequency motion with a steady motion (a very low frequency motion). The second set referred to as High Frequency Data represents combinations of high and low frequency periodic motions where the high frequency motion is indicative of a fixed platform.

In the section devoted to the SSPA data we describe briefly the experiment and the measurement constraints and our data processing procedure utilizing the IPM. One of the advantages of the IPM used with the SSPA data is that IPM coefficients can be computed from startup to termination of each Test Run.

DEVELOPMENT OF THE IPM EQUATION

To apply the IPM to a vertical cylinder moving along a straight line path consider the system of Figure 2.1 . The potential flow pressure distribution, given by Lamb¹⁰, is

$$P/\rho = a \dot{U} \cos \theta - 2 U^2 \sin^2 \theta + F(t) \quad (1)$$

for a circular cylinder of radius a , confined to move along the x-axis with velocity U and acceleration \dot{U} .

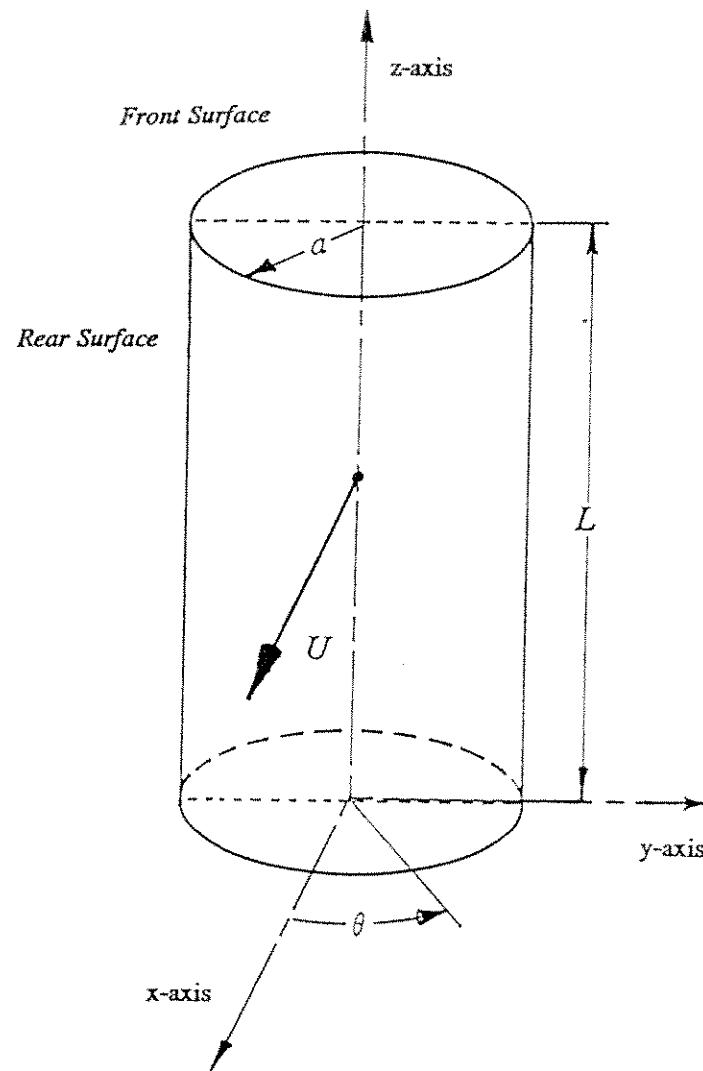


FIGURE 2.1

VERTICAL CYLINDER MOVING WITH VELOCITY U ALONG THE X-AXIS

A more convenient form is achieved by referencing the pressure to the minimum pressure on the cylinder surface P_{\min} , which occurs at the angular position on the surface θ_{\min} (Theta-min). Using $\Delta P = P - P_{\min}$, the potential flow pressure distribution can be written as:

$$\Delta P/\rho = a \dot{U} (\cos \theta - \cos \theta_{\min}) - 2 U^2 (\sin^2 \theta - \sin^2 \theta_{\min}) \quad (2)$$

This pressure acting over a differential segment, $L a d\theta$, of the cylinder surface yields the differential pressure force component in the x-direction:

$$dF_x = -\Delta P a L \cos \theta d\theta \quad (3)$$

Now to account for deviations from the potential flow pressure distribution consider the pressure coefficients C_f and C_r which modify the pressure on the "front" and "rear" halves of the cylinder. C_f is applied to the pressure on the surface for $-90^\circ < \theta < 90^\circ$ and C_r is applied to the pressure for $90^\circ < \theta < 270^\circ$.

Integration of the pressure force over the surface yields the x-component of the hydrodynamic force. Using the symmetry about the x-axis in performing the integration yields:

$$-F_x/\rho a L = 2C_f \int_0^{90} \Delta P \cos \theta d\theta + 2C_r \int_{90}^{180} \Delta P \cos \theta d\theta \quad (4)$$

Evaluation of the integrals using the expression for ΔP results in an algebraic expression which can be written as:

$$F_x/\rho DL = -[(C_f + C_r)/2] \pi D \dot{U}/4 + (C_f - C_r)(4/3 U^2 + R) \quad (5a)$$

with $D = 2a$ and

$$R = -[a \dot{U} \cos \theta_{\min} + 2U^2 \cos^2 \theta_{\min}] \quad (5b)$$

The expression for Theta-min, the minimum pressure angle, is obtained by setting to zero the differential of the pressure expression, Equation (1). This yields three conditions:

$$\text{for } \dot{U}D/8U^2 \leq -1 \quad \text{then} \quad \theta_{\min} = 0^\circ, \quad (5c)$$

$$\text{for } -1 < \dot{U}D/8U^2 < 1 \quad \text{then} \quad -\cos \theta_{\min} = \dot{U}D/8U^2, \text{ and} \quad (5d)$$

$$\text{for } \dot{U}D/8U^2 \geq 1 \quad \text{then} \quad \theta_{\min} = 180^\circ. \quad (5e)$$

USING THE IPM ALGORITHM

The set of Equations (5) is referred to as the "IPM algorithm". With this algorithm it is possible to predict instantaneous hydrodynamic forces on a cylinder moving through a fluid with velocity U and acceleration \dot{U} . Using this algorithm, it is also possible to determine instantaneous drag and inertial coefficients from instantaneous force and kinematic data.

The procedure for using the algorithm is straight forward and can be facilitated by an understanding of some of the quantities which appear in these expressions. Below we have outlined a procedure for using the IPM algorithm which includes a discussion of some of the "new" quantities and concepts.

The three steps in using Equations (5) are:

(1) Compute the instantaneous quantity θ_{\min} , Theta-min, from the instantaneous velocity and acceleration using Equation (5c), (5d), or (5e). Theta-min is determined by the kinematics of the motion only. A discussion of the behavior and importance of it will be given in a later section. Recall that it is the angular position on the cylinder surface where the potential flow pressure distribution would have a minimum value, and this angular position sweeps over the surface during the cycle. In parts of the flow cycle for which the velocity is large and the acceleration is small Equation (5d) would be used and the solution would tend to 90° . When the acceleration is dominant either Equation (5c) or (5e) is used and the values tend to 0° or 180° depending on the direction of the acceleration.

(2) With instantaneous values of Theta-min, velocity, and acceleration the quantity R is computed using Equation (5c). R is call the "interaction force term" and arises in our derivation from the use of the minimum pressure as a reference for the pressure distribution. The value of R is usually small because $\cos \theta_{\min}$ is small when the velocity is significant. When the acceleration is significant, $\cos \theta_{\min} \approx 1$, and R contributes as an

inertial term multiplied by a drag coefficient. For most force predictions the R term can be neglected. We retain it however in determining IPM coefficients from force and kinematic data.

(3) Force predictions follow from Equation (5a) using instantaneous coefficient, kinematic, and R values. The Equation (5a) is identified as the "IPM equation"

COMMENTS ON THETA-MIN

A strong correlation between instantaneous values of Theta-min and the IPM coefficient has been noted in our previous studies. Examples of this Theta-min Correlation were presented in Figures 1.2 and 1.3. The apparent reason for the correlation is that the IPM coefficient is a measure of the extent of flow separation and Theta-min is related to the potential for flow separation.

Recall that regions of adverse pressure gradient are necessary for separation and that the Theta-min position on the cylinder is the demarcation between segments of the cylinder subjected to "favorable" and "adverse" pressure gradients. Thus the pattern of Theta-min sweeping over the cylinder surface establishes conditions for flow separation and separation characterizes the value of the IPM coefficient.

The sweeping of Theta-min can best be followed by considering the sinusoidal motion of a cylinder depicted in Figure 2.2. Beginning our observation as the cylinder moves through the null velocity with peak acceleration in the negative direction. At this point the value of $(\dot{U}D/8U^2)$ would be a large negative number. For this condition Eq.(5c) indicates Theta-min is at the 0° position and none of the surface is subjected to an adverse pressure gradient. Theta-min dwells in this position for a fraction of the cycle. The dwell time depends on the amplitudes of \dot{U} , D, and U^2 . Eq.(5d) applies as the instantaneous value of $(\dot{U}D/8U^2)$ exceeds -1 and Theta-min sweeps away from 0° toward the 90° position. During this portion of the flow cycle a spreading region of adverse pressure exists between the $\pm\theta_{\min}$ locations on the cylinder. This adverse pressure gradient would influence the flow on the rear surface. As U^2 achieves a maximum value, the acceleration becomes positive and Theta-min sweeps through 90° and on toward 180° . During this portion of the cycle a significant region of adverse pressure exists. This half cycle of negative motion for the cylinder concludes with $\theta_{\min} = 180^\circ$ for a fraction of the motion for which $(\dot{U}D/8U^2)$ exceeds +1, Eq.(5e).

The dwell times of θ_{\min} at 0° and 180° and the duration of the flow cycle when $\theta_{\min} = 90^\circ$ are determined by $(\dot{U}D/U^2)$, which is the Iversen parameter, which is the reciprocal of the KC-Number. For small KC-Numbers the dwell at 0° and 180° is significant and the sweep through 90° is rapid. By contrast with large KC-Numbers the dwells at 0° and 180° are short and the minimum pressure is in the vicinity of 90° for

most of the cycle. One can think of $\cos \theta_{\min}$ as an instantaneous KC-Number.

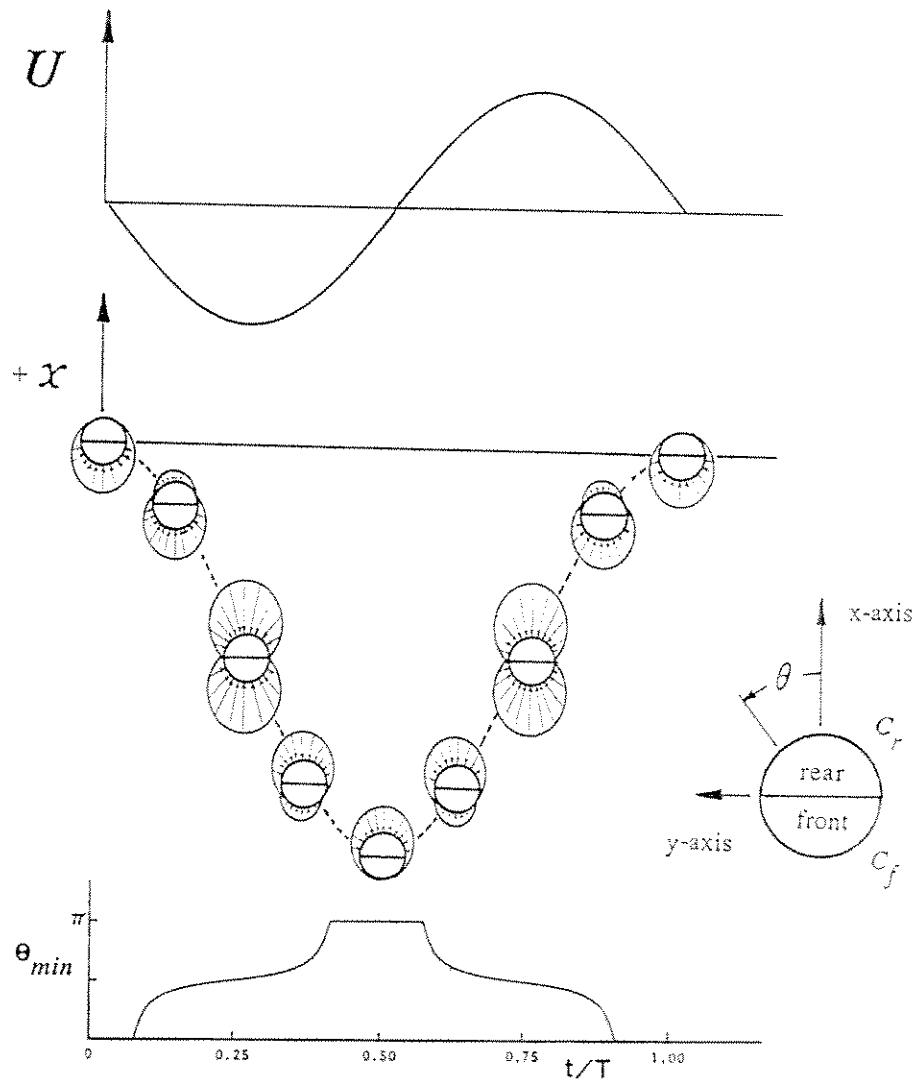


FIGURE 2.2

TIME SERIES REPRESENTATION FOR A MOVING CYLINDER

Relationship between the Velocity of a Cylinder and Its Position, Pressure Distribution, and Theta-min

MORISON AND IPM EQUATIONS

The similarity between the forms of the Morison equation and the IPM equation are significant and may be noted in the comparison below. These forms are both for a cylinder moving through a fluid.

Morison Equation:

$$F_x/\rho DL = -C_a \pi D \dot{U}/4 - C_d 1/2 |U| U \quad (6)$$

IPM Equation:

$$F_x/\rho DL = -(C_f + C_r)/2 \pi D \dot{U}/4 + (C_f - C_r)(4/3 U^2 + R) \quad (7)$$

In contrasting the expressions the following items should be noted:

- (1) That the IPM pressure coefficients have the value of 1 when the surface's pressure is that of potential flow. When flow separation reduces the pressure below that of potential flow the coefficients become less than 1.
- (2) That when potential flow occurs on both the rear and front surfaces $C_f = C_r = 1$ and the IPM inertial coefficient $(C_f + C_r)/2 = 1$ and the IPM drag term $(C_f - C_r) = 0$. For this "ideal" flow condition the IPM equation yields the classic expression for the hydrodynamic force on a moving cylinder:

$$F_x = -\rho(L \pi D^2/4) \dot{U} \quad (8)$$

which indicates an inertial force only which is equal to the product of cylinder acceleration and displacement mass and is in opposition to the acceleration. For motion of a cylinder in an ideal fluid the Morison equation inertial coefficient C_a is unity. Clearly the equivalency of the inertial terms and of the limiting values of their coefficients for these two equations has been established.

- (3) That it appears both equations have two coefficients which must be supplied for force predictions. For the IPM equation, the deviation of pressure coefficients from unity controls the values of the drag and inertial coefficients. Consider the "deviation", δ , of the front coefficient from unity so $C_f = 1 - \delta$. For this the value of the IPM drag coefficient $(C_f - C_r) = -\delta$ and the IPM inertial coefficient $(C_f + C_r)/2 = 1 - \delta/2$. A similar analysis considering the rear coefficient confirms that the value of $(C_f - C_r)$ is a measure of this "deviation" from the ideal flow pressure distribution and that this "deviation" results in a reduction of the inertial coefficient. Thus we observe that the drag and inertial coefficients are coupled so that the development of drag results in a

reduction of the inertial coefficient. An empirical observation of this relationship has been reported by several investigators.

(4) That from the above only the IPM coefficient ($C_f - C_r$) is needed. With it the deviation of the other coefficient ($C_f + C_r$) from unity can be determined.

D-FORCE FORM OF EQUATIONS

Incorporating the above ideas into the Morison and IPM equations yields the useful forms given below.

Morison Equation:

$$F_x / \rho DL + \pi D \dot{U} / 4 = C'_a \pi D \dot{U} / 4 - C_d 1/2 |U| U \quad (9)$$

IPM Equation:

$$F_x / \rho DL + \pi D \dot{U} / 4 = (C_f - C_r) (\pi D |\dot{U}| / 8 + 4/3 U^2 + R) \quad (10)$$

For the Morison equation we have replaced the inertial coefficient C_a with $(1 - C'_a)$. The coefficient C'_a is referred to as the inertial correction.

For the IPM equation the use of the absolute value of acceleration is a consequence of the sign switching of the IPM coefficient. The IPM coefficient ($C_f - C_r$) is used as a single coefficient and not as separate values of C_f and C_r . The notation is somewhat confusing and cumbersome; however, we have retained it to emphasize that this coefficient is the difference in pressure coefficients on the front and rear surfaces. Also positive values of ($C_f - C_r$) are associated with $C_r < 1$ or separation on the rear surface, and the switching to negative values of ($C_f - C_r$) is associated with $C_f < 1$ or separation on the front surface.

Comparisons of the drag terms reveals that $C_d = 8/3 (C_f - C_r)$. Note that nominal values of the IPM coefficient are less than 1.

The combination of terms (in-line hydrodynamic force and the ideal inertial force) on the left-hand side of the above equations is referred to as the "defect-force" or "D-Force". In the data reduction performed in this study the D-Force is computed and noted as a measure of the drag contribution to the total force.

The above D-Force form of the IPM equation reveals the simplicity of determining instantaneous values of the IPM coefficient from instantaneous force and kinematic data. The D-Force divided by the kinematic term $(\pi D |\dot{U}|/8 + 4/3 U^2 + R)$ yields the coefficient. It should be noted that this kinematic term is never zero so the coefficient is always finite.

SSPA DATA

The data base for this study came from a test program "Fluid Forces on Cylinders in 2-Dimensional Flows", organized by Shell Development Company and conducted by the Maritime Dynamics Laboratory of the Swedish Maritime Research Center (SSPA).

The data from this program are force and kinematic time series, sampled at 50 hz, for the motion of a vertical circular cylinder about the 88 x 39 x 3.5 meter basin at the Swedish Maritime Research Center. The test cylinder with a nominal diameter of 1 meter had an instrumented central section for force measurement which was 1 meter in length. The cylinder was supported by a bridge and sub carriage structure which could be moved about the basin. A large surface plate and the bottom of the basin formed the boundaries which assured 2-dimensional flow about the 3 meter cylinder length.

The force transducer's resolution was 4 Newtons/bit. They were calibrated to a maximum load of 4700 Newtons.

The kinematic data was derived from accelerometers, mounted with the force transducers. The accelerometers had a resolution of 4 mm/sec²/bit and a $\pm 2g$ range. Further details on the test can be found in the paper by Rodenbusch and Kallstrom⁶.

For this study only a fraction of the test conditions were analyzed. This study used the data involving the planar motion of the smooth cylinder for the test conditions described as:

Combinations of Steady Tow and Sinusoidal Motion (Low Frequency Data)

Combinations of Two Sinusoidal Motions (High Frequency Data)

We have chosen to identify these test conditions with the abbreviations in parentheses.

UNCERTAINTIES IN THE DATA

Three sources of uncertainty in these data are the force resolution, the acceleration resolution, and the acceleration noise.

For observed D-Force amplitudes above 300 Newtons the force resolution of 4 Newtons does not represent a significant problem. In some of the Low Frequency data with high currents the peak of the minimum force falls below 100 Newtons. For these conditions, which are very important to this study, the uncertainty from force resolution may approach 10%. In the high frequency tests the amplitude of the high frequency D-Force component is of the order of 20 to 30 Newtons so force resolution is a critical item in the interpretation of these data.

As the acceleration resolution of 4 mm/sec^2 is much less than the observed acceleration noise of 20 mm/sec^2 , it does not influence the uncertainties in D-Force. However, it results in a condition that we have termed "velocity drift". For all tests the velocity time series were determined from numerical integration of the acceleration. Thus a small off set in the acceleration zero, when integrated over the record, gives rise to a linear variation of the velocity over the record. This apparent velocity drift correlates with the acceleration resolution and can be easily eliminated by any one of several techniques which yield the same result.

The acceleration noise is the order of 20 mm/sec^2 and is relatively constant over the range of test conditions. As the amplitude of periodic acceleration is inversely proportional to the KC-Number, the noise is a significant problem for the high KC-Number Runs. For the highest KC-Number of 63 the acceleration amplitude is of the order of 100 mm/sec^2 and the noise represents a 20% uncertainty. For a KC-Number of 31 this uncertainty is less than 10%.

DATA REDUCTION

For the kinematic data, the acceleration was measured. The acceleration was numerically integrated to yield a velocity time series. The velocity was corrected for "velocity drift". The result was a consistent unfiltered velocity and acceleration time series.

For the force the "raw" data was first corrected of the d'Alembert loading of the force transducer by the 103 kg mass of the test segment. The difference between the resulting Hydrodynamic force and the Raw force was difficult to perceive on a plot. The Hydrodynamic force, F_x , and the acceleration of the cylinder, \dot{U} , are combined in the expression:

$$[F_x + \rho(L \pi D^2/4) \dot{U}]/\rho L D \quad (11)$$

to yield the D-Force time series.

The D-Force is a basic element in this study. It represents the Hydrodynamic force decreased by the ideal inertial load. It is the basis for force prediction comparisons and for computation of the IPM coefficient.

The computation of the IPM quantities followed the procedure outlined earlier in this Chapter: θ_{\min} computed from kinematics via Equation (5c), (5d), or (5e); R computed with Equation (5b); and the IPM coefficient with the above and the D-Force with Equation (11).

For the Low Frequency tests the above data were used in their unfiltered form for a variety of exploratory studies. For the High Frequency tests the above data were used in both their unfiltered and in smoothed form, FFT filtering to enhance the significant small signals and remove the noise.

CHAPTER 3

ANALYSIS OF LOW FREQUENCY DATA

This Chapter is devoted to the data combining a low frequency periodic motion with a steady flow. These data are to be represented by constant coefficient data appropriate to the RV approximation of the Morison equation. The low frequency data includes tests with periodic motion KC-Numbers in the range of 3.2 to 63 combined with steady currents which are 0.1, 0.5, 1, and 2 times the periodic velocity amplitude.

The objective in this Chapter is to translate the time dependent IPM coefficient pattern into constant coefficients for the Morison equation. Even a casual comparison of the IPM and Morison equations reveals the clear relationship between them and their coefficients. For the Morison equation the drag coefficient, C_d and a corrective inertial coefficient, C_a' , will be determined. Note that the IPM coefficient has the combined role of drag and corrective inertial coefficients.

The Theta-min correlation pattern of the IPM coefficient serves as an effective guide for Morison coefficient selection. On a plot of the IPM coefficient vs Theta-min the regions of drag and inertial dominance occur in different parts of the pattern. The IPM coefficients at the velocity extrema (Theta-min = 90°) translate to Morison drag coefficients for high and low velocity parts of a flow cycle. The different values of the IPM coefficient at the beginning and end of the Theta-min correlation indicate that different values of the inertial coefficient should be used at the beginning and end of both the high and low velocity parts of the flow cycle.

The logical application of these observations on the pattern of Theta-min correlation leads to a hierarchy of constant Morrison coefficient approximations. In this Chapter three levels of this hierarchy are presented.

Using this procedure uncertainties in the coefficient data are easily determined. A major uncertainty arises from the in-line transverse force contribution.

A. DATA AND NOMENCLATURE

The combined motion tests considered below are comprised of combinations of a steady motion with velocity, U_s , with periodic motion with velocity amplitude, U_p , and period T. The periodic KC-Number for these data range from 3.1 to 63 with periodic Reynolds Numbers of 0.44 and 0.88×10^6 . Parameters for each of the Runs considered in this Chapter are listed in the Table of Appendix A.

In identifying the data we have used U_s/U_p , the ratio of steady to periodic velocity, and A_x/D , the amplitude to diameter ratio for the periodic motion. The latter parameter is equal to the periodic KC-Number divided by 2π . The data are also identified by Run Numbers. A guide, relating the velocity ratio, the amplitude to diameter ratio, and Run Number, is supplied by Table 3.1.

TABLE 3.1
TABLE OF RUN NUMBERS

	A_x/D				
	0.5	1	2	5	10
U_s/U_p					
0.1		364	365	366	367
0.5		368	369/370	371/372	
1		375	376/377		
2	378/379	380/381			

Most investigations of the combined motion problem use the Reduced Velocity as a parameter. Denoted by V_R and computed by $U_s T/D$, the Reduced Velocities for the test parameters are listed in Table 3.2.

TABLE 3.2
TABLE OF REDUCED VELOCITIES: V_R

	A_x/D				
	0.5	1	2	5	10
U_s/U_p					
0.1		.63	1.3	3.1	6.3
0.5		3.1	6.3	15	
1		6.3	12.6		
2	6.3	12.6			

In discussing our data we shall refer to high current Runs and low current Runs. The data at U_s/U_p of 0.1 and 0.5 are referred to as low current and represent data in which flow reversal occurs. The data at 1 and 2 are referred to as high current for which no flow reversal occurs.

This terminology should not be confused with our reference to the high and low velocity parts of the cycle. In the high velocity part of the cycle the steady and periodic velocities add. The low velocity part of the cycle is the remaining fraction of the period of motion.

CORRELATION KC-NUMBERS

We have refrained from presenting our data correlated with the IPM based KC-Number despite the evidence that the pattern of the IPM coefficient, as well as the Morison coefficient data, correlates with an IPM based combined motion KC-Number:

$$N_{KC} \cdot (1 \pm U_p/U_s)^2$$

where N_{KC} is the usual periodic KC-Number. This correlation is based upon the argument that the KC-Number is the ratio of convective and temporal inertial terms :

$$2\pi U^2 / D \dot{U}.$$

A second approach is based upon using UT/D with the velocity replaced by the combined velocities and the period replaced by the zero crossing periods of the combined flow. A rational argument can be made for this form using the particle motion argument as the basis for the KC-Number:

$$2\pi A_x / D.$$

Other combined motion KC-Numbers have been proposed. One which is a simple combination of periodic KC-Number and Reduced Velocity i.e. :

$$(U_s + U_p)T/D$$

is the most frequently used but the least rational in origin.

Curves relating these three approaches to their modified KC-Number for combined flow problems are presented in Figure 3.1 . One problem with the last two is that they do not provide a correlation KC-Number for $U_s > U_p$.

None of these correlation KC-Numbers are used in this study and are provided to the user as a convenient reference.

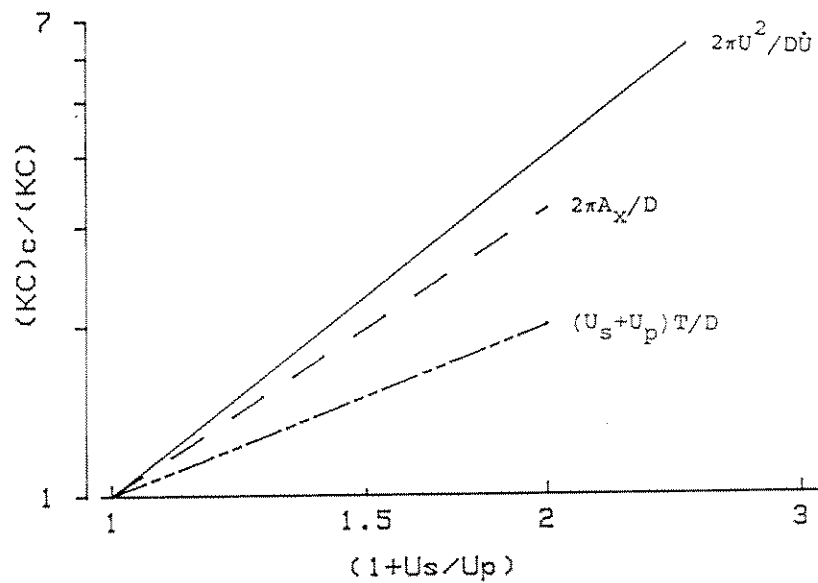


FIGURE 3.1

RELATIONSHIP BETWEEN PROPOSED CORRELATION KC-NUMBERS FOR COMBINED MOTION

IPM TIME SERIES DATA

In Appendix A we have included IPM time series data indicative of the Runs considered in this Chapter. These have been plotted as the superposition of successive cycles. Three frames of data have been presented for each Run: In each frame the velocity has been plotted as a reference. The width of the curve of velocity data is indicative of how well we were able to superimpose successive cycles. The tic marks of the time scale are at one second intervals for all plots. The three frames of data are the D-Force, the IMP coefficient ($C_f - C_r$), and the Theta-min angular position Θ_{\min} .

The quantity D-Force, here plotted as points, is the in-line hydrodynamic force less the ideal inertial force. Thus it is comprised of the drag force and the correction to the inertial force. D-Force time series plots will provide the basis for force prediction comparisons. Each force scale tic represents $F/\rho DL = 0.1$ where $\rho DL = 1000$ Newtons.

The IPM coefficient scale is from -1 to 1. The Theta-min scale is from 0 to 180° with the axis at 90°.

Note should be made of the "scatter" in both the Force and Coefficient plots. Three factors contribute to the spread of these plots. In order of their contribution, they are: (1) the in-line transverse force contribution, (2) high frequency acceleration noise, and (3) improper superposition of successive cycles.

IN-LINE TRANSVERSE FORCE

A word of explanation is appropriate at this point in explaining what is meant by "in-line transverse force contribution" hereafter referred to as the I-T force or I-T effect. The significant portion of the transverse force observed in these Runs arises from the motion of vortices along the in-line direction (x-axis) and is related through the cross product of velocity and vorticity. However, not all vortex motion is in the x-direction. Motions in the y-direction are introduced in the process of vortex shedding and sweeping around a cylinder. Though the cross product relation this transverse motion gives rise to in-line force impulses. These are observed as in-line force perturbations which we have termed as the in-line transverse force contribution (I-T Force).

In this study the I-T Force has not been closely examined. However, we have observe, that to a good approximation, its amplitude is a fraction ($\approx 20\%$) of the transverse force, and its frequency is twice that of the transverse force. Clearly it is not an artifact of improper alignment in the test apparatus.

OBSERVATIONS ON IPM DATA

A few observations on the scatter in the data are appropriate. First examining the low KC-Number Runs 364, 365, and 368 at low current. The scatter for these is dominated by vortex shedding at a low frequency which approaches that of the flow cycle. However, the asymmetry introduced by the current resists the build up of the transverse force. This results in a beating (build up and decay) of the transverse force amplitude so that the transverse force builds to twice the in-line force amplitude. Thus, with the I-T Force scaling as 20% of the transverse, the I-T effect easily accounts for most of the scatter or shift in these Runs. The very prominent low velocity force hump in Run 368 is an I-T perturbation resulting from the vortex shed during the high velocity part of the cycle showing up as the dominant feature in the low velocity part.

One can clearly see the difference between the high frequency noise and the lower frequency I-T effect by considering the higher KC-Number Runs 370 and 372. Here the transverse force frequency is much larger than that of the flow. Additional clarity is achieved by plotting only a few cycles. The perturbation pattern in both the force and coefficient time series, particularly near peak velocity, is indicative of the I-T Force.

Finally attention is directed to the erratic behavior of the IPM coefficient in the minimum velocity part of Runs 375 and 376. This "spiking" of the coefficient is not a cause for concern as it is the result of the sensitivity of the coefficient algorithm to acceleration noise when the primary signal is small. Good force predictions for these conditions are achieved by ignoring the spiking and using a smooth curve connecting adjacent well behaved portions of the coefficient pattern.

B. MORISON COEFFICIENTS FROM IPM

There are several procedures that one can conceive of using to convert the time dependent IPM coefficient into constant coefficients appropriate to the Morison methodology. The numerical conversion of the C_d being 8/3 times the IPM coefficient has already been noted.

CONCEPT

The procedure used in this study is simple and logical and can best be understood by referring to Figure 3.2. Central to this figure, as well as the concept, is a standard Theta-min Correlation plot (IPM Coefficient vs Theta-min). Here it is contrasted with velocity and acceleration which have also both been plotted vs Theta-min. In this figure one can appreciate the very narrow peak of the velocity plot.

We see that, for drag, the significant value of the coefficient occurs at $\Theta_{\min} = 90^\circ$, the extreme value of the velocity.

Recall that the IPM coefficient has both the properties of a drag coefficient and an inertial coefficient correction. From this figure we see that the significant values of the acceleration correspond to the "ends" of the Theta-min plot where the IPM coefficient values portray the inertial correction. This indicates the plausibility of using different inertial coefficients in the beginning and end of a "half cycle" with a drag coefficient determined at $\Theta_{\min} = 90^\circ$. This pattern yields the highest level of our Morison hierarchy and is referred to as Level III.

LEVELS OF HIERARCHY

For Level III different values of C_d may be used in the high and low velocity portions of the cycle each with pairs of C_a' . The coefficients are constant with time over the "half cycle" with the inertial coefficients changing values at the zero acceleration point.

Level II, a less complicated approximation, is achieved by using only a single value of C_a' in the low velocity part and a different value in the high velocity part. Thus a C_d and C_a' are used in each "half cycle".

Level I, which should be of most interest to designers, uses a single value of C_d and a single value for C_a' for the complete flow cycle and for all Runs. For this study, Level I was $C_d = 0.67$ and $C_a' = 0.67$.

Clearly, there is another Level of approximation which has not been used. This is the most common approximation found in compilations of test data and uses a single C_d and C_a' for each Run. The approximation would be at a level between I and II. One has this approximation if the high velocity coefficients of Level II are considered to apply through out the cycle. The intent was not to formally identified this level as it reflects the maximum force philosophy which has dominated wave force work. For damping we are interested in the extreme values of the force as well as the points in between.

ADVANTAGES OF THE PROCEDURE

Our approach, which uses the IPM coefficient as a guide to obtain Morison coefficients, has several advantages over the more conventional methods, such as least square and Fourier averages. First, the IPM base method can easily examine high and low velocity data separately. Second the method allows one to see the scatter in

the data and to quantify this uncertainty in the Morison coefficients. Third the approach logically leads to the hierarchy of approximations and allows one to see where and why they may be good approximations.

It is difficult to conceive of a constant coefficient Morison approximation beyond Level III. From a practical point of view one may not be interested in going to Level III.

Our approach is similar to an early technique which computed drag coefficients at maximum velocity and inertial coefficients at maximum acceleration points. Our method supports the logic of this earlier approach while superseding it in accuracy and implementation.

LEVEL II DATA

The values of the coefficient data for Level II are presented in Figures 3.3 to 3.6 . The Figures represents velocity ratios (steady to periodic) of 0.1, 0.5, 1, and 2 respectively. Each presents separate plots of C_d and C'_a as a function of the amplitude to diameter ratio for the high and low velocity parts of the cycle. The solid curve represents the effective mean value of the coefficient. The dashed lines are the extreme values observed from the IPM coefficient data and tested with the constant coefficient Morison equation. The extreme values of C_d yield the envelope of the D-Force data when used with the corresponding mean value of C'_a . Similarly, when inertia effects are dominant, the extreme values of C'_a yield the observer D-Force envelope with a mean C_d .

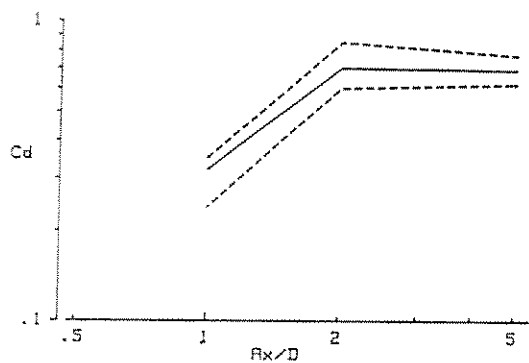
LEVEL III DATA

For Level III the C_d values of Level II would be used with the C'_a values from Table 3.3 . The 1st and 2nd refer to the initial value used and the final value used respectively in their high and low velocity parts of the flow cycle.

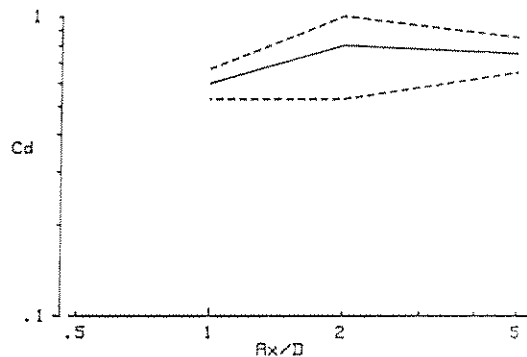
OBSERVATIONS ON COEFFICIENT DATA

In reviewing the data in Figures 3.3 to 3.6, one should remember:

$$C_a = 1 - C'_a$$



$U_s/U_p=0.1$ for High Velocity Part of Cycle



$U_s/U_p=0.1$ for Low Velocity Part of Cycle

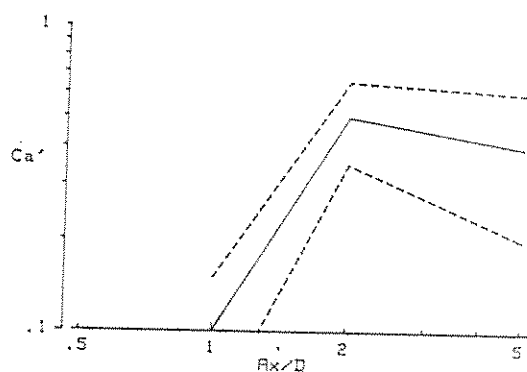
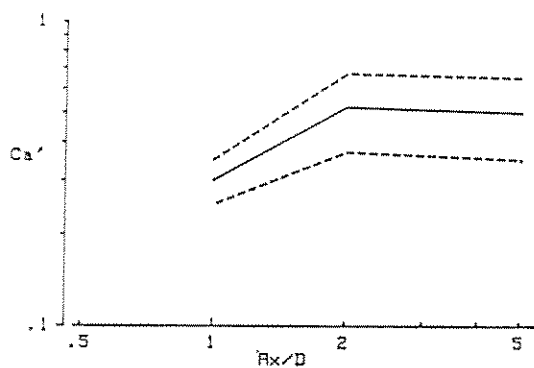
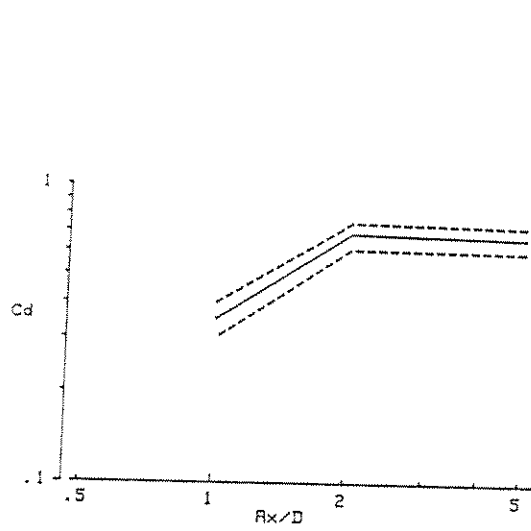


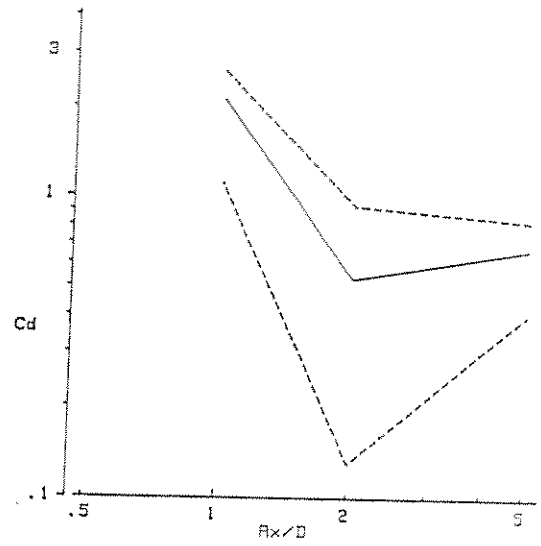
FIGURE 3.3

LEVEL II COEFFICIENT DATA

Morison Drag and Inertial Correction Coefficients applicable to the low and high velocity parts of a combined motion flow cycle. The motion combines a steady and periodic motion of the cylinder with a steady to periodic velocity ratio of 0.1 .



$U_s/U_p=0.5$ for High Velocity Part of Cycle



$U_s/U_p=0.5$ for Low Velocity Part of Cycle

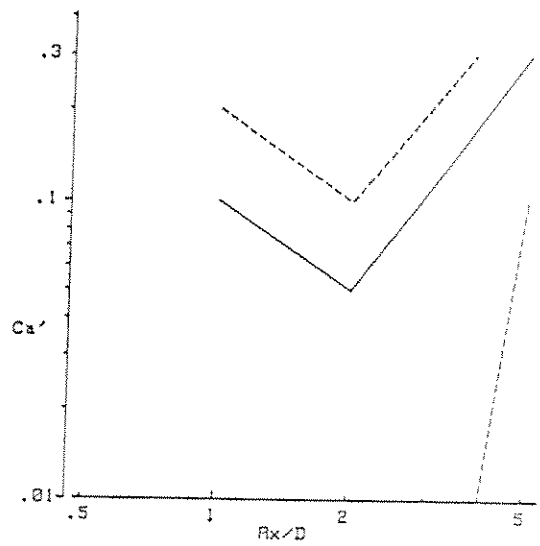
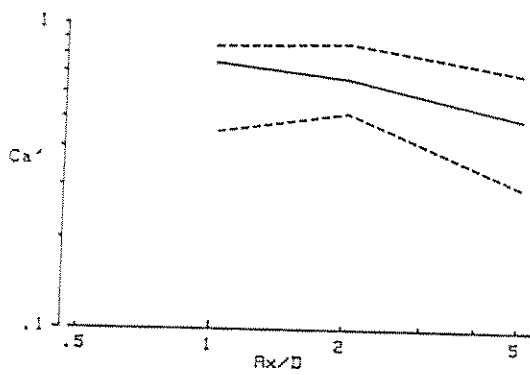
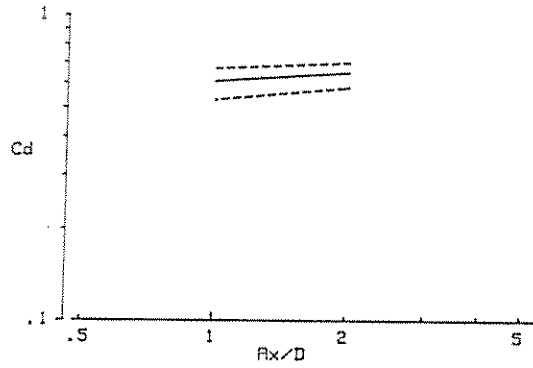


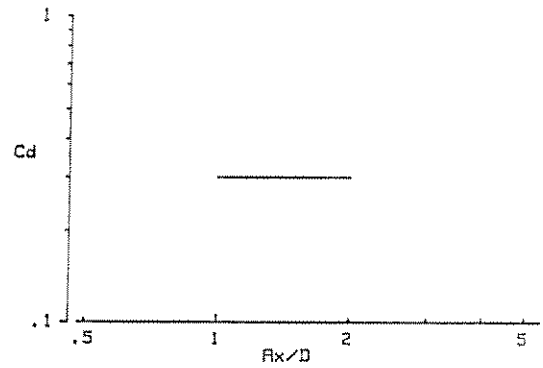
FIGURE 3.4

LEVEL II COEFFICIENT DATA

Morison Drag and Inertial Correction Coefficients applicable to the low and high velocity parts of a combined motion flow cycle. The motion combines a steady and periodic motion of the cylinder with a steady to periodic velocity ratio of 0.5.



$U_s/U_p=1$ for High Velocity Part of Cycle



$U_s/U_p=1$ for Low Velocity Part of Cycle

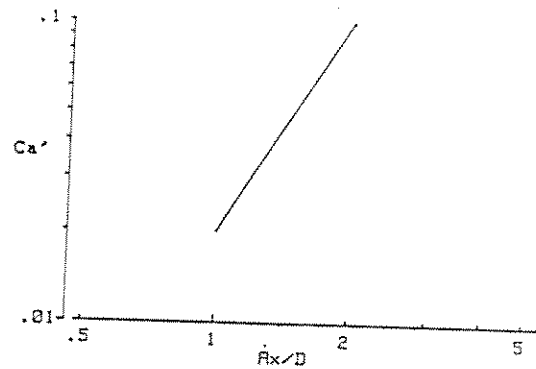
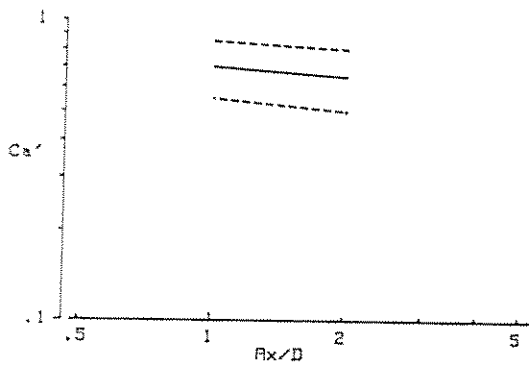


FIGURE 3.5

LEVEL II COEFFICIENT DATA

Morison Drag and Inertial Correction Coefficients applicable to the low and high velocity parts of a combined motion flow cycle. The motion combines a steady and periodic motion of the cylinder with a steady to periodic velocity ratio of 1.0 .

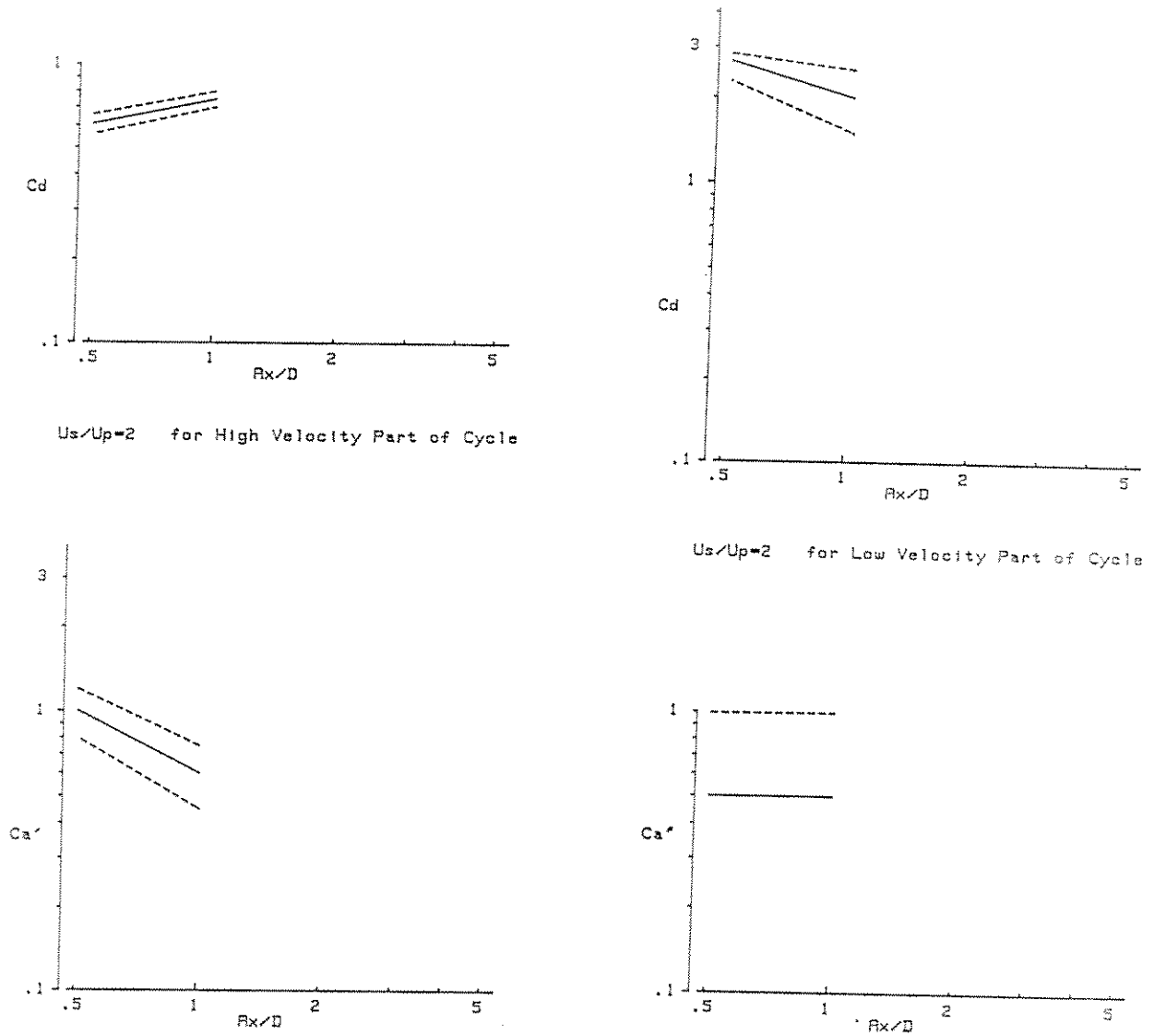


FIGURE 3.6

LEVEL II COEFFICIENT DATA

Morison Drag and Inertial Correction Coefficients applicable to the low and high velocity parts of a combined motion flow cycle. The motion combines a steady and periodic motion of the cylinder with a steady to periodic velocity ratio of 2.0 .

TABLE 3.3

C_a VALUES FOR LEVEL III

A_x/D	U_s/U_p	<i>High Velocity</i>		<i>Low Velocity</i>	
		<i>1st</i>	<i>2nd</i>	<i>1st</i>	<i>2nd</i>
1	0.1	0	0.3	0	0.1
2	0.1	0.7	0.5	0.3	0.5
5	0.1	0.37	0.5	0.2	0.5
1	0.5	1.0	0.6	0.25	0
2	0.5	0.9	0.6	0	0.1
5	0.5	0.3	0.55	0.2	0.4
1	1	0.5	0.75	-	-
2	1	0.9	0.6	0	0.1
0.5	2	1	0.8	-	-
1	2	1	0.6	-	-

So for high KC-Number, drag dominated flows, C_a' should approach 1. Likewise for low KC-Number, inertial dominated data, the correction coefficient should be small.

Also, the high velocity part of the flow cycle tends to a high KC-Number behavior while the low velocity part tends to a low KC-Number behavior. The amount of shift in KC-Number is open to question as indicated by Figure 3.1 .

One should recall the observations, made in an earlier section, on the scatter in the D-Force and IPM coefficient data and the relationship of uncertainties to the I-T effect.

All data for the high velocity parts of flow cycles are well behaved from the point of uncertainty and follow the expected pattern of increasing drag with KC-Number. Noteworthy is the lack of the "mid range peak" in coefficient data. This peak is observed for KC-Numbers in the range of 10 to 15 ($A_x/D \approx 2$) in zero current Runs. This peak is an I-T effect. Clearly, current opposes the build up at these conditions. The high current data are all at low periodic KC-Numbers but clearly have a high KC-Number behavior.

The logic of assigning the value of 0.67 to both C_d and C_a' for the Level I approximation is evident from Figures 3.3 to 3.6 . These values fit well within the uncertainty of most of the data. However, these values are not unique.

The coefficient data from the low velocity part of a cycle shows a larger uncertainty band. For low A_x/D values, an erratic behavior of the coefficients is observed. For the low current data with amplitude ratio of 1, the C_a' s are small as expected but the C_d s are much higher than expected. We have discussed these data in an earlier section and attributed this behavior to the I-T effect. For the highest current data, the low velocity C_d s are surprisingly large. Because the behavior of the latter data is difficult to rationalize, the high current data will be analyzed further with the high frequency data as we consider the RV vs IF question in Chapter 5.

CHAPTER 4

LOW FREQUENCY PREDICTIONS

In this study we will have done two things which, though obvious, are rarely done in wave force studies: (1) quantified the uncertainty in our Morison coefficient data and (2) shown how well the coefficient data predict the observed force. The uncertainty in the coefficient data and the coefficients ability to reproduce data are two distinctly different questions. However, both involve the limitations of the Morison methodology.

The uncertainty is comparatively easy to understand and quantify. It is simply the variation of the coefficients achieved through the data reduction procedure. If the procedure is either least square or Fourier averages and the entire data record is used, it is impossible to state the uncertainty, as the procedure yields a single value. Cycle-by-cycle analysis is required to determine uncertainty in constant coefficient data.

Using coefficients within the uncertainty range does not assure accuracy in a force prediction. The accuracy of a force prediction is difficult to quantify in a meaningful way, although "goodness of fit" and standard deviation are most frequently used. The ability to predict the maximum force is also used; however, for damping one has equal interest in maximum and minimum force values. It is the variation about a mean that comes to mind when considering damping forces.

In this study our standard for accuracy of a force prediction is: "how much of the prediction falls within the scatter of the observed data".

The quality of the predictions will be judged on how well they reproduce the D-Force which is the observed hydrodynamic force minus the ideal inertial force. In some studies, force comparisons are based on the observed hydrodynamic force; however, this may be deceiving particularly at low KC-Number conditions where the dominance of the inertial force will obscure the drag force. The D-Force which is comprised of drag and corrective inertial contributions is a better standard for judging drag or damping predictions.

Predictions with our coefficients indicate the ease with which the Morison equation accurately yields maximum forces. However, there is a problem in predicting the off-peak forces which are important in determining damping. The poor results with the high current data led us to reexamine these data in the RV and IF analysis considered in Chapter 5.

LEVEL I PREDICTIONS

In considering the force predictions of our hierarchy of Morison coefficient representations we shall start with Level I.

In Figures 4.1 to 4.4 the force predictions of Level I are compared to the observed force time series. The Figures are organized in order of increasing steady to periodic velocity ratio with the plots of lowest A_x/D at the top of the Figure. The force plots are on the same scale as those presented in Appendix A except these data are presented as curves rather than just points.

The predictions, at all Levels with these low frequency data, were made with unfiltered kinematic data. From the width of the band and the high frequency perturbations of the predicted force curves, we can see the influence of high frequency noise and any problems posed by errors in alignment of successive cycles.

LEVEL II PREDICTIONS

For Level II, similar D-Force time series plots comparing observed with predicted forces are presented in Appendix B. In these a separate page is devoted to each test condition. The plot at the top of each page presents the high velocity^{*} prediction. This prediction, though appropriate only for the high velocity part of the cycle (last part of the plot), has been presented for the entire cycle. The low velocity prediction is seen on the middle plot and should be compared in the initial part of the plot. The Level I prediction is repeated as the bottom plot for easy reference in seeing improvement from Level I to II. These Figures are organized into groups of increasing current. Within these groups for the same current the plots are in order of increasing amplitude to diameter ratio.

No plots are presented for Level III. However, a summary of comments on each Run and for each Level is presented in Tables 4.1, 4.2, and 4.3.

*NOTE: We have selected the Runs and organize the data so the high velocity part is positive and plotted in the last half of the cycle. This results in a negative D-Force in the last half of the cycle. Run 375 is the exception and was the only Run for this test condition. Its maximum velocity is in the negative direction and was plotted in the second half of the cycle.

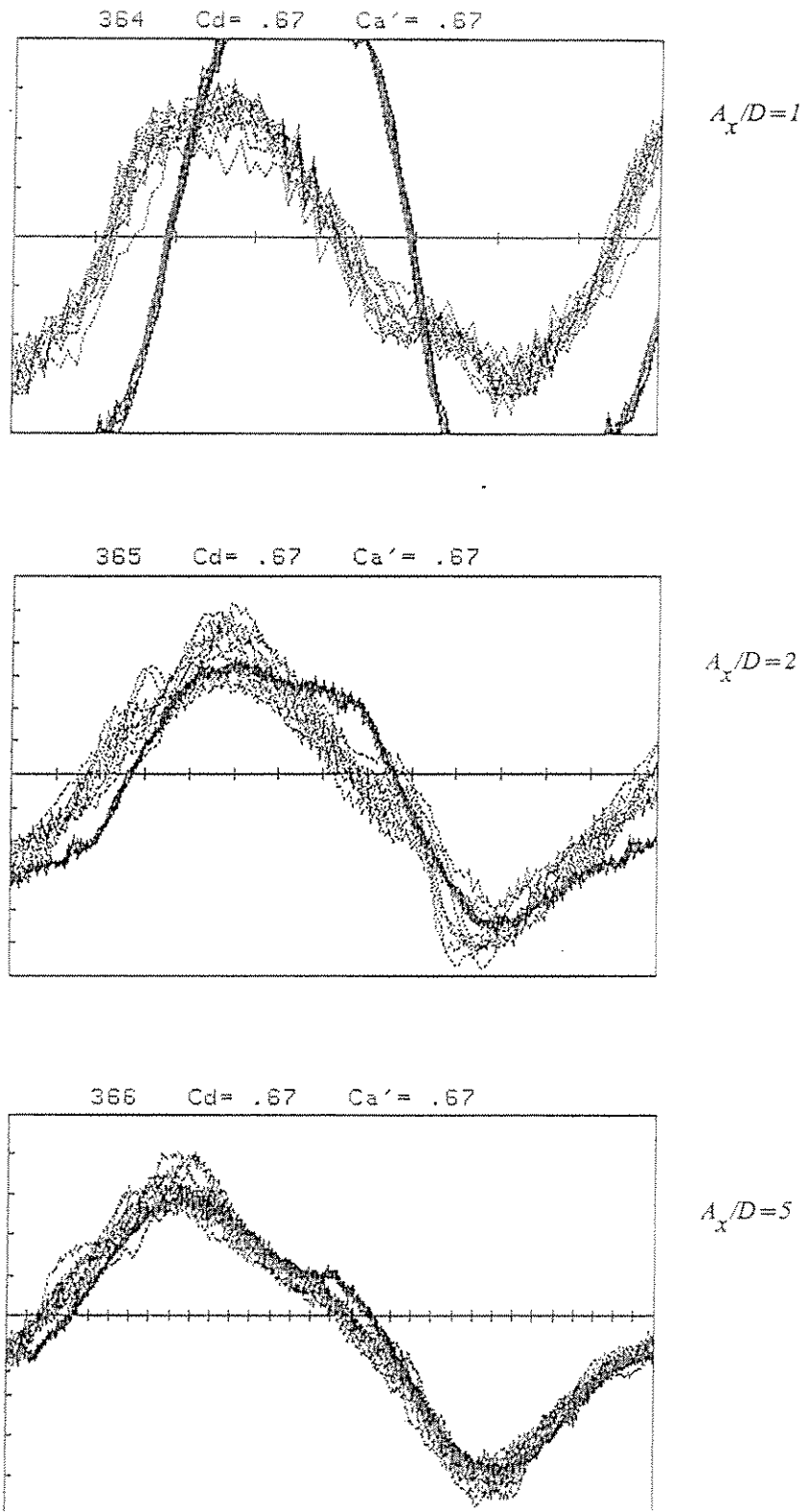


FIGURE 4.1

COMPARISON OF D-FORCE OBSERVED TO PREDICTIONS WITH LEVEL I
 $U_s/U_p = 0.1$

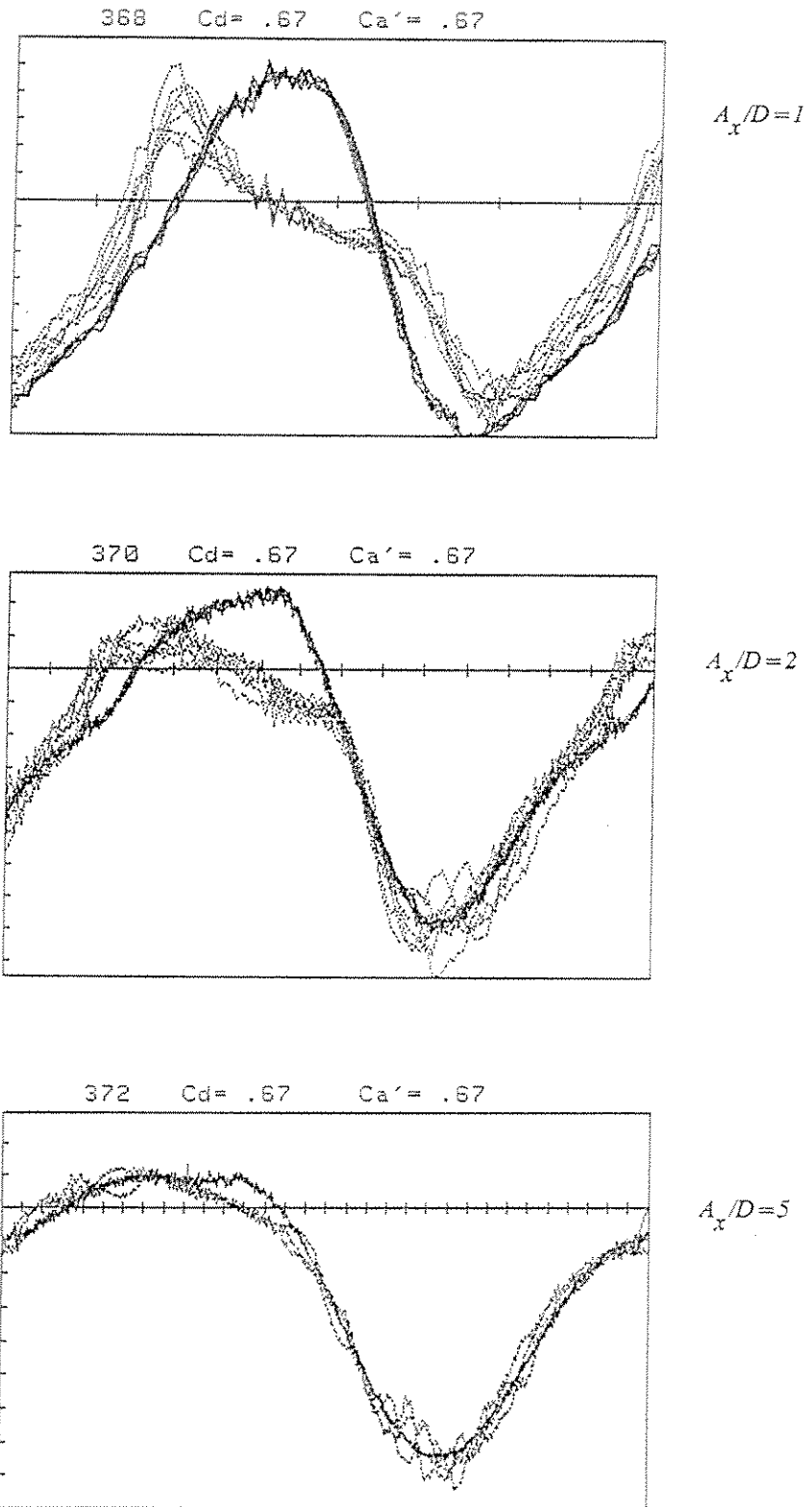


FIGURE 4.2

COMPARISON OF D-FORCE OBSERVED TO PREDICTIONS WITH LEVEL I
 $U_s/U_p = 0.5$

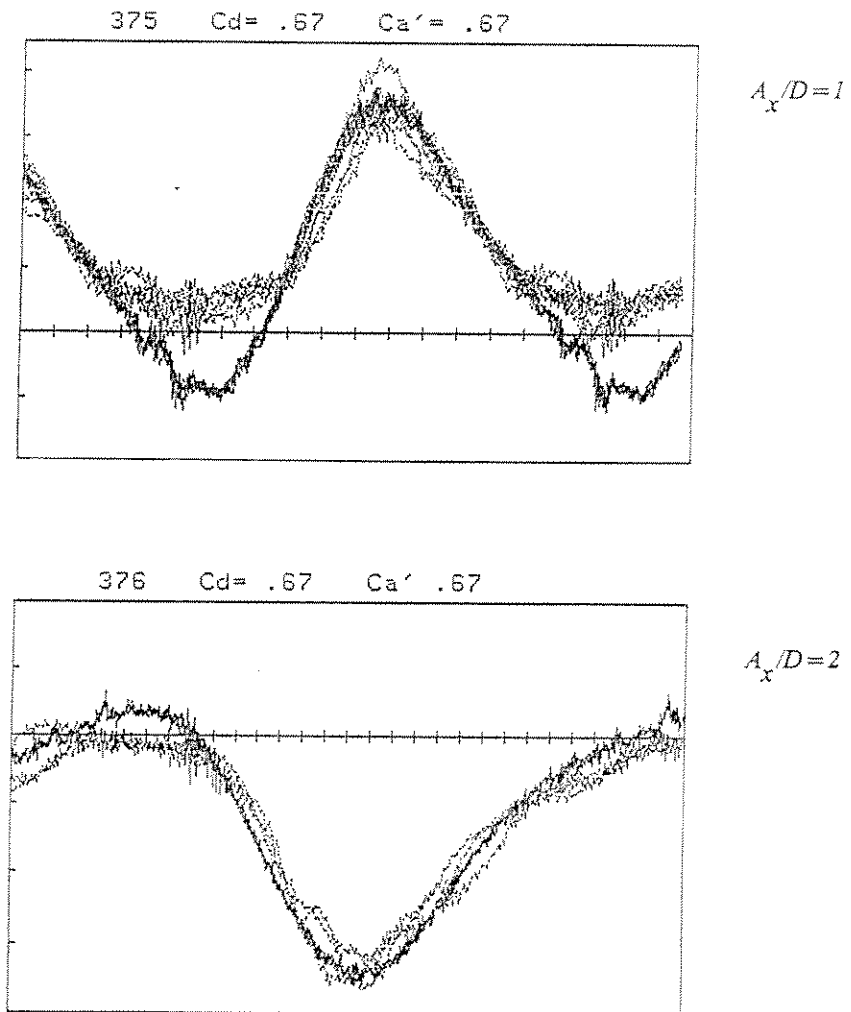


FIGURE 4.3

COMPARISON OF D-FORCE OBSERVED TO PREDICTIONS WITH LEVEL I

$$U_s/U_p = 1.0$$

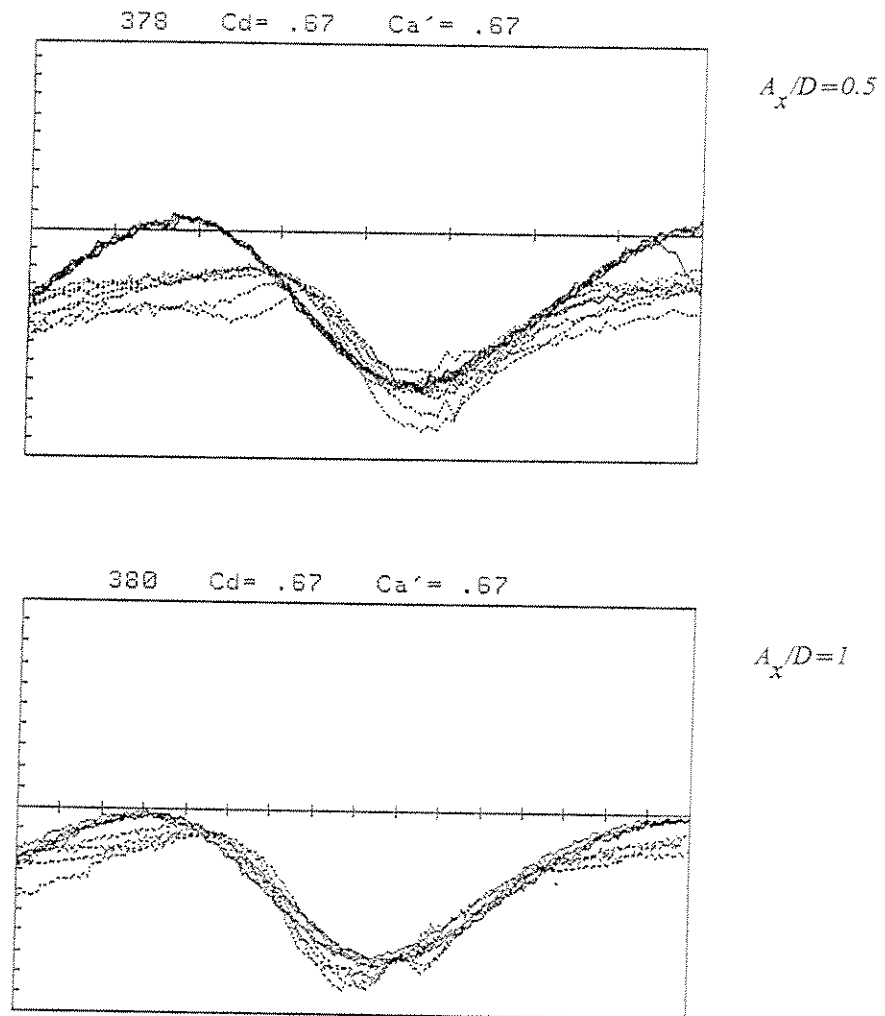


FIGURE 4.4

COMPARISON OF D-FORCE OBSERVED TO PREDICTIONS WITH LEVEL I

$$U_s/U_p = 2.0$$

TABLE 4.1

COMMENTS SUMMARY

OBSERVATIONS ON PREDICTIONS MADE WITH
THE HIERARCHY OF MORISON COEFFICIENT LEVELS
PRESENTED IN THIS STUDY FOR LOW CURRENT DATA $U_s/U_p = 0.1$

Run 364 $U_s/U_p = 0.1$ $A_x/D = 1$

Level I Very poor prediction

Level II Low Velocity: Good prediction
High Velocity: Peak force region good with bumps elsewhere

Level III Low Velocity: Further improvement, 70 % within scatter band
High Velocity: Significant Improvement

Run 365 $U_s/U_p = 0.1$ $A_x/D = 2$

Level I Prediction 70 % within scatter band

Level II Prediction 85 % within scatter band; reduced bumps

Level III Prediction 85 % within scatter band; better centering
in scatter band; bump reduction requires variable C_a'

Run 366 $U_s/U_p = 0.1$ $A_x/D = 5$

Level I Prediction 80 % within scatter band

Level II Prediction 100 % within scatter band

Level III Prediction 100 % within scatter band; better centering
in scatter band

TABLE 4.2

COMMENTS SUMMARY

OBSERVATIONS ON PREDICTIONS MADE WITH
THE HIERARCHY OF MORISON COEFFICIENT LEVELS
PRESENTED IN THIS STUDY FOR LOW CURRENT DATA $U_s/U_p=0.5$

Run 368 $U_s/U_p=0.5$ $A_x/D=1$

Level I Poor prediction; amplitude OK but out of phase

Level II Prediction 60 % within scatter band

Level III Prediction 70 % within scatter band

Run 370 $U_s/U_p=0.5$ $A_x/D=2$

Level I Prediction 55 % within scatter band

Level II Prediction 83 % within scatter band

Level III Prediction 85 % within scatter band; slight improvement
with better centering in scatter band

Run 372 $U_s/U_p=0.5$ $A_x/D=5$

Level I Prediction 78 % within scatter band

Level II Prediction 90 % within scatter band

Level III More than 90 % of prediction within scatter band;
better centering in scatter band

TABLE 4.3

COMMENTS SUMMARY

OBSERVATIONS ON PREDICTIONS MADE WITH
THE HIERARCHY OF MORISON COEFFICIENT LEVELS
PRESENTED IN THIS STUDY FOR HIGH CURRENT DATA

Run 375 $U_s/U_p = 1.0$ $A_x/D = 1$

Level I Prediction 60% within scatter band, but poor prediction for low velocity part where amplitude error is 65 %

Level II Prediction 85 % within scatter band; improvement for low velocity part

Level III NA

Run 376 $U_s/U_p = 1.0$ $A_x/D = 2$

Level I Prediction 75 % within scatter band; 23 % error in amplitude prediction in low velocity part

Level II Prediction 83 % within scatter band

Level III Slight improvement

Run 378 $U_s/U_p = 2.0$ $A_x/D = 0.5$

Level I Prediction 55 % within scatter band; 88 % error in amplitude prediction in low velocity part

Level II Large bump in low velocity part, can not be eliminate with constant coefficients

Level III NA

Run 380 $U_s/U_p = 2.0$ $A_x/D = 1.0$

Level I Prediction 53 % within scatter band; 55 % error in amplitude prediction in low velocity part

Level II Small bump in low velocity part, but hard to eliminate with constant coefficients

Level III NA

OBSERVATIONS ON PREDICTIONS

As stated earlier our standard for accuracy is how much of the prediction falls within the scatter band. This is exemplified in Table 4.1 by "prediction 80% within scatter...", for Run 366. This indicates that for 80% of the period the prediction is within the scatter. The descriptive statement "better centering..." conveys an improvement in quality which needs no explanation.

For most of the data, further quantifying of the prediction accuracy was not done, feeling that with the comparative time series one would prefer to use their own standards. The exception to this is found in the high current Runs. For these data we have noted an error in prediction of the minimum force amplitude. The "amplitude error" reported as a percentage in Table 4.3 is the difference between prediction and observation divided by the prediction amplitude. The prediction amplitude is half the difference between the extrema of the prediction and is indicative of the amplitude of oscillation about the mean.

A quick look at all the data tends to reinforce the classic observation that: "the Morison equation is better at high KC-Numbers than low". This observation is valid at all Levels and is exemplified by comparisons such as Runs 364 and 366.

A further generalization is that predictions which are 60 to 70 % within the scatter can be achieved with our lowest Level with a few exceptions. The exceptions are at low amplitude to diameter ratios and at high currents.

COEFFICIENT COMPATIBILITY

A careful review of the predictions and the coefficient data indicates a problem of coefficient compatibility for certain Runs. The most dramatic examples of this are the highest current Runs 378 and 380 with the Level II predictions, see the Appendix. Here we observe the high and the low velocity predictions do not intersect. This is caused by the very large coefficients required for predictions in the low velocity part of the cycle. To a lesser degree this is seen in the low A_x/D Runs 364 and 368.

GRADES FOR RUNS

Based on the coefficient data and the predictions it is possible to assign a grade A through D to each Run. This grade indicates how well behaved the prediction is relative to the observer force.

Grade A would be assigned to those Runs which are 85% or better within the scatter band. These are the high A_x/D Runs with low current, Runs 365, 366, 370, and 372.

Grade B would be assigned to those Runs which are 85% or better within the scatter band but which present slight problems in the low velocity part of the cycle. Here it seems that the coefficients can't be adjusted to achieve better centering of the predictions within the scatter band. The high current Runs 375 and 376 with $U_s/U_p = 1$ are grade B.

Grade C would be assigned to Runs 368 and 380. For these Runs the problems of prediction have increased and the problem of coefficient compatibility is slight. Both have $A_x/D = 1$. Run 380 is a high current and 368 a low current. The I-T effect was noted previously to influence the 368 data.

Grade D is assigned to the severest problem Runs 378 and 364. These represent extreme test conditions: low A_x/D combined with the lowest and highest currents. Coefficient compatibility is severe. In adjusting the coefficients for these Runs one sees the need for more coefficient variation over the cycle. In particular variation of coefficients is needed in the turn on and terminal phases of a "half cycle".

MORISON "BUMP"

The error in prediction is largely due to the "Morison bump". This is our own terminology. It identifies a significant feature in all the comparisons of predicted and observed forces.

In a modest form it is seen in Figure 4.1 on Run 366 as a slight bump in the prediction at the zero crossing for the force. The "bump" is more pronounced for the lower A_x/D data. The bump is always associated with the region of minimum absolute velocity. So, as the current increases, its phase relationship to the cycle shifts. This shift is evident in comparing the low current data of Figure 4.1 with the slightly higher current data of Figure 4.2. And for the highest currents of Figures 4.3 and 4.4 the bump shifts to a position where it represents a significant problem in predicting the minimum force amplitude.

Contrasting the plots of Level I and Level II indicates how the bump can be reduced by careful selection of the Morison coefficients. To aid in this observation consider the two runs plotted in Figure 4.5. The two predictions on each of the plots indicate how the bump was reduced by adjusting the inertial correction, C_a' . The bump is a more persistent problem at low KC-Numbers and for high currents.

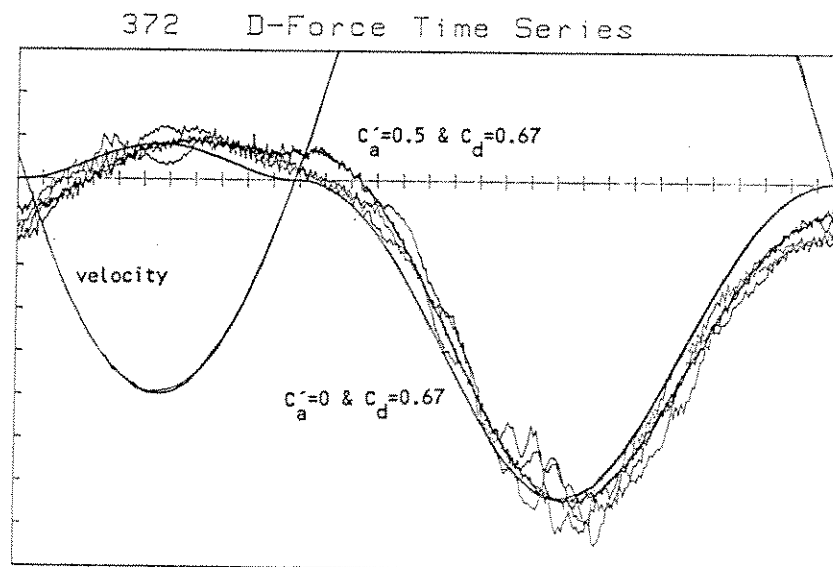
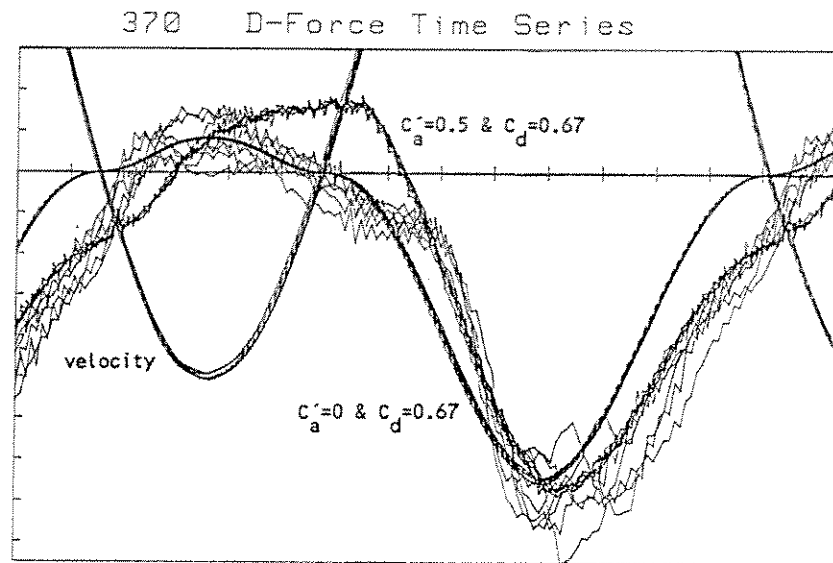


FIGURE 4.5

COMPARISON OF D-FORCE OBSERVED TO MORISON PREDICTIONS

Influence of change in coefficients upon force predictions. For Run 370 the $A_x/D=2$ and for Run 372 the $A_x/D=5$. The $U_s/U_p=0.5$ for both.

An obvious question is: Are the bump and other problems, such as the I-T effect and coefficient compatibility, related? Both bump and coefficient compatibility occur in the turn on and termination phase of the flow half cycle. Both could be reduced by a variation of the coefficient in this region. Clearly the bump and coefficient compatibility are manifestations of the same problem.

The relationship between the bump and I-T is not as clear. We know that the I-T force is most prominent in regions where the bump is not evident; however, we do not know whether the bump is a I-T effect occurring in the turn on and termination phases. It could be associated with the first vortex or the sweeping of the last back over the cylinder. In the case of Run 368 we see clear evidence of the coincidence of the bump and I-T effect. Questions of the I-T effect and the Morison bump deserve further study.

CHAPTER 5

RV AND IF APPROXIMATIONS

If the original plan of this study had been followed this Chapter would have been devoted entirely to a short presentation of coefficient data for the High Frequency* SSPA tests. However, in the pursuit of the original plan we found several inconsistencies that led us to widen the scope of the study in so far as the high frequency data are concerned. The two most significant inconsistencies were: (1) some of the high frequency data seemed to fit into the classic pattern of the RV form of the Morison equation while others seemed to fit the IF form and (2) criteria, such as that cited by Reference 11, failed to identify the proper Morison form for these data. Furthermore, the criteria also failed with the low frequency data presented in the previous Chapters. This situation led us to the broader subject which is the title of this Chapter.

The high frequency data and the high current low frequency data have an interesting feature in common -- no flow reversal for significant periods of observation. This is significant as: (1) the functional behavior of the IPM U^2 and the Morison $|U|U$ are identical, (2) the fluctuations of the IPM coefficient are similar for the high frequency data and the low frequency high current data, (3) wake return questions do not arise. In short the IPM seems ideally suited to the resolution of the inconsistencies.

The approach that is used in the resolution of the RV vs IF question is to consider the expansion of the IPM drag term consisting of the fluctuating IMP coefficient and velocity. The resulting expression consists of a series of terms which favors either the RV or the IF form depending upon the relative magnitudes of the coefficient and velocity fluctuations. This analysis applies equally well to the small amplitude high frequency data of this Chapter and the higher amplitude low frequency data of Chapter 4. The results of this analysis can be portrayed on a plot which defines the conditions for applicability of the RV and IF forms.

On the basis of this plot, as well as confirming IPM based force dissection, we can justify the algorithm used for damping force predictions and the values of the Morison coefficients presented for each of the high frequency Runs. One unexpected dividend from the analysis was a rational justification for neglecting or filtering out the very high frequency noise that plagues tests similar to the SSPA.

The Chapter concludes with an appraisal of I-T effects that modify the transverse force pattern and possibly influence the damping pattern.

*NOTE: Recall high frequency data involve the combination of high frequency periodic motion with a low frequency periodic motion. Expressions for the RV and IF forms of the Morison equation are included on Figure 5.3

RV MORISON OVERPREDICTION

The problem of over prediction of "damping forces" with the RV form of the Morison equation is most clearly seen in an illustrative example which compares observed and predicted forces. As in the previous Chapters the comparisons should be of the D-Force time series.

For the illustration we have chosen Run 437 from the set of High Frequency SSPA data. The dominant features of this Run are associated with the low frequency motion which is characterized by a KC-Number of 12.5. The high frequency motion has a amplitude which is 1/20 of the low frequency motion.

In the comparison two predicted forces are used. One is based upon the Morison drag term using only the low frequency kinematics. The other combines the low and high frequency kinematics in the RV form. In the lower plot of Figure 5.1 the low frequency prediction is compared to the observed force (identified as the noisier curve) to indicate that we have achieved a good average prediction of the observed low frequency features. Clearly we have made a reasonable selection for the drag coefficient.

In the upper plot the prediction is based upon the same drag coefficient but using the RV form. The comparison is to the same observed force time series.

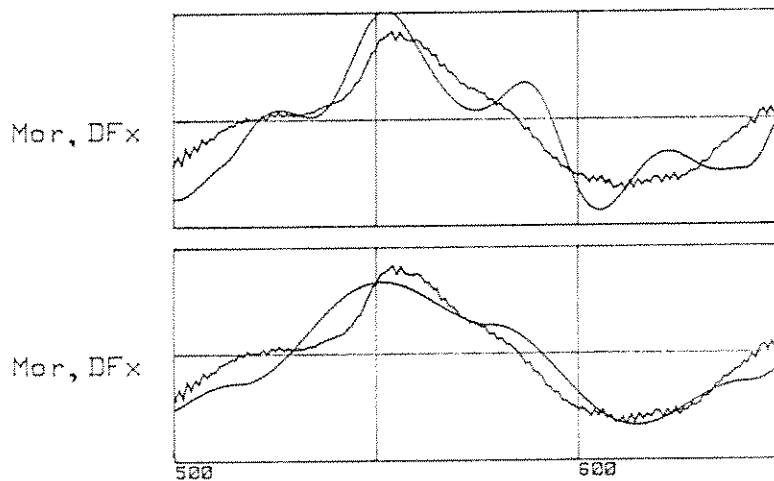


FIGURE 5.1

COMPARISONS OF OBSERVED AND PREDICTED FORCES

For high frequency Run 437 two predictions were made with the Morison equation using identical drag coefficients. The upper plot prediction was based on the RV form. For the lower plot prediction the high frequency motion was neglected.

These plots clearly illustrate how the RV form of the Morison equation over estimates the damping force (high frequency component). For this Run the RV's damping force prediction is over 10 times the observed.

To rationalize this illustrated failure of the RV prediction we turned to a review paper¹¹ which discusses the "region of applicability of the relative velocity and independent flow fields" forms in terms of the parameters, periodic KC-Number and Reduced Velocity. The cited work holds that below a threshold in the range of 10 to 15 for either of these parameters the independent flow fields approximation should apply. According to this the IF form should be applicable to all the high frequency SSPA Runs. However, for some of the high frequency Runs the RV form seemed to be a good predictor, and these were the most unlikely cases of low KC-Number and reduced velocity.

When this cited criteria was tested with the low frequency data it proved to be unreliable. Most of the data, that was handled well with the RV form in the previous Chapter, fell below the threshold for RV applicability.

BRIEF REVIEW OF RV, IF, AND OTHER FORMS

Recall that the Relative Velocity (RV) idea combines two or more motions vectorially and substitutes the resulting velocity into the Morison equation with a single time invariant drag coefficient. The Independent Flow Fields (IF) idea typically is realized by using a Morison drag term, with its own coefficient, for each motion. Expressions and graphical representations for each are given in Figure 5.3.

Before pursuing the RV vs IF question further it is well to review some ideas on drag and damping. For this it is useful to visualize the perturbations which are indicative of the various damping and/or drag approximations on force vs velocity plots. Thus, for the classic case of linear damping, we would envision the variation of the force perturbation with damping velocity as shown in Figure 5.2A. Positive velocities result in negative loading forces and negative velocities for the cylinder result in positive forces. The slope of the curve is the damping coefficient. Note that despite the negative slope of this line the damping coefficient would be positive. Negative damping would be indicated by forces in the first and third quadrants of such a plot.

A similar plot of the classic Morison drag term has the parabolic or quadratic appearance as shown in Figure 5.2B. In contrasting these two classic renderings it should be clear that the linearization of this Morison form is not easily achieved with rational arguments.

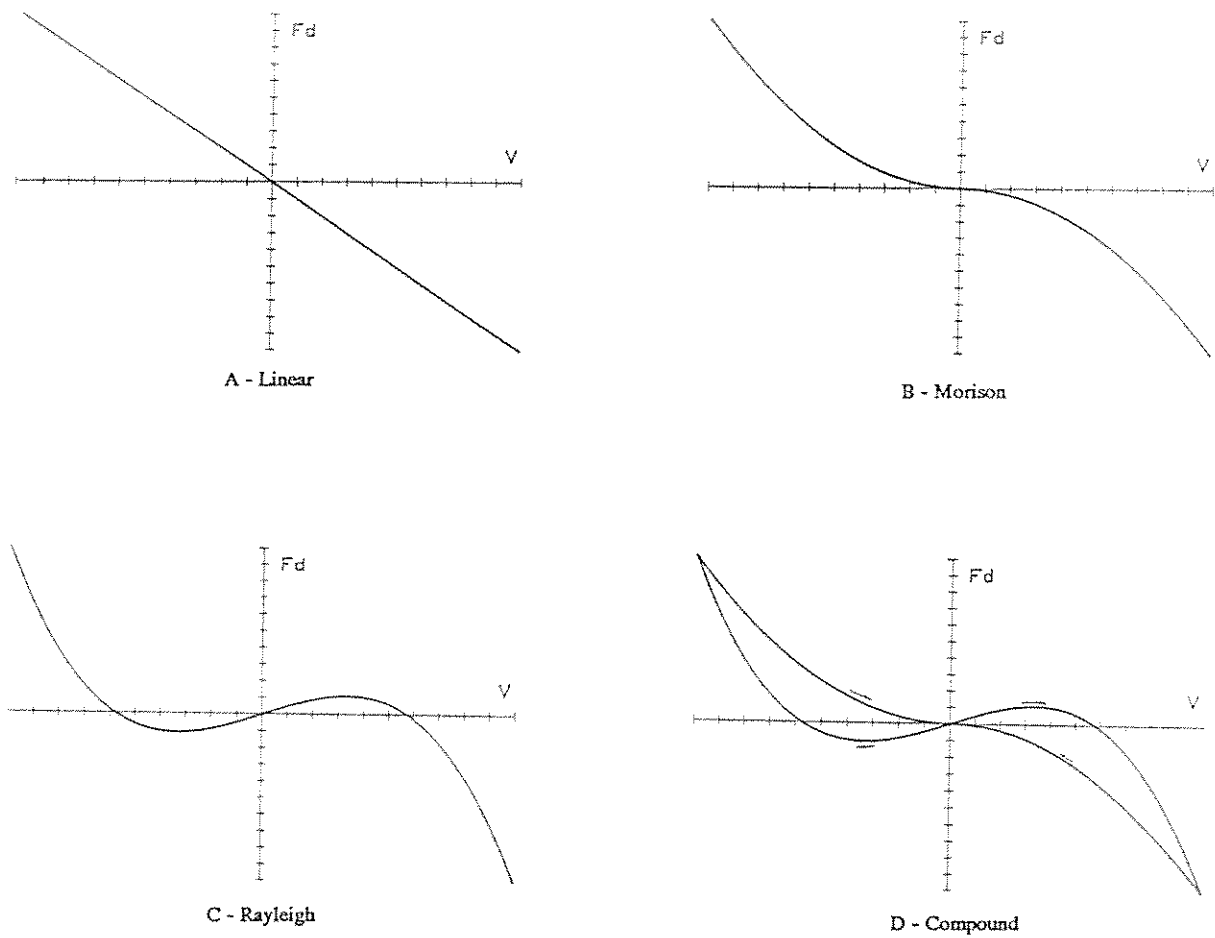


FIGURE 5.2

DAMPING FORCE AS A FUNCTION OF CYLINDER VELOCITY

- A. Linear approximation with a constant damping coefficient
- B. Morison drag term $C_d |V| V$ with constant drag coefficient.
- C. Rayleigh's equation (van der Pol) involving negative damping during part of the cycle.
- D. Compound representation of Rayleigh & Morison. This is a good approximation of an observed pattern with negative damping in the early portion of each half cycle.

Now, for the combination of a primary motion of large amplitude and low frequency with a secondary motion of small amplitude and high frequency, we should expect the RV Morison approximation fits the Morison curve. In Figure 5.3A this RV Morison form is presented. In this plot we have "frozen" the primary motion and have shown the secondary or perturbation effect as the solid segment of the curve. The force fluctuates along the solid curve as a result of the secondary motion. The solid curve in turn moves along the dotted curve as a result of the primary motion. As opposed to the earlier Morison plot, it is easy to envision a linear damping approximation for the secondary motion on this plot. This linear form would be especially good for small amplitudes of the secondary motion.

A similar plot for the IF approximation is presented in Figure 5.3B. Here the primary motion has been "froze" to show the secondary motion as a small segment of a Morison curve which is transverse to the dotted primary motion curve. One should envision the secondary motion segment as sliding along the primary curve. The resulting combination would be a rather complex pattern of loops about the primary curve.

With the Morison IF form, the achievement of a linear damping approximation is not possible as with case 5.2.B three paragraphs above. However, if one drops the Morison constraint on the IF idea, then a rich pattern of damping forms become available. With this less doctrinaire approach, one would simply postulate a linear behavior for the high frequency perturbation and test it against observation. Equally interesting alternatives for the "independent" high frequency motion would be Rayleigh damping, Figure 5.2C, or a combination of Rayleigh with quadratic damping, Figure 5.2D.

Using this expanded IF idea with an IPM based drag force dissection, we found some of the SSPA data approximated these more exotic plots. Figure 5.4 presents such a pattern for data from a high frequency SSPA Run. Good arguments can be presented for this force pattern, and it fits the observed force data. However, this intriguing option was not pursued further in this study; as, it can not be represented by a Morison form and we have focused on Morison based approximations in presenting data.

Returning to the RV and IF patterns of Figure 5.3, an interesting question is: how closely do the observer force patterns fit these Morison idealizations? Using IPM based force dissection, plots of force versus velocity were generated for all SSPA data. Two example plots are shown in Figure 5.5. At the top is Run 443 (low KC-Number primary motion) which fits a RV pattern. The high frequency secondary motion is nearly superimpose on itself and moves along the primary low frequency pattern. At the bottom is Run 439 (high primary motion KC-Number) which shows a complex pattern indicative of two independent effects. The width of the pattern is indicative of the high frequency perturbation being skew to primary motion pattern. Note that the skewness of the secondary pattern appears reduced as the primary velocity is reduced; so at low velocities the pattern approaches a RV form.

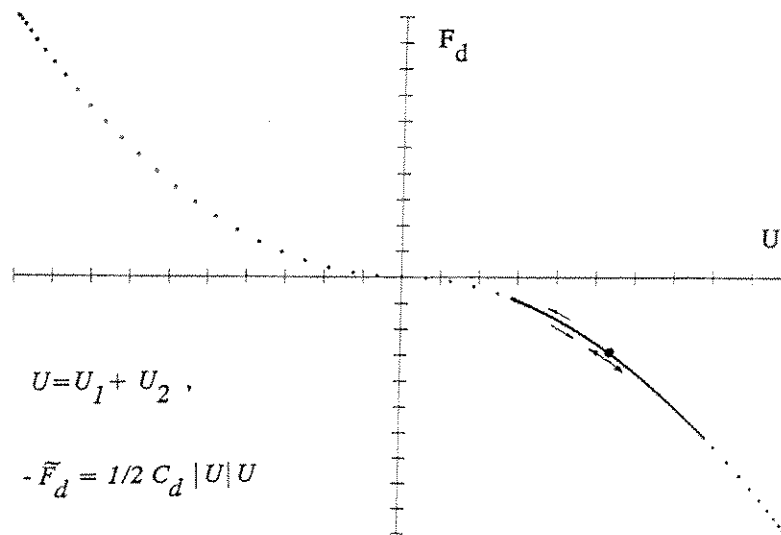


FIGURE 5.3A

RV COMBINED MOTION FORCE AS A FUNCTION OF CYLINDER VELOCITY

Representation for the Morison Relative Velocity (RV) approximation. The high frequency secondary motion, U_2 , (solid curve segment) is shown superimposed on the primary motion, U_1 , (dotted curve).

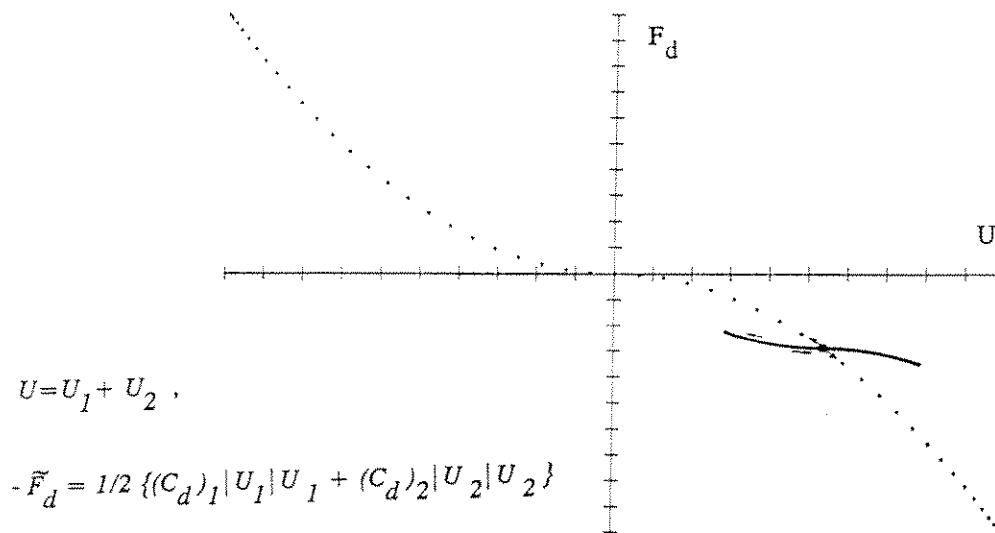


FIGURE 5.3B

IF COMBINED MOTION FORCE AS A FUNCTION OF CYLINDER VELOCITY

Representation for the Morison Independent Flow Fields (IF) approximation. The high frequency secondary motion, U_2 , (solid curve segment) is shown superimposed on the primary motion, U_1 , (dotted curve).

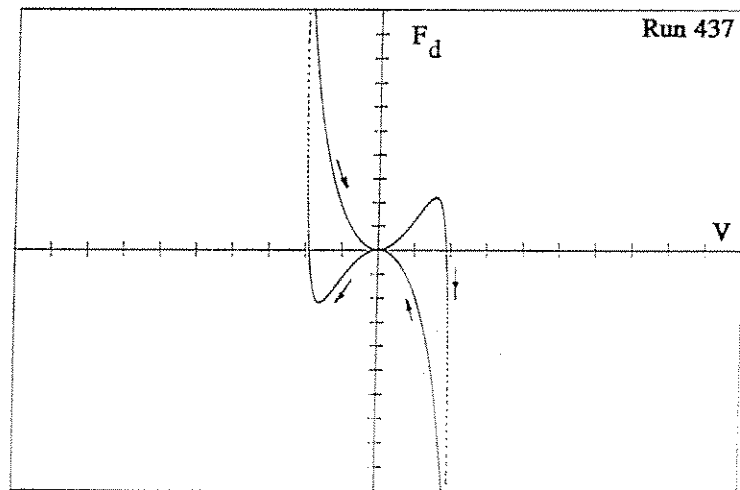


FIGURE 5.4

OBSERVER DAMPING FORCE PATTERN

The above variation of the high frequency component of force with the high frequency component of velocity was obtained from IPM force dissection. The pattern results in negative damping in the initial part of each half cycle.

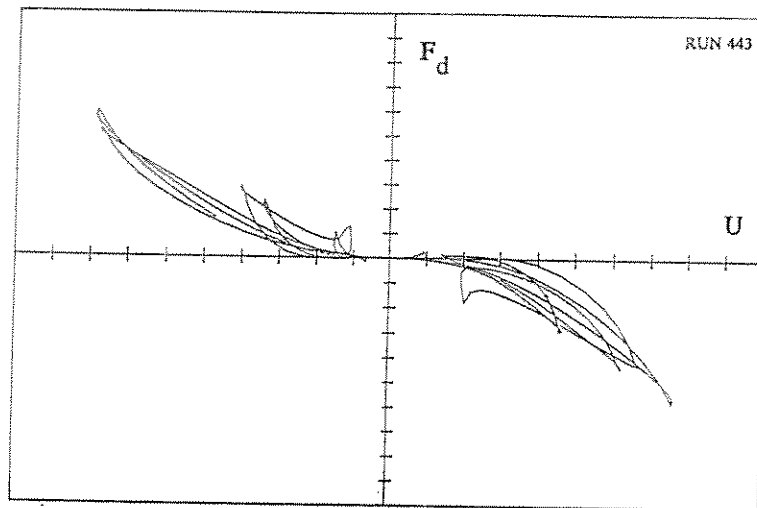


FIGURE 5.5A

REALIZATION OF THE RV APPROXIMATION

Total drag force vs combined motion velocity for low KC-Number Run 443. The plot show a good relative velocity pattern with the high frequency segments falling along the same curve.

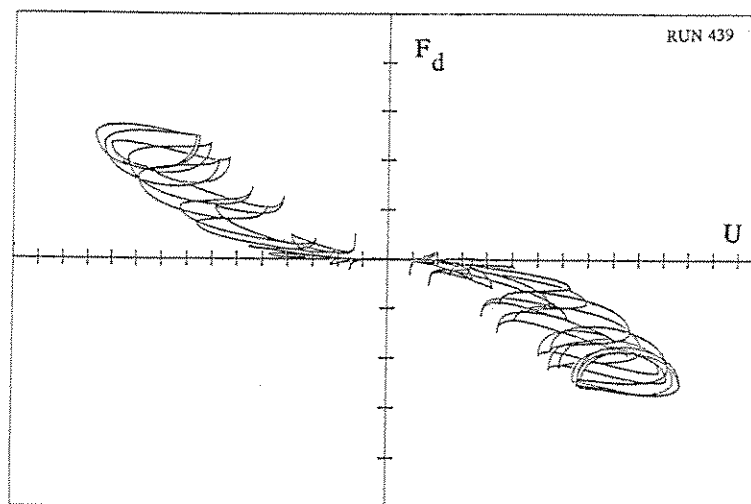


FIGURE 5.5B

REALIZATION OF THE IF APPROXIMATION

Total drag force vs combined motion velocity for high KC-Number Run 439. The plot show a independent flow fields pattern with the high frequency segments transverse to the average curve for the pattern.

Although we have not attempted to make an exhaustive survey of the literature for RV vs IF criteria, none was found which adequately covers the SSPA data. However, with the IPM based dissected force patterns we can clearly discern those Runs best suited to the RV or the IF approximation.

Force dissection is the process of combining instantaneous IPM coefficients with the square of the velocity to yield an IPM based drag force time series. When this is plotted against the combined motion velocity we have the useful patterns of Figure 5.5. Plots such as these are straight forward; however, it would be more meaningful if the origin of the differences in the dissected force pattern were understood. Clearly the two determinants of the pattern are the IPM coefficient and the velocity. So to pursue a more general view of the RV vs IF question let us examine the IPM coefficient.

IPM COEFFICIENT PATTERN

It is our view that the IPM coefficient pattern not only provides a means of understanding the relationship between the different high frequency Runs but also of relating them to the high current Runs that represented a problem in the previous Chapter.

The overview of the IPM coefficient time series pattern for the high frequency SSPA data is similar to those depicted in Figure 5.6 and is characterized by a low frequency variation of the coefficient with a high frequency perturbation superimposed. A more informative view is achieved by focusing on several cycles of the high frequency pattern occurring at maximum values of the low frequency velocity. The similarity of this coefficient pattern to that of the high current Runs is seen in Figure 5.7. In the lower plot is a focused view several cycles of the high frequency pattern of Run 439; at the top is the single cycle pattern for the high current Run 380. Although their time and amplitude scales may differ, the character of the two patterns is similar, and they each have similar relationships to their velocities.

In Figure 5.7 for Run 439, the amplitude of the low frequency motion has produced a "current" equal to that of Run 380. The perturbations on this "current" are for A_x/D motions of 0.1 (KC-Number 0.63) for Run 438 and of 1.0 (KC-Number 6.3) for Run 380.

Note that the velocity and coefficient perturbations are in phase, and the primary (mean) values are of opposite sign, i.e. out of phase. Also in the interval depicted neither the velocity or coefficient undergoes a reversal of sign. Thus for this interval of observation both U^2 and $|U|U$ would have an identical functional form.

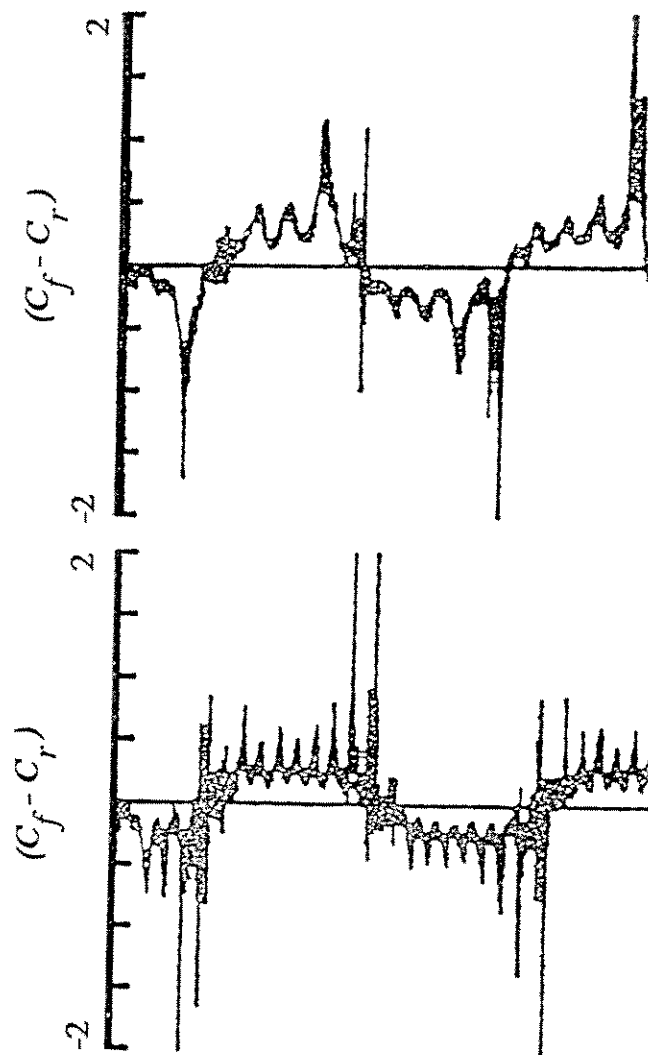
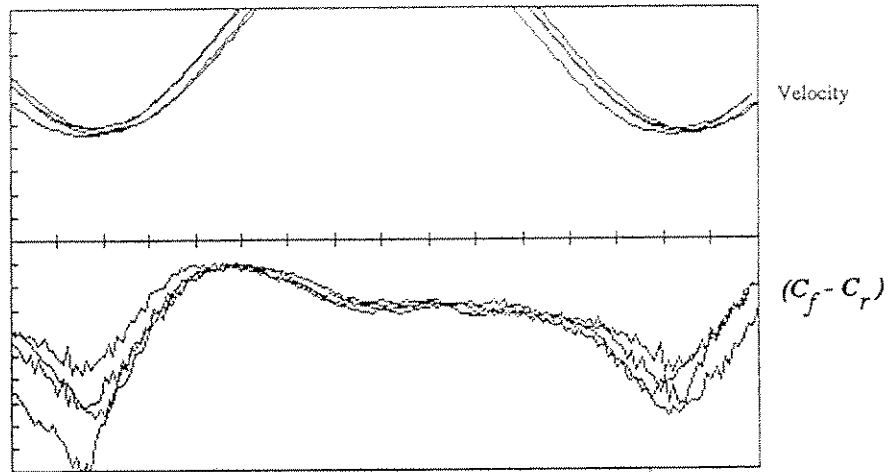


FIGURE 5.6

HIGH FREQUENCY IPM COEFFICIENTS

Comparison of IPM coefficient time series of two high KC-Number Runs 438 (top) and 439. Note the high frequency perturbations of the coefficient. The time scale have been adjusted so the low frequency periods look similar. The data used to generate these plots was neither filtered or smoothed. The extreme spikes in the plots are due to single data points and may be neglected.

Run 380 IPM Coefficient and Velocity Time Series



Run 439 IPM Coefficient and Velocity Time Series

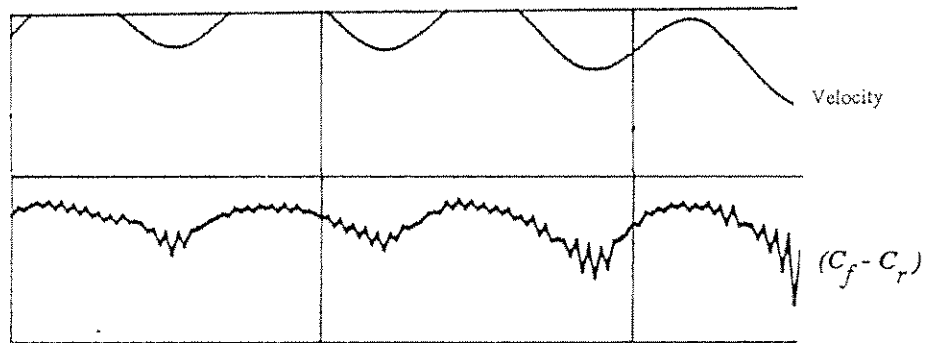


FIGURE 5.7

COMPARISON OF IPM COEFFICIENT TIME SERIES

Each plot shows the relationship between variations in the velocity and the IPM coefficient. Note the similarity of the patterns of the two Runs. The mean velocity for the two is approximately 1 m/s. For the high-frequency Run 438 the period is 3.3 sec and $A_x/D=0.1$. For the low frequency Run 380 the period is 12.5 sec and $A_x/D=1$

ANALYTICAL APPROXIMATION OF PATTERN

It is useful to envision these patterns as a primary value (taken to be a mean value) and a perturbation value so that:

$$U = U_o + V \text{ with } V = U' \sin \omega t \quad \text{and} \quad (C_f - C_r) = -C_o + C' \sin \omega t$$

These expressions represent first approximations to the patterns in Figure 5.7; as, clearly, higher harmonics and phase relations were neglected.

Taking the square of this velocity multiplied by the coefficient approximation we achieve an analytical expression:

$$\begin{aligned} \tilde{F}_d &= 4/3 (C_f - C_r) U^2 \\ &= -4/3 \{ C_o (U_o)^2 + [2 C_o U_o U' - C' (U_o)^2] \sin \omega t + \\ &\quad [C_o (U')^2 - 2 C' U' U_o] (\sin \omega t)^2 - C' (U')^2 (\sin \omega t)^3 \} \end{aligned} \quad (12a)$$

which represents the salient features of the IPM force dissection and thus the key to the RV and IF patterns. A clear expression of the functional form and parametric dependence is achieved by factoring out the mean value term $C_o U_o^2$ and by using the dimensionless perturbation velocity:

$$\tilde{V} = (U'/U_o) \sin \omega t$$

So the above expression for the drag force becomes:

$$\tilde{F}_d = -4/3 C_o U_o^2 [1 + 2a\tilde{V} + b\tilde{V}^2 - c\tilde{V}^3] \quad (12b)$$

with coefficients determined by the ratio of the IPM coefficient and the velocity perturbation ratios $c = (C'/C_o)/(U'/U_o)$ so that $a = (1 - c/2)$ and $b = (1 - 2c)$.

The above expression indicates the dominance of the "mean value term". This term scales as the square of the velocity and fits the dotted primary value curve of Figure 5.3. However, for this analysis the term is a stationary value and corresponds to the dot on these Figures about which the secondary perturbations oscillate.

THE PERTURBATION PATTERN

To understand the behavior of Equation (12b), in so far as it relates to the RV vs IF behavior, we need to focus only on the square bracketed expression. Its governing parameters are the perturbation ratios; the IPM coefficient ratio (C'/C_0) and the perturbation to mean velocity ratio (U'/U_0) . The significance of each term in the polynomial is determined by the value of its coefficient and the perturbation velocity ratio. For this study the maximum value of these ratios is 1. So for the small values expected in damping motion the terms involving squares and cubes will be of reduced significance. The coefficient of each term is determined by the relative magnitudes of the above mentioned ratios which are considered to be positive. Thus the coefficients a and b can be positive, negative, or zero.

A detailed study of the above expression could be very informative. Such was not warranted at this point; however, we should note three observations:

- (1) For zero amplitude of the coefficient perturbation, i. e. $C' = 0$, the value $c = 0$ so that $a = b = 1$. For this condition our bracketed expression takes on the classic RV Morison form;

$$[1 + 2\tilde{V} + \tilde{V}^2] = (1 + \tilde{V})^2 \quad (13)$$

but with an IPM coefficient basis.

- (2) A careful examination of Equation (12b) fails to yield the classic Morison IF form.

- (3) For small velocity perturbations, the terms involving its square and cube may be neglected leading to the linear expression:

$$[1 + 2a\tilde{V}] \quad (14)$$

Now consider two cases for this expression. First, note that for small values of c the value of a approaches 1 which corresponds to the linearization of the RV form. The perturbations occur along a line tangent to the curve segment of Figure 5.3A. As the second case consider a significant IPM coefficient perturbation so that the coefficient perturbation ratio increases relative to the velocity ratio. For this condition c increases from the small values of the previous case. This results in a decrease in a which determines the slope of the perturbation line. Thus the linear pattern is no longer tangent to the quadratic curve. The pattern is skew to the dotted curve as in Figure 5.3B, but the curve segment is linear.

APPLICABILITY PLOT

To express these observations in a way suitable to guide the choice of an approximation for damping forces is our objective. The suitable guide is the "map" shown in Figure 5.8 . The mapped space is defined by the now familiar velocity and IPM coefficient ratios.

In the area labeled IF, an independent flow field approximation with the skewed high frequency pattern applies. For the area RV, the conventional relative velocity form applies. In MOD-RV a modified relative velocity form (linear) of the Morison equation is accurate. RV' defines a problem area in which a more comprehensive RV form is required, usually involving careful consideration of the variation of the force coefficients over the cycle.

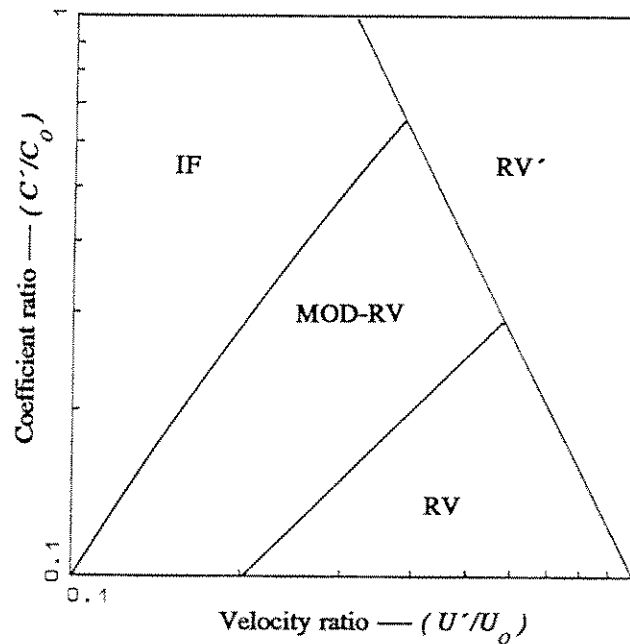


FIGURE 5.8

APPLICABILITY MAP

The region RV' requires a comprehensive RV form, the region RV neglects the cubic term and uses the classic RV form, the region MOD-RV uses the linear form with an independent coefficient, the region IF has very skewed patterns. The defining parameters are the ratios of the perturbation amplitudes of the velocity U' and the IPM coefficient C' to their respective mean values U_o & C_o .

The delineation of these regions of applicability on this plot are achieved by the application of three criteria.

Criterion I: $c\tilde{V}^3 = 0.1$ To determine where the full polynomial is required for an accurate description we have chosen the condition where the highest order term (the cubic) is just 10 % of the primary term. This criteria is expressed as the line which runs down and to the right with -2 slope. The line divides the plot into two regions. In the region labeled RV the cubic term contributes more than 10 % and so in this region a comprehensive view of coefficient variation is required with the RV form to achieve good accuracy. In the balance of the mapped space (sub-RV) are the regions of the linear and square terms.

Criterion II: $b = 0$ Determines the boundary of the RV approximation. It is the condition where the square term changes sign. On this boundary the linear approximation is exact. This condition is met on the line of unit slope which separates the RV and Mod-RV regions.

Criterion III: $2a\tilde{V} = 0.1$ This expresses the conditions for which the linear term becomes small (10 % contribution) and provides the IF to MOD-RV boundary. One should note that the reference to IF is not to the Morison IF form but to the linear IF form in which the linear perturbation force pattern is significantly skewed to the mean quadratic pattern.

In reviewing the criteria and the plot one should realize that the criteria are arbitrary and can be argued over if one is so disposed. In their defense we would argue that they capture the observed features of the Equations (12) and are adequate to the first order features this expression was intended to represent. Clearly a more comprehensive study extending these ideas would be useful.

Because of their arbitrariness, the boundaries on the map should be viewed as fuzzy and should be used only in a qualitative way. As a case in point consider the MOD-RV region. In this region the linear form is dominant and there is a gradation from a quadratic tangent pattern of the RV to the distinctly skew pattern of the IF. Clearly with such a gradation it is difficult to draw boundaries.

PERSPECTIVE

On the subject of the "applicability plot or map" it is easy to slip into an interminable discussion of its features and their extensions; however, the important question at this point is : How is such a plot useful?

Recall that we have on the basis of F_d vs U plots (Figure 5.5) been able to determine whether the RV or IF approximation is best for each of the high frequency Runs. The above map incorporates the observed behavior of the F_d vs U plot as influenced by the velocity (U'/U_o) and IPM coefficient (C'/C_o) perturbation ratios. The map alleviates the plotting and interpretation of F_d vs U plots.

The map is intended as a guide to the best approximation for representing the drag and /or damping force prediction. Thus for a high frequency or high current Run, one determines its perturbation ratios and then locates the point on the map associated with these values. The labeled area enclosing the point specifies the best approximation. In this study the map will be used as such a guide; however, the intent will be somewhat reversed as we demonstrate the validity of this map on the basis of known F_d vs U plots which have been constructed on each Run. In the process of locating the Runs on this map some new insights on the characteristics of these data will be gained. These items will be treated in the sections to follow.

VALID APPROXIMATIONS FOR SSPA DATA

The position of each high frequency Run is shown on Figure 5.9. Also shown are the troublesome high current cases from the low frequency Runs. For the high frequency data the average perturbation amplitude of the velocity and the IPM coefficient were used to compute the ratios with the mean values selected at the peak of the low frequency velocity cycle.

The position of the high current data, Runs 375, 376, 378, and 380 in the RV' region is expected as our experience with them indicated a comprehensive treatment of the coefficient variation was required to achieve good accuracy. You may recall the exception was Run 380 for which the Level I approximation worked well. The position of Run 380 on the RV' boundary confirms its less troublesome RV behavior.

Note that all of the high frequency Runs fall well below the RV' boundary indicating that they can be accurately represented with a less rigorous approximation. Thus despite the similarity of the fluctuating coefficient patterns of the high current Runs and the high frequency Runs, they differ significantly due to the magnitudes of both the velocity and coefficient perturbations.

Recall that Run 443 was presented in Figure 5.5 as a realization of the RV approximation, while Run 439 was presented as the IF illustration. Runs 443 and 440 have similar force vs velocity patterns. And Runs 437, 438, 439, and 441 have similar skewed patterns. From such comparisons we can conclude that the data supports the characterizations of the map.

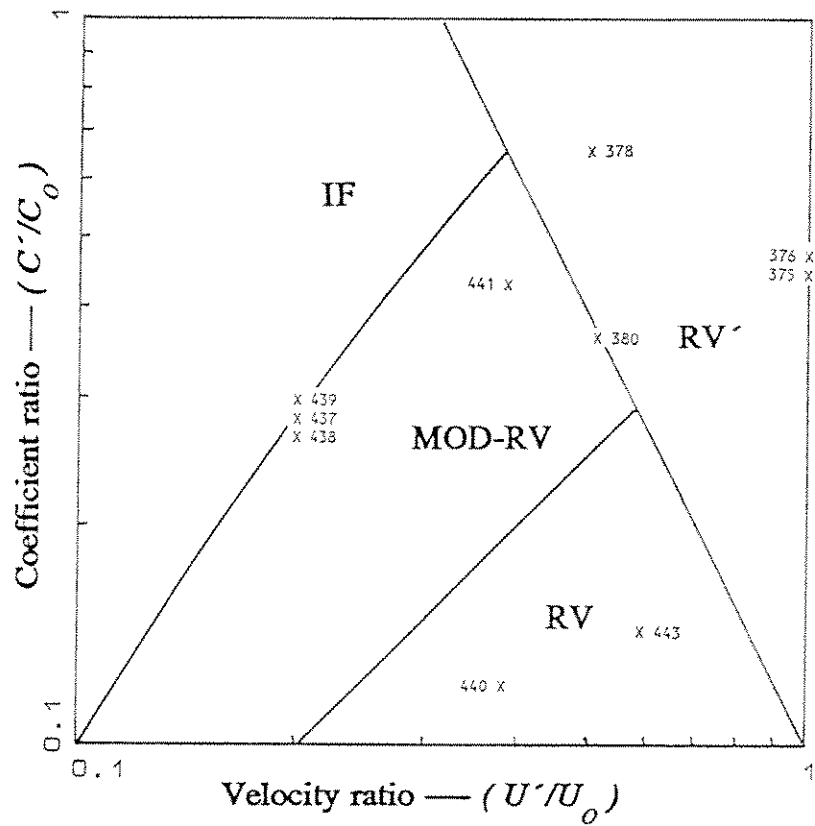


FIGURE 5.9

APPLICABILITY MAP WITH SSPA DATA

Plotted perturbation ratios for the High Frequency Data and the High Current Low Frequency data showing the approximation requirements for each Run.

For the sub-RV region, if one envisions a series of parallel lines running diagonally at 45° upward and to the right, one would see the coefficient pattern (constant " a " lines of Equation (12b) & (14)). Each line would represent a value for the coefficient with the largest at the lower right. Thus the coefficients of Runs 440 and 443 are expected to be similar and larger than the values of Runs 437, 438, 439, and 441. The proximity of these four Runs to the same constant " a " line and to the IF to MOD-RV boundary (0.1 linear term) indicates similar small coefficients with a valid linear approximation. Although Runs 440 and 443 fall in the RV region, their proximity to the boundary where the quadratic term is zero, prompts one to consider a linear representation for them also. Examination of each of the Runs indicates the linear approximation is good.

One can achieve a feeling for the variation of the damping coefficient over a low frequency cycle by realizing that the points portrayed on this plot are instantaneous values and the mean values of the coefficient and velocity vary. The plotted point for a Run will shift to the right as the low frequency velocity goes through its cycle. This indicates that the damping tends toward a RV form in the low velocity parts of the cycle whereas its IF behavior occurs at the extrema of the velocity. This pattern is evident in the time series data. Thus the damping coefficient varies over the low frequency cycle, and negative or small damping occurs at the velocity extrema.

As a final item with this map, consider the problem of very high frequency noise that plagues many experiments such as the SSPA tests. The question is: are we justified in filtering out and thus ignoring sizable signals characterized by a small velocity amplitude at very high frequency? Considering the map one can surmise that such points would be off the plot to the left. Thus in the independent region. So we would be justified in considering their contribution to be independent of the lower frequency data and in deleting the signal. Even with this justification due consideration must be give to possible physical coupling and to signal processing considerations.

HIGH FREQUENCY DATA

Many of these Runs have been used earlier in this chapter as illustrations. The Run numbers and parameters of the high frequency test conditions treated in this study are given in Table 5.1 .

The dominance of the high frequency acceleration is clearly seen in the last column of this table.

These conditions supply a comprehensive test of the ideas presented thus far and provide an insight into a significant in-line transverse (I-T) coupling phenomena which may influence damping.

TABLE 5.1
SUMMARY OF TEST CONDITIONS FOR HIGH FREQUENCY DATA

Low frequency motion						High frequency motion					
Run No.	f_o	A_o	U_o	Re-No.	KC-No.	f'	A'	U'	KC-No.	U'/U_o	\dot{U}'/\dot{U}_o
	(Hz)	(meters)	(m/s)			(Hz)	(meters)	(m/s)			
437	0.0796	2	1	0.88×10^6	12.5	0.3	0.1	0.2	0.63	0.2	0.76
438	0.032	5	1	0.88×10^6	31	0.3	0.1	0.2	0.63	0.2	1.9
439	0.016	10	1	0.88×10^6	61	0.3	0.1	0.2	0.63	0.2	3.8
440	0.0796	1	0.5	0.44×10^6	6.2	0.3	0.1	0.2	0.63	0.4	1.5
441	0.016	5	0.5	0.44×10^6	31	0.3	0.1	0.2	0.63	0.4	7.6
443	0.0796	1	0.5	0.44×10^6	6.2	0.3	0.15	0.3	0.94	0.6	2.3

The tests cover a range of low frequency motion KC-Numbers at two values of the Reynolds Number. With the exception of Run 443 the high frequency (damping) motions are identical (0.3 Hz and $A_x/D = 0.1$). The constraint on the values of Re-Number provided an interesting contrast of low and high frequencies over a range of KC-Numbers.

To illustrate this point consider the 6.2 KC-Number Runs 440 and 443 with the mid range 12.5 Run 437. For these KC-Numbers, the transverse force frequency is well known to be twice the primary frequency. Thus transverse forces at 1/2 the high frequency are expected with their I-T effects at or near the high frequency of 0.3 Hz. This would indicate not only interaction between the low and high frequency phenomena but and overlap of their spectral features. By contrast, for the higher KC-Number Runs 441, 438, and 439, the low and high frequencies are widely separated so dissection of the low and high frequency spectral features is simple.

The spectral features of both kinematics and forces were carefully studied with a variable interval FFT program. In all Runs the high and low frequency features could be dissected with confidence. The mid range conditions of Run 437 presented the greatest challenge due to the complexity and proximity of the two sets of spectral features. In general the low frequency features of the D-Force spectra were a 1'st harmonic (the low frequency primary motion) and a 3'rd harmonic. The 3'rd was a good approximation of 20% of the 1'st. The 1'st harmonic amplitudes were 50 to 70 Newtons for the low Re-Number Runs and 300 to 450 Newtons for the high Re-Number Runs.

The high frequency features of the D-Force data consisted of a line at 0.3 Hz with amplitude in the range of 20 to 40 Newtons and an equivalent amplitude line on either side at an interval of twice the low frequency. These two "side band" lines * provide the beat envelope for the damping force and thus represent the time variation of the damping during the low frequency cycle. With the constant coefficient constraint this feature could not be treated; so a time average of the high frequency force over the low frequency cycle was used. There is evidence that the damping becomes negative during a portion of the low frequency cycle for some of the Runs.

A very high frequency noise feature of approximately 20 Newtons above 4 Hz was a problem for all the Runs.

DAMPING FORCE ALGORITHM

The outstanding question now is: how do we compute the drag and/or damping force?

For the force determination we could use the perturbation values (U'/U_o) and (C'/C_o) with Equation (12). This would provide both the equation and the coefficients. Because only a first order approximation was used to represent the perturbation coefficient contribution, this might limit its accuracy. This option will not be used at this point. However we shall use the functional form suggested by Equation (12), and determine its constant (average) coefficients independent of the IPM, as a best fit to the observed data.

Thus the damping force expression suggested for the high frequency Runs of this study is:

$$(\tilde{F}_d)' = \tilde{F}_d - (\tilde{F}_d)'_o = -1/2 [2 C_d' U_o U'] \quad (15)$$

*NOTE: The spectral features of the RV form of the Morison drag term were examined by Dello Stritto and Horton³. Such side band lines were found in that study, but the amplitudes were much smaller than those found in these data.

where the $()_o$ referrers to the low frequency contribution and $()'$ referrers to the high frequency contribution. The expression states that the damping force is the difference between the observed force and the low frequency force. Where the low frequency contribution:

$$(\tilde{F}_d)_o = F_d / \rho DL = - 1/2 C_d |U_o| U_o \quad (16)$$

is the conventional Morison expression involving only the low frequency motion. In Equation (16) the symbol U_o represents the instantaneous low frequency velocity. In Equation (15) this symbol is a constant, the velocity amplitude.*

The linear dependance of Equation (15) on the high frequency velocity is clearly an advantage in design and analysis applications.

Moreover, this is a rational expression following from Equation (12). Due consideration was given to the cubic and quadratic terms; however, for the high frequency data of this study their inclusion was not justified considering: (1) the small contribution of these term for these data and (2) the errors imposed by the constant coefficient constraint.

An advantage of the above expression is that the transition from IF to RV forms is achieved through the coefficient C_d' . As it tends toward the low frequency C_d , the RV form becomes increasingly appropriate. The increasing "skewness" referred to as a characteristic of the IF form, occurs with small values of C_d' .

As a final note concerning the form of the damping force expression, we have found noting to support the "classic" IF form $|U'| U'$.

*NOTE: The dependance of this term on the low frequency motion is an important issue. There are two aspects (1) the variation of low frequency velocity U_o and (2) the variation of the coefficient C_d' . We have constrained this effort to constant coefficients. There is evidence of significant variation of the coefficient over the low frequency cycle, and consideration of the velocity variation only would be misleading. At this point the use of the constant term is the consistent option. If a low frequency time dependance is required, a first approximation would use the square of the normalized low frequency velocity; however, this approximation has a problem in that it yields zero damping at zeros in the low frequency velocity.

COEFFICIENTS FOR HIGH FREQUENCY RUNS

For the drag force forms of Equations (15) and (16), the drag coefficient data are presented in Table 5.2 for both the low frequency motion term and the high frequency motion term. The values applicable to the low frequency Morison term are labeled "TM analysis" and were obtained by the methods used in Chapters 3 and 4. The values for C_d' are listed under the header "Eq. (15)". They were obtained from this Equation using average values of the dissected D-Force which were phase aligned with the high frequency velocity.

The data under headers "TM analysis" and "Eq.(15)" are consistent with the Morison equation in its expanded form, Equation (15).

TABLE 5.2
DRAG COEFFICIENTS FOR HIGH FREQUENCY DATA

Run Number	C_d (Low frequency)			C_d' (High frequency)		
	Spectral analysis		TM analysis	Spectral analysis		Eq. (15)
	Shell	HYDAMP		Shell	HYDAMP	
437	0.86	0.96	0.93	0.12	0.10	0.07
438	0.75	0.81	0.84	0.07	0.11	0.09
439	0.66	0.76	0.75	0.03	0.03	0.02
440	0.38	0.45	0.40	0.26	0.26	0.16
441	0.44	0.58	0.66	0.10	0.11	0.07
443	0.32	0.39	0.40	0.28	0.28	0.18

These data should be contrasted with two other sets presented under the header "Spectral analysis". The values labeled "Shell" were taken from the Shell SSPA Report and represent their spectral method. We have also used a spectral procedure to achieve the set labeled "HYDAMP". The similarity of the spectral data sets indicates that our procedure and Shell's method were similar. Our spectral procedure used the 0.3 Hz spectral components of the D-Force and of the RV form of the Morison drag term. Equating these components, with due consideration for phase relationships, yields a corrective coefficient.

There are several critical comments that can be made on this spectral procedure. First the procedure presumes the RV form to apply and uses its spectral features as its basis. The procedure then corrects the spectral features with coefficients as if they were "independent terms". This procedure, while seeming to be empirically advantageous, is not rational. The only logical way to arrive at a similar procedure is with the variable coefficient arguments used to develop Equation (12). If the above spectral procedure were applied to a simple periodic motion, it would yield separate corrective coefficients for the 1'st, 3'rd, 5'th,... harmonics terms of the Morison equation. A second and more crucial criticism is that the procedure supplies no information on the scaling of the component with either low or high frequency velocity. Without such scaling it is not possible to achieve predictions at adjacent conditions and the data is restricted to the point observed.

Despite the significant difference between the spectral and Eq. (15) values for the high frequency coefficients, the two sets seem to have a common ordering. Also the ordering of the coefficients follows that presented earlier in the discussion of Figure 5.9 . The contrast between the high and low frequency coefficients for a Run indicates the tendency toward independent behavior for these motions.

There are several sources of uncertainty in the high frequency data. The primary being the variation of the damping over the low frequency cycle. In some cases this leads to negative damping. The sizable noise problem has been mentioned earlier. Considering the phase resolution, we have assessed a 40% uncertainty to these high frequency coefficients.

OTHER OBSERVATIONS -- AN I-T EFFECT

The Shell Report notes a reduction in both the in-line and the transverse forces when the high frequency motion is present. It states: "...the high frequency oscillation are disturbing the formation of vortices....the reduction in the transverse lift forces...". In their work the reduction in the transverse force for Run 441 was shown as an illustration.

In our study, using the results of force dissection, an extensive comparison of Theta-min Correlation Plots was undertaken and reported on in a early HYDAMP participants meeting (May 11, 1990). The results presented at that time were in the form of superimposed transparencies of Theta-min Correlation Plots (IPM Coefficient vs Theta-min). Note was made of the similarity of the low frequency character of comparable high frequency and simple periodic Runs. The noted exception was Run 441; however, the differences were in the "wings" and would primarily affect the low frequency inertial coefficient and not the drag coefficient. Our conclusion was that the modifications of the low frequency in-line forces and coefficients for the high frequency Runs were not as significant as those observed in low frequency Runs with current.

By contrast we have observed that the transverse force patterns are significantly modified by the high frequency motion. A study of the transverse forces was not part of the original proposed study; so the items presented below are qualitative and tentative.

We have observed both increases and decreases in the transverse force. These changes were dramatic, generally by greater than a factor of 2.

The transverse force frequency for all the high frequency Runs peaked at or very near 0.15 Hz (half the high frequency of 0.3 Hz). For low and mid KC-Number Runs 440, 443, and 437 this was expected with their low frequency motion. Using the usual Strouhal Number arguments, the transverse force frequencies for Run 441 should have been less than 0.1 Hz and for Runs 438 and 439 approximately 0.2 Hz.

The transverse amplitudes of the low Re-Number Runs 440, 441, and 443 were reduced by more than a factor of 2 while the high Re-Number Runs 439 and 438 were increased by more than a factor of 2 and Run 437 was not changed significantly.

Changes in the in-line force were not as large as these cited for the transverse force.

For the high Re-Number Runs the transverse force is of the order of hundreds of Newtons; so it is plausible to ask if the I-T effect could influence damping. The I-T effect would yield a 0.3 Hz in-line force and amplitudes of 30 to 60 Newtons could be expected based upon a 10 to 20 % transfer from transverse to in-line.

The influence of the in-line high frequency motion on the transverse force is irrefutable from these data, although we have not done a comprehensive quantitative study as yet. The evidence for the reverse influence, the transverse on the damping, is more difficult to see; however the evidence is in the variation of the high frequency force over the low frequency cycle.

Using the I-T evidence presented in earlier Chapters and guided by a IPM based rational, one explanation for the transverse force behavior is that physically the high frequency fluctuations of the Theta-min position on the cylinder surface facilitate vortex formation and shedding. During half of a high frequency cycle the vortex is formed and then released during the second half. Evidence of this was presented in an earlier Chapter where Run 368 was cited as an illustration. Thus we have the half cycle relationship between the high frequency motion and the transverse force frequency. Applying the idea of the IPM based correlation KC-Number, page 22, we find an expression for the high frequency Run KC-Numbers which depends upon the dominant low frequency velocity and the dominant high frequency acceleration. The value of this IPM based KC-Number

can be obtained by dividing the low frequency KC-Number of Table 5.1 by the acceleration ratio, the last column. The resulting value and its relationship to the transverse force is shown below.

Run 440: low frequency KC-number 6.2, IPM base KC-Number 4, transverse force reduction.

Run 441: low frequency KC-number 31, IPM base KC-Number 4, transverse force reduction.

Run 443: low frequency KC-number 6.2, IPM base KC-Number 3, transverse force reduction.

Run 437: low frequency KC-number 12.5, IPM base KC-Number 16, transverse force unchanged.

Run 438: low frequency KC-number 31, IPM base KC-Number 16, transverse force increased.

Run 439: low frequency KC-number 61, IPM base KC-Number 16, transverse force increased.

Clearly, Runs experiencing reductions in KC-Number to 3 or 4 should experience significant vortex reductions. While Runs 438 and 439 have experienced reductions in KC-Number to 16 which is known to be an enhanced vortex shedding condition. For Run 437, the mid range KC-Number shift from 12.5 to 16 is insufficient to change the transverse force pattern significantly.

The above phenomena are very evident. Our explanation for them, although conjectural and tentative at this point, illustrates the utility of the IPM.

The problem is significant and deserves further quantitative study. If the transverse force through the I-T effect influences the high frequency in-line force, then we can achieve an explanation for the increasing independent behavior of some of the Run, the variation of damping over the low frequency cycle, and the negative damping.

CHAPTER 6

FINAL OBSERVATIONS AND COMMENTS

The objectives of HYDAMP were to address the Combined Motion Problem by:

1. Demonstrating the utility of the IPM in the combined motion environment,
2. Providing an understanding of the Problem, and
3. Providing Morison based data.

In the course of this investigation several HYDAMP meetings have been held to familiarize participants with the work and to provide feedback to the investigation. These meetings tended to supply background and as a result focused on items 1 and 2 with concerns such as: Can the IPM do the job? What is the character of the information that the IPM provides? What generalizations can we draw from the IPM? The heavy emphasis on the IPM was to provide an understanding of the method and what it reveals about the current problem.

In contrast to the meetings this Report has focused on the Morison data derived from the IPM and observations on that effort. This Report has not attempted to reproduce the qualitative material of the meeting presentations. Implicitly it has relied on them for background, but this Report has concentrated on item 3 and quantitative results. With the exception of the initial Chapters, the IPM has played an important but supporting role to that objective. The approach we hope has created a more focused and less confusing document by reducing the mixing of methodologies.

THE IPM DILEMMA

The procedure of Chapter 3 for determining Morison coefficients from the IPM is a excellent illustration of how the IPM was intended to be used in this study. One can see the logic of the hierarchy of representations based on the IPM pattern of coefficient variation. Moreover, this procedure can be translated into a technique which can be used without a knowledge of the IPM.

The simple description of the technique would prescribe selection of drag coefficients at the velocity extrema to yield the observed force. Then by adjusting the inertial coefficient one "rotates" the Morison prediction about the fixed maximum velocity point to achieve the best alignment of the Morison prediction curve with the observed force. Clearly one can in this manner adjust the curves on either side of the fixed point independently and thus achieve the Level III approximation. This is a simple concise description easy to understand and simple to use.

However, if one used this procedure one is not likely to achieve the accuracy of Chapter 3 because of inaccuracies in locating the maximum velocity and unfamiliarity with the variation of the coefficient at that point. This illustrates how IPM findings can be translated into a quite conventional tool. It also illustrates that the tool that results from the translation is not as sharp as the original.

In a sense this is a theme of this Report, to take a sharp tool and transform it into something not so sharp but thought to be better understood.

DATA REDUCTION PROCEDURES

Several final comments are appropriate on the techniques used in the data reduction. The technique used with the low frequency data could also be used with the high frequency data. In that application it is very effective in finding the perturbations in the coefficient and in quantifying their variation over the low frequency cycle. Also the technique of describing coefficient perturbations used with the high frequency data in Chapter 5 is applicable to a portion of the low frequency data (high current). It could have been extended to apply to all the low frequency data. Finally, for the high current data, the region RV' of Figure 5.8 could have been explored and divided as with the sub- RV' region.

LOW FREQUENCY DATA

A unique accomplishment with the low frequency data was quantifying both the uncertainty in the coefficients as well as the error in prediction resulting from their use. One of the advantages of the low frequency technique is that it can be used to study cycle to cycle variation so deterministic relations to other phenomena could be explored. It can also be used as a coefficient generator for statistical analyses of uncertainties. We feel that if constant coefficient data is to be used, then this technique yields the most reliable values.

Force Predictions:

The author's view is that there is an undeniable variation of the force coefficients over the flow cycle and thus to achieve desired predictions variable coefficients are required. Despite this view the author was surprised and pleased at the accuracy of the predictions achieved with our hierarchy of "constant" Morison coefficients.

My variable coefficient view is supported by two observations from the current data set:

The first is that problems such as the bump and coefficient compatibility obviate the need for a variable coefficient to eliminate these "local" problems. This becomes obvious as one works with the Morison equation trying to fit the predictions in these local intervals.

The second is that when we use an approximation such as Level III, we are then dealing with variable coefficients both philosophically and practically. From the practical standpoint, with Level III, we would have to supply a computer with more information than with the IPM prediction scheme discussed in connection with Figure 1.2 . Clearly Level III is of limited practical interest.

The usual practice, which corresponds to the data set generated in Shell's SSPA study, is to use an approximation which we shall term Level I'. Level I' is comprised of only our Level II high velocity coefficients. There is a set of coefficients for each Run. The question is whether Level I' is worth the effort as compared to Level I. Most of its predictions are comparable to Level I. The simplicity of using the same coefficients for all computations overrides the marginal gain in accuracy.

I feel a Level I approximation fits the level of accuracy inherent in the Morison equation.

Predictions with Level II are superior but are still limited by the bump and low KC-Number problems. Low KC-Number problems not only arise from low periodic flow KC-Numbers but also in the low velocity fraction of a combined motion flow cycle where the correlation KC-Number is small. For these conditions small force amplitudes are expected, and these forces can easily be dominated by the I-T force. Clearly before a correlation of Level II coefficient data is achieved the I-T effect must be understood and quantified.

Coefficient Correlation:

The viability of Level II will depend on the resolutions of: (1) Quantifying the I-T effect and (2) Correlation of the coefficient data. The first is a major impediment to the second.

Clearly by "correlation" we are referring to a more comprehensive representation of the coefficient data than the conventional plots supplied in Chapter 3 . We feel a comprehensive correlation will use the IPM based KC-Number presented in Figure 3.1. We have resisted using this correlation except in explaining the transverse force behavior in the high frequency data sat. For those data the correlation fits the evidence in a remarkable fashion.

Correlations of IPM Coefficient patterns have been presented in several HYDAMP meetings. We have shown how the Theta-min correlation patterns vary systematically with KC-Number and Velocity ratio by using the IPM based correlation (upper line on Figure 3.1). An illustration of this is Figure 1.3 where, as in our meetings, our proof follows from the superposition of two or more plots. Clearly the mechanics of such comparisons are suited to meeting presentations but are not as effectively handled in text presentations. The data shown in such correlation presentations is largely that of the dominant high velocity part of the flow cycle.

Our contention is that if such correlations can be demonstrated using the IPM coefficient pattern then the Morison coefficients should follow the same correlation given the relationship between them.

We have not attempted such a comprehensive correlation of the Level II data for two reasons:

- (1) The high velocity data could have been correlated with the IPM base KC-Number of Figure 3.1, but there could be arguments about its uniqueness.

One aspect of the uniqueness problem arises from the proximity of the IPM and the A_x/D curves in this Figure. The argument would be that if you can correlate with one you can correlate with the other. This seems to be a valid point; however, the rejoinder is that the A_x/D based correlation can not predict the behavior of the high current Runs while our IPM based correlation correctly places these data on a common curve with other data. The matching of the two high current Runs of Figure 1.3 would not have been suggested by the other techniques in Figure 3.1. The IPM based correlation shows that the presence of a large current can shift a small KC-Number motion to a high KC-Number condition.

The second aspect of the uniqueness problem arises from this shift in KC-Number. Although the data, with one exception*, fit the shifted pattern, this would not be a decisive proof. As one can see in Figures 3.3 to 3.6 the values are quite similar so shifting them along a horizontal is prosaic. (This is the basis for our

*NOTE: The exception is Run 368 plotted on Figure 3.4 for $A_x/D = 1$. For this Run the steady motion shifts the KC-Number to 14 in the mid-range. For this condition large transverse forces should be present giving rise to a sizable I-T contribution. This I-T contribution is the source of the large drag coefficients observed in the mid-range in simple periodic flows. In Run 368 one has the opportunity to observe a mid-range KC-Number flow stripped of its I-T force. As discussed on page 25 the transverse and I-T forces appear as a residual contribution in the low velocity part of the cycle.

observation earlier on Level I' vs Level I.) The decisive proof is not with the Morison coefficients; its is with the rich pattern of the IPM coefficients.

(2) The above concerned the high velocity data correlation, but our second and decisive reason concerns the low velocity data. To be meaningful both the low and high velocity coefficients must be correlated, and one would hope they would share the same correlation curve. There is some evidence of this in the data. The low velocity points are shifted to low KC-Numbers and their coefficients should be small. However, among these coefficients we find inordinately large values which are due to the residual I-T force from the high velocity part of the cycle playing a dominant role in the low. Before a correlation of the low velocity data can be achieved the I-T force contribution must be understood.

Uncertainties --- the Bump and the I-T effect:

In our investigation the sources of uncertainties have been carefully tracked. Of these the Morison Bump and the I-T Effect are the only remaining sources which are cause for concern in using the HYDAMP data.

The Bump is a purely Morison artifice. It has been observed even in simple periodic flows at high KC-Numbers, a region where the Morison equation is alleged to provide its best predictions. For a simple periodic environment, the bump occurs at the zero crossing points of the force. Thus for static design analyses it is not a concern. With currents the position of the bump shifts to a region of importance and thus should be a concern particularly in dynamic analyses.

For the I-T effect much has already been said in this Chapter. It is easy to ascribe everything you don't understand to unquantified phenomena. I trust that I am not guilty of that here. In our case, the transverse force pattern and its relationship to a higher frequency contribution to the in-line force has been studied sufficiently to know that this is a very real phenomenon, which has also been observed in other experiments. We know with certainty it is the major source of uncertainty at high KC-Number conditions. In contrast, some Runs, with correlation shifts to lower KC-Numbers, provide clear glimpses of I-T's dominant role in their force patterns. At meetings we have presented clear illustrations of its role in the large drag coefficients associated with simple periodic flows at mid-range KC-Numbers.

We can say with confidence that the I-T effect is the major source of uncertainty in the HYDAMP data and that it can be understood and quantified. With the IPM and SSPA we had the technique and the data to achieve this.

The importance of the I-T effect transcends data reduction for HYDAMP. It is a phenomena that must be understood so that its influence can be intelligently integrated into design procedures. Clearly, currents alter the transverse force pattern for a partial cycle of the flow as the KC-Number shifts, and high frequency motion modifies the transverse force pattern as a result of KC-Number modification. These influences obviously present problems to the designer; however, a more important question is whether they can be converted from problems to advantages.

Summary observations:

1. Our hierarchy of approximations provides the best data sets for constant coefficient Morison equation force predictions.
2. The RV form of the Morison equation should be used with our data sets.
3. The influence of current can be understood as a shift in the KC-Number for both the low and high velocity parts of the flow cycle.

HIGH FREQUENCY DATA

In the original proposed effort for HYDAMP the linear approximation was not to be the "be all and end all" approximation for the high frequency data set. The linear representation was viewed as an approximation at the bottom of a hierarchy. A hierarchy similar to that for the low frequency Runs was envisioned. In fact the preproposal thinking on the high frequency data was the genesis of the hierarchical concept, and as originally conceived it would be based on a series expansion of the IPM coefficient time series (used in Chapter 5 and in our May presentation). From such an analysis one arrives at a rational hierarchy of approximations capable of representing the high frequency data, but they are not constant coefficient Morison compatible.

The flavor and length of Chapter 5 must reflect our struggle with the problem. In the Chapter we have tried to convey the reader from the delineation of the RV vs IF representations to a final rational expression consistent with the constant coefficient Morison constraint. Our Linear Expression, which some would argue is neither RV or IF, is also the only practical Morison compatible expression which represents the observed high frequency data.

Review of analysis:

At this point it is well to briefly recall the essentials of the process described in Chapter 5. It started with the question of whether the RV or the IF form was appropriate to the various Runs of high frequency data. The problem arose from the apparent failure of the existing criteria to indicate which should apply.

Using plots of force vs velocity from IPM force dissection, one could distinguish the two patterns. Figure 5.5 illustrates the distinguishing patterns for such plots. In the RV pattern the high frequency contribution tends to align with the low frequency contribution. For IF behavior the high frequency force contribution tends to be skewed across the low frequency pattern.

By a series expansion of the IPM drag term, in terms of high frequency perturbations of both the IPM coefficient and the velocity, one is able to achieve a useful expression, Equation (12), that is equivalent to the Morison equation for a non flow reversal case. This flow description is a good approximation for a significant portion of the high frequency data as well as the high current low frequency Runs. The expansion contains an expression that is the RV form of the Morison equation; however, the classical Morison IF expression was not found. A less restricted IF form which includes linear behavior is evident.

The findings from the expansion have been portrayed on an Applicability Map, Figure 5.8, and the Map has been validated with available SSPA data. The Map indicates that a Linear Expression, Equation (15), applies to all the high frequency Runs. For these Runs the cubic and quadratic terms in the expansion were observed to be small because of the magnitudes of their velocity and coefficient perturbations.

For this Linear Expression the drag coefficient approaches the low frequency value, and thus the linearized RV form, if the perturbations of the IPM coefficients were very small. Large IPM coefficient perturbations tended to act counter to the velocity perturbations resulting in a reduction in the drag coefficient and thus inducing an IF behavior. The countering of the coefficient and velocity perturbations can produce negative drag coefficients (negative damping). In the high frequency drag coefficient data presented in Chapter 5 one observes Runs which tend to RV behavior while others with much smaller drag coefficients tend to IF behavior.

Further comments on results:

The primary products of the above process were the Linear Expression and the Map. Some further comments associated with these two products are appropriate at this point.

On the expression for the high frequency force: Our linear expression represents a "natural" transition from RV to IF behavior which is an obvious advantage. If one were so disposed to create a classical Morison IF form, it can be achieved by multiplying and dividing Equation (15) by U' . The IF coefficient would then be $2 C_d' U_o / U'$. It should be noted that no 0.9 Hz force component (the 3rd harmonic of 0.3 Hz), indicative of a classical Morison IF behavior, was observed among the spectral features of the high frequency Runs.

On the map: The map can be improved and used in ways other than discrimination between RV and IF behavior. We have used it only on a qualitative level. It demonstrates that the RV or IF characterization depends not only on the velocity perturbation, which most authors have claimed, but also on the coefficient perturbation. It is the coefficient perturbation that leads to the IF behavior. Because the IPM coefficient perturbations lead to IF behavior, this suggests a course for future investigations which would consider IF to be a partial-cycle rather than whole-cycle behavior. There is evidence for this in the data patterns.

High frequency observations beyond the Morison constraint:

Let us start with the broader view of the IF behavior. To distinguish this view we could identify it as the "Independent Motion" Idea. If we dissect a time series into high frequency and low frequency patterns and are not constrained by the Morison equation, then a rich hierarchy of representations becomes available with this idea. One example representation, which was observed, is presented in Figure 5.4 .

Focusing on the independent high frequency pattern we must consider two aspects which could not be treated under the constant coefficient Morison constraint. These are: (1) the form of the high frequency force pattern and (2) the observed variations over a low frequency period. Clearly there can be longer period variations but the above seem to involve most of the pertinent behavior.

Illustrations of behavior over the high frequency period are found in Figures 5.2 and 5.4. Although linear behavior is one of these high frequency forms, the general situation likely involves nonlinear expressions.

The second item is the variation of the amplitude and the high frequency form over the period of a low frequency oscillation. In some of the Runs we have seen evidence that this variation can be quite extreme. Ranging from negative damping in portions of the cycle to near RV behavior in other parts.

Now could these patterns be modeled? Yes, but the implications of the I-T effect need to be understood first. Recall the final item in the Chapter is the qualitative explanation, using the IPM, of why the transverse force for some Runs is increased by the 0.3 Hz motion while others are significantly decreased. The I-T implications of this need to be carefully considered. Should these be modeled? Yes; in an environment in which negative damping exists and force patterns characteristic of self excitation are observed the concern is clear.

Summary observations:

1. Our Linear "damping force" Expression and companion coefficient data provides the only rational, practical, and accurate Morison representation of the high frequency data.
2. The Applicability Map provides an effective portrayal of the appropriate approximations for a wide range of combined motion problems.
3. The IPM provides an understanding of several high frequency phenomena including the modification of transverse forces by high frequency motion.

FINAL OBSERVATIONS ON THE I-T EFFECT

It should be clear that an understanding of the I-T effect will improve force prediction. Even with our imperfect knowledge of it, the qualitative implications to design can be illustrated by consider two loading environments. One is characterized by a random sea state and the other by a periodic motion such as the dragging of a riser or tendon by vessel motion. In the first case the I-T effect does not have an opportunity to build-up so low values of drag coefficients would be expected. By contrast in the periodic motion case the I-T could build-up requiring larger drag coefficients for accurate predictions. An understanding of the I-T effect would be the first step toward controlling it to the benefit of a design.

We feel that studies of the I-T effect will also contribute to our understanding of the "why" of IF behavior. The evidence for this is in the both the high frequency Runs and the low velocity partial cycles of the low frequency Runs.

RECOMMENDATIONS FOR FUTURE STUDIES

We have in the course of this document noted many promising areas for investigation. Most of these would provide important contributions to our state of knowledge. However, we feel that one of the problems, the investigation of the I-T effect, is a critical path item.

Thus in furthering the state of our current study we feel two items should have priority:

1. A companion study of the SSPA roughened cylinder data and
2. A quantitative treatment of the I-T effects observer in the current study.

The roughened cylinder would provide a logical companion data set to that in this Report and a useful test of the items developed in this Report. Such a study would also supply additional data for testing the findings of the I-T investigation.

The need for the I-T study has been discussed adequately in the section above as well as in other sections of this Report.

REFERENCES

1. Keulegan, G. and Carpenter, L., "Forces on Cylinders and Plates in an Oscillating Fluid", *Journal of Research of NBS*, vol 60, no 5, pp 423-441, (1958).
2. Verley, R. and Moe, G., "The Effect of Cylinder Vibration on the Drag Force and Resulting Hydrodynamic Damping", *Mechanics of Wave-Induced Forces on Cylinders*, pp 521-531, (1979).
3. Dello Stritto, Fr. and Horton, T., "Harmonics of Wave Forces Predicted by the Morison Equation", *OMAE Proceedings*, pp 165-176, (1984).
4. Demirbilek, Z., Moe, G., and Yttervoll, P., "Morison's Formula: Relative Velocity vs Independent Flow Fields Formulations for a Case Representing Fluid Damping", *OMAE Proceedings*, pp 25-31, (1987).
5. Teng, C. and Nath, J., "Periodic Waves on Horizontal Cylinders", *OMAE Proceedings*, pp 391-399, (1988).
6. Rodenbusch, G., and Kallstrom, C., "Forces on a Large Cylinder in Random Two-Dimensional Flows", *OTC Proceedings*, pp 127-136, (1986).
7. Horton, T., and Feifarek, M., "The Inertial Pressure Concept of Determining the Wave Forces on Submerged Bodies", *Journal of Energy Resources Technology*, vol 104, no 1, pp 47-52, (1982).
8. Horton, T., Fekifarek, M., and Rish, J., "Formulation of the One-Dimensional Wave Force Algorithm Using the Inertial Pressure Concept", *OMAE Proceedings*, pp 59-64, (1982).
9. Rish, J., "Correlation of Time-Dependent Force Coefficients for Cylinders in Oscillatory Flow", *AIAA Paper* 84-0083, (January 1984).
10. Lamb, H., *Hydrodynamics*, Cambridge University Press, 6'th Ed, pp 76-77, (1932).
11. Chakrabarti, S., "Recent Advances in High-Frequency Wave Forces on Fixed Structures", *Journal of Energy Resources Technology*, vol 107, pp 315-328, (1985).

APPENDIX A

LOW FREQUENCY DATA PROCESSED BY IPM

PARAMETERS FOR LOW FREQUENCY RUNS

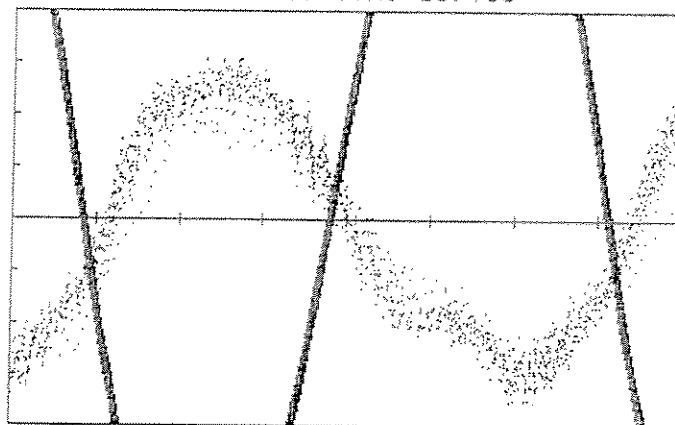
Run Number	A(m)	f(hz)	U _s (m/sec)	U _s /U _p	(N _{KC}) _p	(N _{Re}) _p /10 ⁶	Appendix Page
364	1.0	0.16	0.1	0.1	6.3	0.88	1
365	2.0	0.08	0.1	0.1	12.6	0.88	2
366	5.0	0.032	0.1	0.1	31.4	0.88	3
367	10.0	0.016	0.1	0.1	63.0	0.88	-
368	1.0	0.16	0.5	0.5	6.3	0.88	4
369	2.0	0.08	0.5	0.5	12.6	0.88	-
370	2.0	0.08	0.5	0.5	12.6	0.88	5
371	5.0	0.032	0.5	0.5	31.4	0.88	-
372	5.0	0.032	0.5	0.5	31.4	0.88	6
375	1.0	0.08	0.5	1.0	6.3	0.44	7
376	2.0	0.04	0.5	1.0	12.6	0.44	8
377	2.0	0.04	0.5	1.0	12.6	0.44	-
378	0.5	0.16	1.0	2.0	3.1	0.44	9
379	0.5	0.16	1.0	2.0	3.1	0.44	-
380	1.0	0.08	1.0	2.0	6.3	0.44	10
381	1.0	0.08	1.0	2.0	6.3	0.44	-

U_s = steady tow velocity

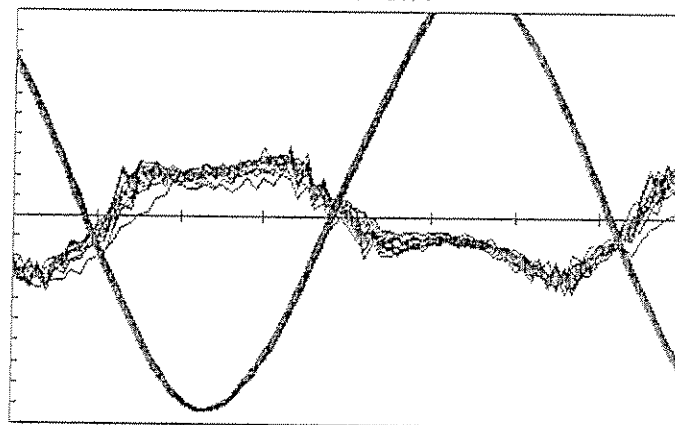
U_p = periodic velocity amplitude

(N_{KC})_p and (N_{Re})_p are "base-point" Keulegan-Carpenter and Reynolds numbers which are associated with the periodic motion only.

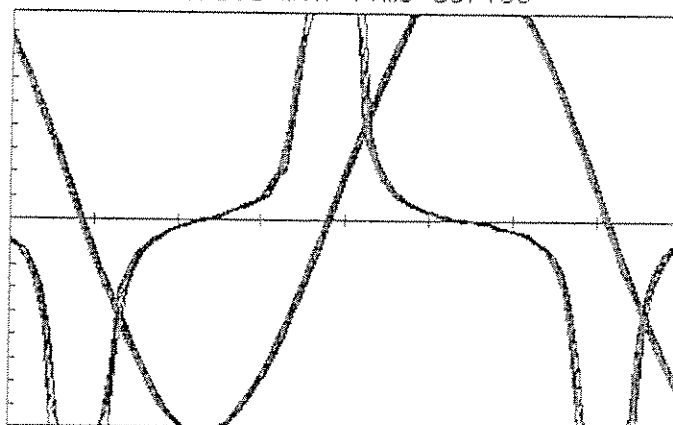
364 D-Force Time Series



364 IPM Coefficient



364 Theta-min Time Series

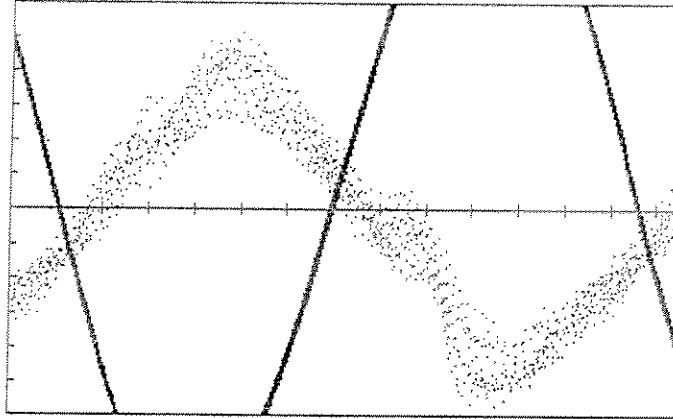


D-FORCE, IPM COEFFICIENT, AND THETA-MIN TIME SERIES
WITH VELOCITY SHOWN ON EACH PLOT

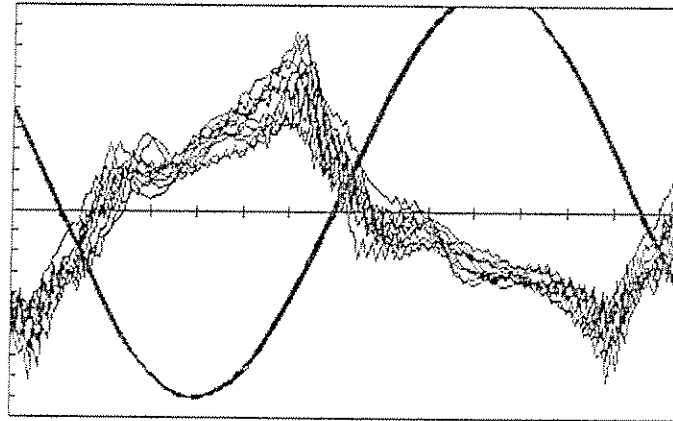
Periodic KC-Number= 6.3 or $A_x/D = 1$ with $U_s/U_p = 0.1$

Time scale 1sec/div, Force scale 100 N/div, IPM Coef. scale 0.1/div, Theta-min scale $10^\circ/\text{div}$

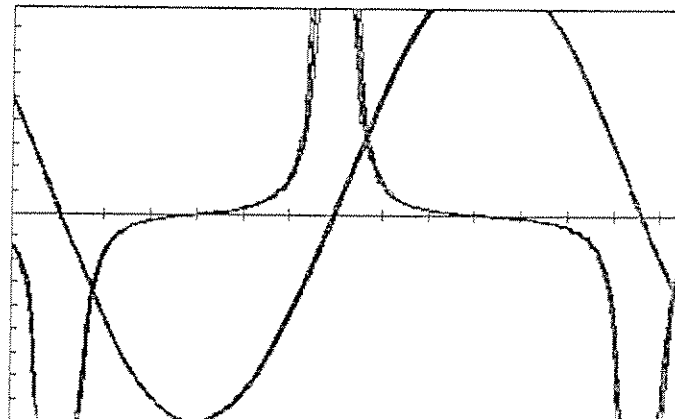
365 D-Force Time Series



365 IPM Coefficient



365 Theta-min Time Series

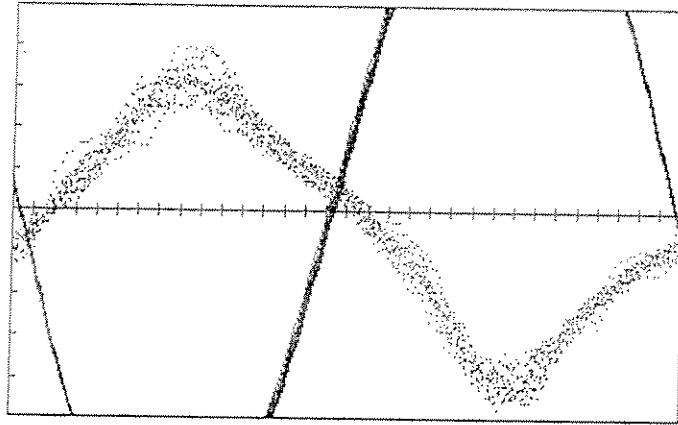


D-FORCE, IPM COEFFICIENT, AND THETA-MIN TIME SERIES
WITH VELOCITY SHOWN ON EACH PLOT

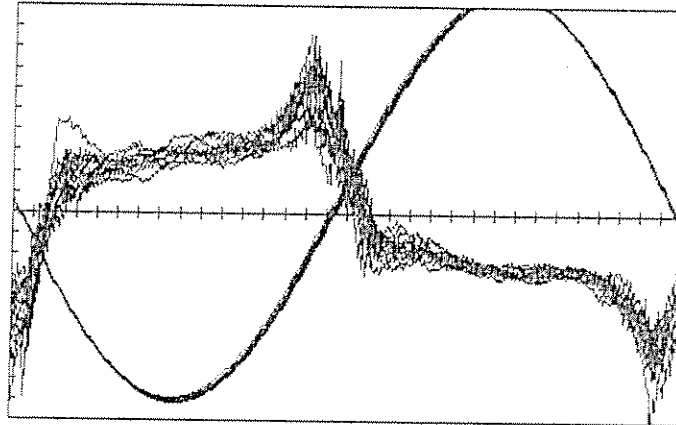
Periodic KC-Number=12.6 or $A_x/D=2$ with $U_s/U_p=0.1$

Time scale 1sec/div, Force scale 100 N/div, IPM Coef. scale 0.1/div, Theta-min scale $10^\circ/\text{div}$

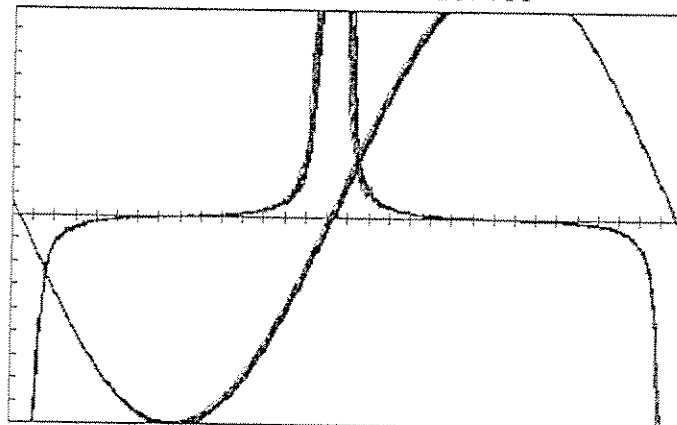
366 D-Force Time Series



366 IPM Coefficient



366 Theta-min Time Series

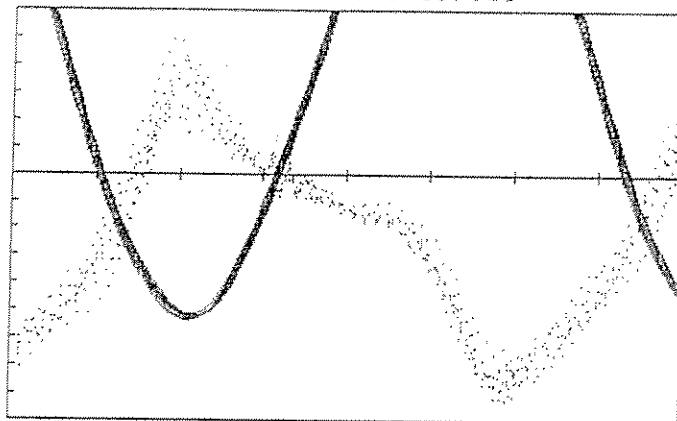


D-FORCE, IPM COEFFICIENT, AND THETA-MIN TIME SERIES
WITH VELOCITY SHOWN ON EACH PLOT

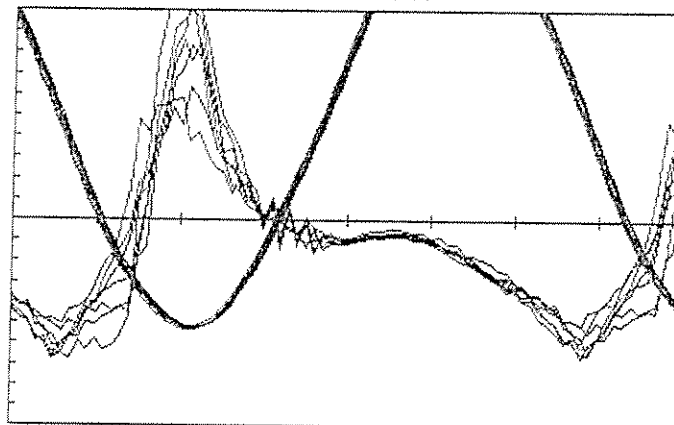
Periodic KC-Number=31.4 or $A_x/D = 5$ with $U_s/U_p = 0.1$

Time scale 1sec/div, Force scale 100 N/div, IPM Coef. scale 0.1/div, Theta-min scale $10^\circ/\text{div}$

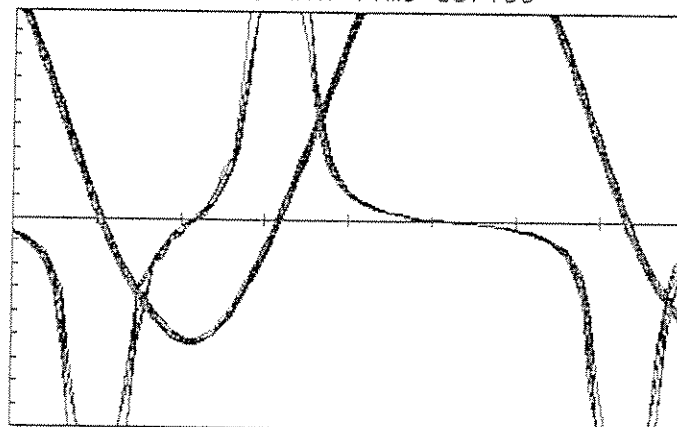
368 D-Force Time Series



368 IPM Coefficient



368 Theta-min Time Series

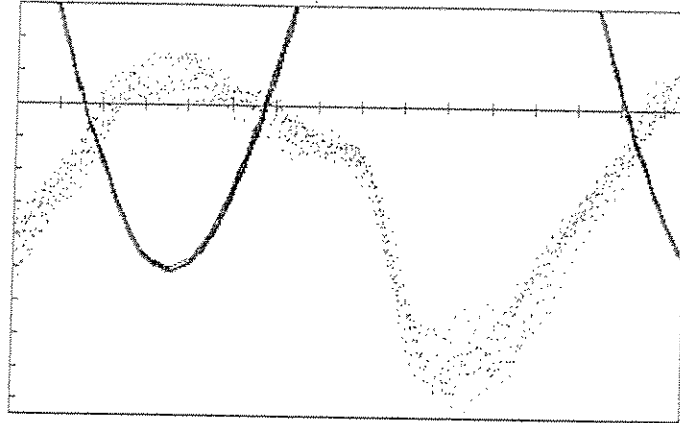


D-FORCE, IPM COEFFICIENT, AND THETA-MIN TIME SERIES
WITH VELOCITY SHOWN ON EACH PLOT

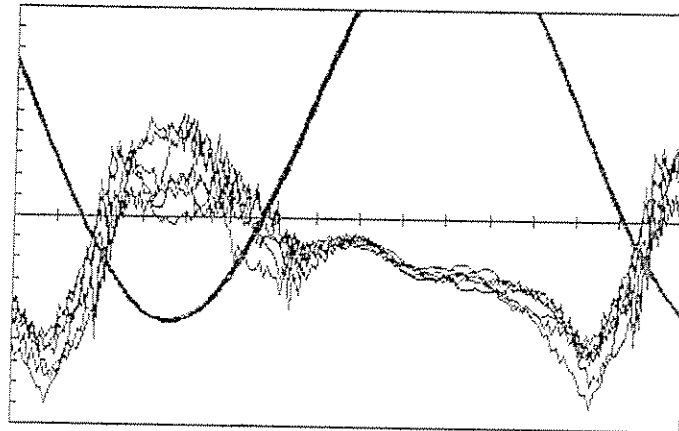
Periodic KC-Number= 6.3 or $A_x/D = 1$ with $U_s/U_p = 0.5$

Time scale 1sec/div, Force scale 100 N/div, IPM Coef. scale 0.1/div, Theta-min scale $10^\circ/\text{div}$

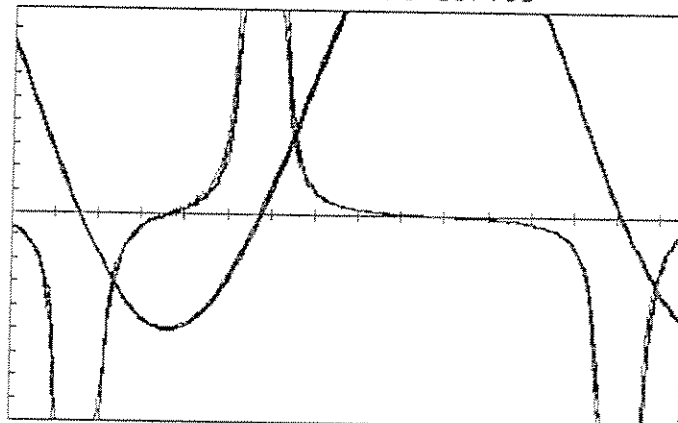
370 D-Force Time Series



370 IPM Coefficient



370 Theta-min Time Series

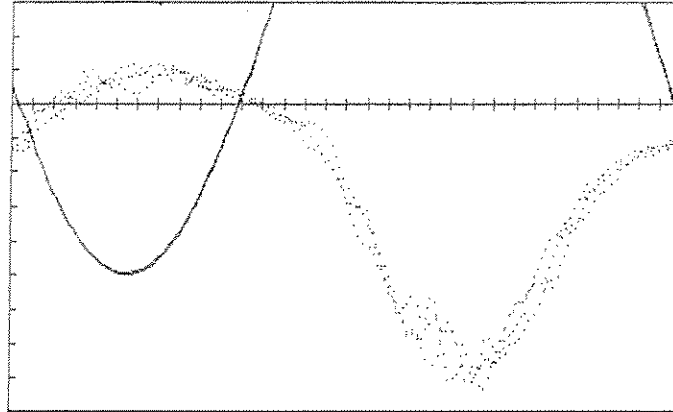


D-FORCE, IPM COEFFICIENT, AND THETA-MIN TIME SERIES
WITH VELOCITY SHOWN ON EACH PLOT

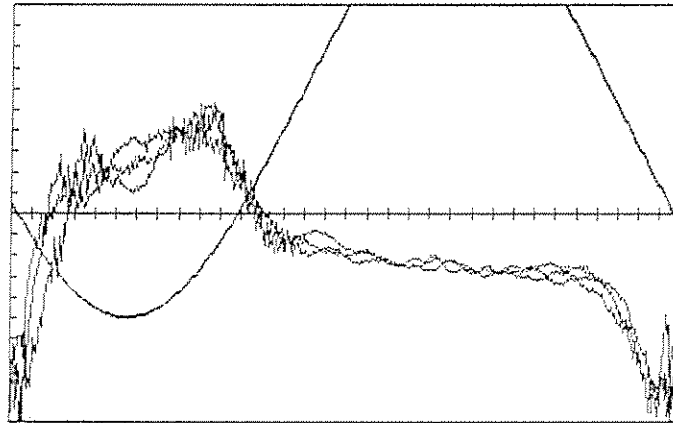
Periodic KC-Number=12.6 or $A_x/D = 2$ with $U_s/U_p = 0.5$

Time scale 1sec/div, Force scale 100 N/div, IPM Coef. scale 0.1/div, Theta-min scale $10^\circ/\text{div}$

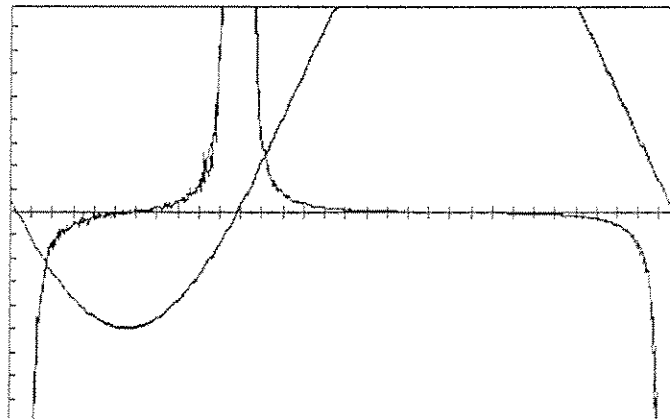
372 D-Force Time Series



372 IPM Coefficient



372 Theta-min Time Series

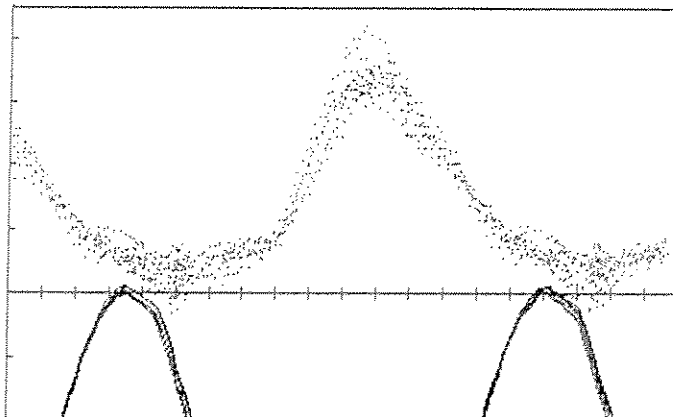


D-FORCE, IPM COEFFICIENT, AND THETA-MIN TIME SERIES
WITH VELOCITY SHOWN ON EACH PLOT

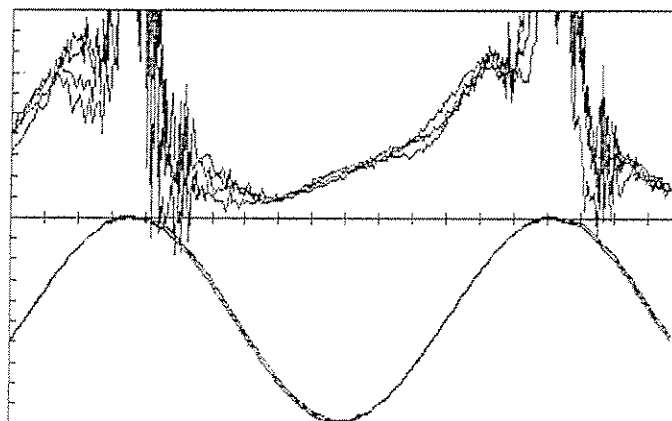
Periodic KC-Number=31.4 or $A_x/D = 5$ with $U_s/U_p = 0.5$

Time scale 1sec/div, Force scale 100 N/div, IPM Coef. scale 0.1/div, Theta-min scale 10°/div

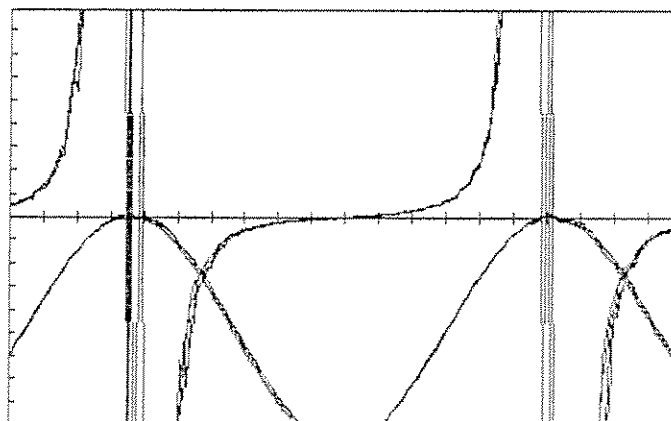
375 D-force Time Series



375 IPM Coefficient



375 Theta-min Time Series

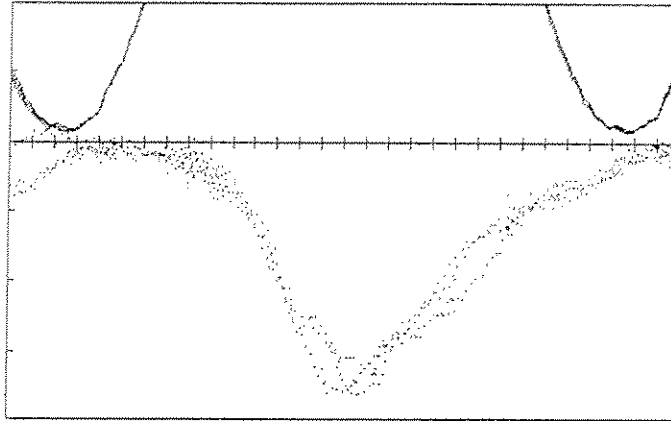


D-FORCE, IPM COEFFICIENT, AND THETA-MIN TIME SERIES
WITH VELOCITY SHOWN ON EACH PLOT

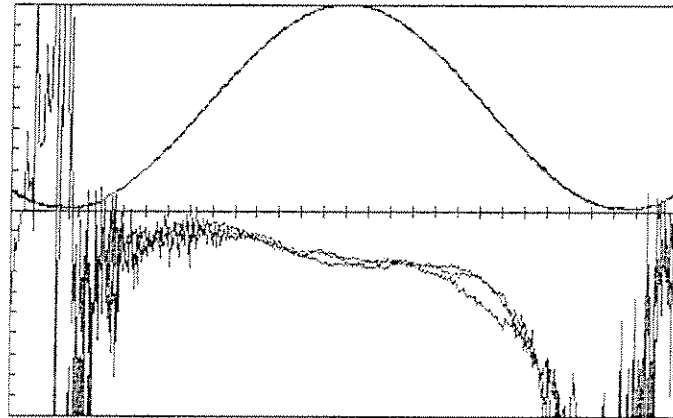
Periodic KC-Number = 6.3 or $A_x/D = 1$ with $U_s/U_p = 1.0$

Time scale 1sec/div, Force scale 100 N/div, IPM Coef. scale 0.1/div, Theta-min scale $10^\circ/\text{div}$

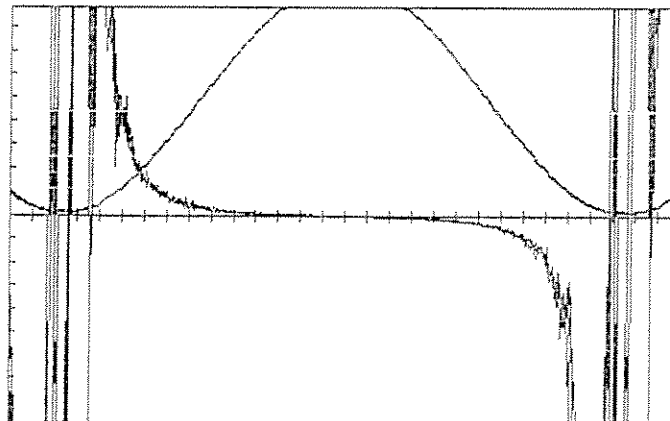
376 D-Force Time Series



376 IPM Coefficient



376 Theta-min Time Series

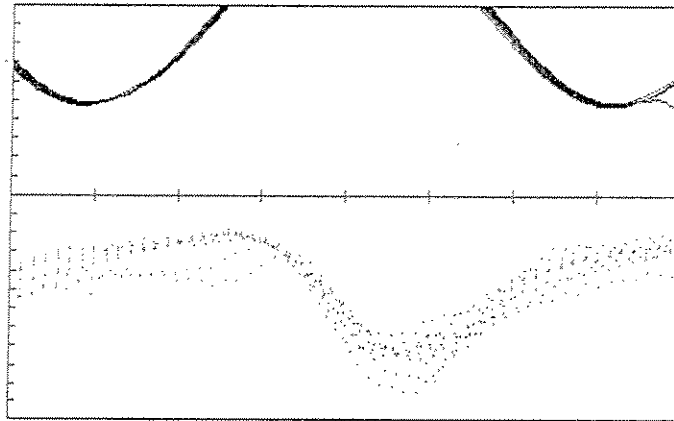


D-FORCE, IPM COEFFICIENT, AND THETA-MIN TIME SERIES
WITH VELOCITY SHOWN ON EACH PLOT

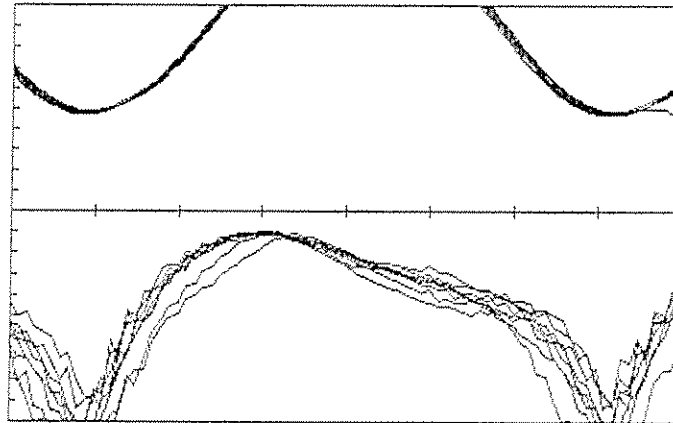
Periodic KC-Number=12.6 or $A_x/D = 2$ with $U_s/U_p = 1.0$

Time scale 1sec/div, Force scale 100 N/div, IPM Coef. scale 0.1/div, Theta-min scale 10°/div

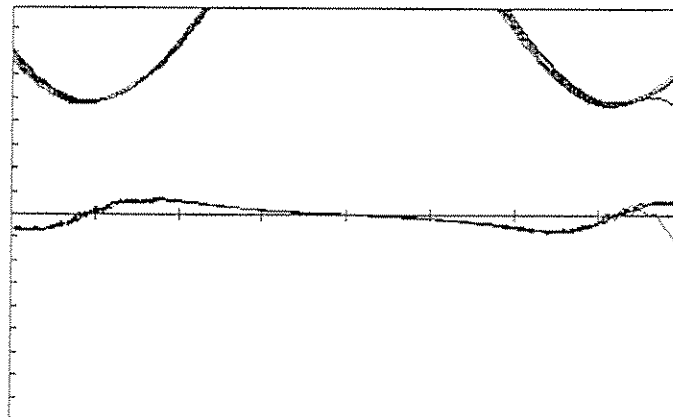
378 D-Force Time Series



378 IPM Coefficient



378 Theta-min Time Series

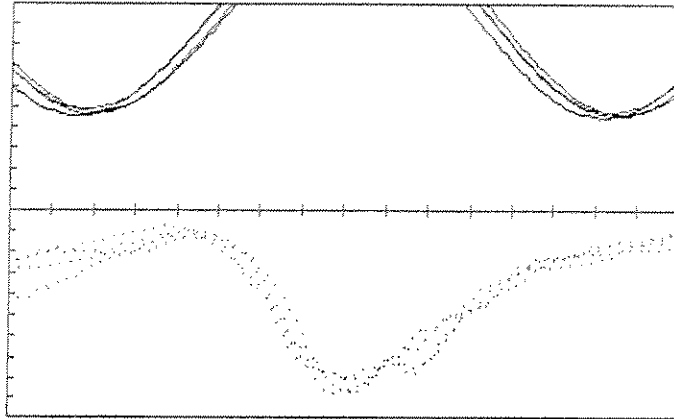


D-FORCE, IPM COEFFICIENT, AND THETA-MIN TIME SERIES
WITH VELOCITY SHOWN ON EACH PLOT

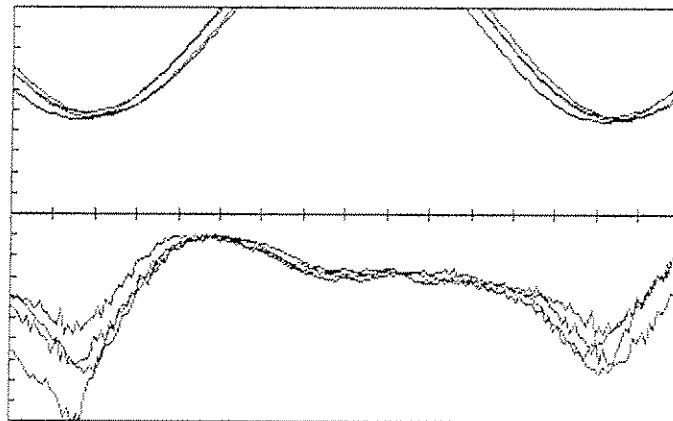
Periodic KC-Number= 3.1 or $A_x/D=0.5$ with $U_s/U_p = 2.0$

Time scale 1sec/div, Force scale 100 N/div, IPM Coef. scale 0.1/div, Theta-min scale 10° /div

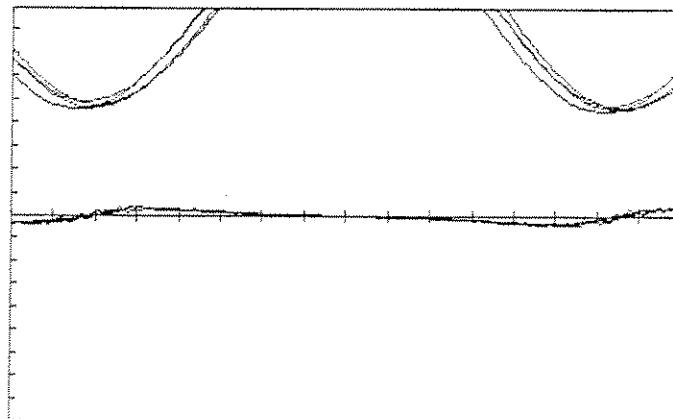
380 D-Force Time Series



380 IPM Coefficient



380 Theta-min Time Series



D-FORCE, IPM COEFFICIENT, AND THETA-MIN TIME SERIES
WITH VELOCITY SHOWN ON EACH PLOT

Periodic KC-Number= 6.3 or $A_x/D = 1$ with $U_s/U_p = 2.0$

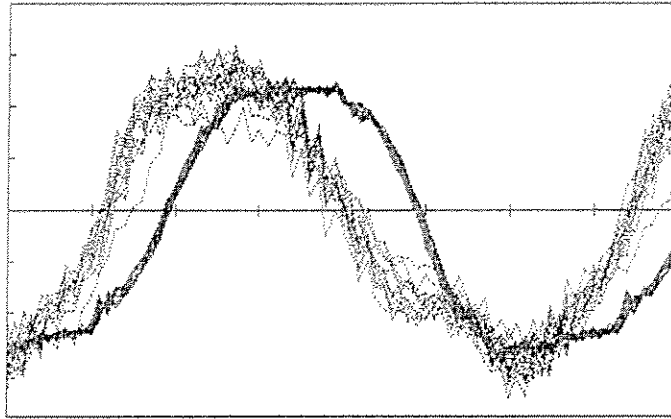
Time scale 1sec/div, Force scale 100 N/div, IPM Coef. scale 0.1/div, Theta-min scale 10° /div

APPENDIX B

FORCE PREDICTIONS WITH MORISON EQUATION USING LEVEL II

B-1

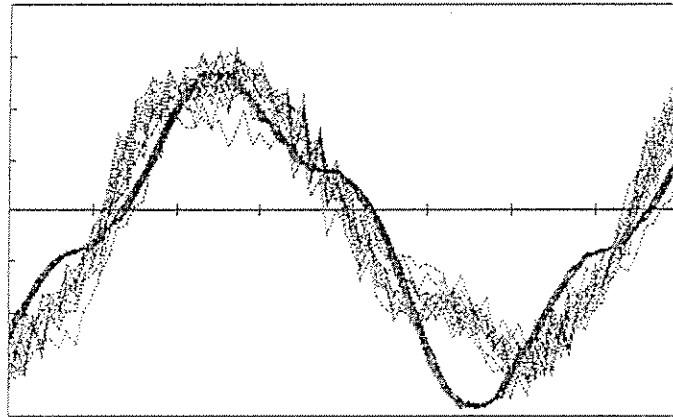
364 $C_d = .32$ $C_a' = .3$



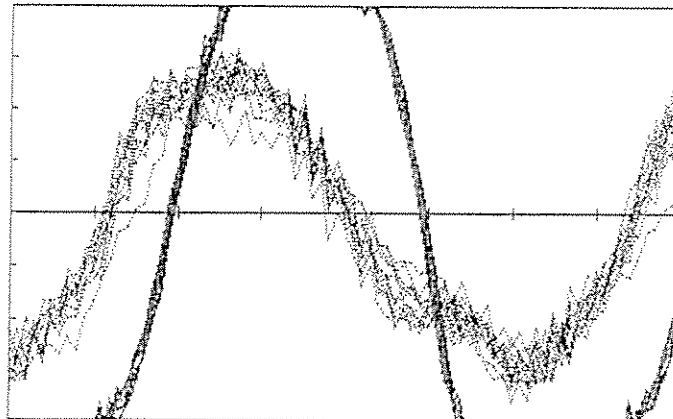
High Velocity
Prediction

364 $C_d = .6$ $C_a' = .1$

Low Velocity
Prediction



364 $C_d = .67$ $C_a' = .67$



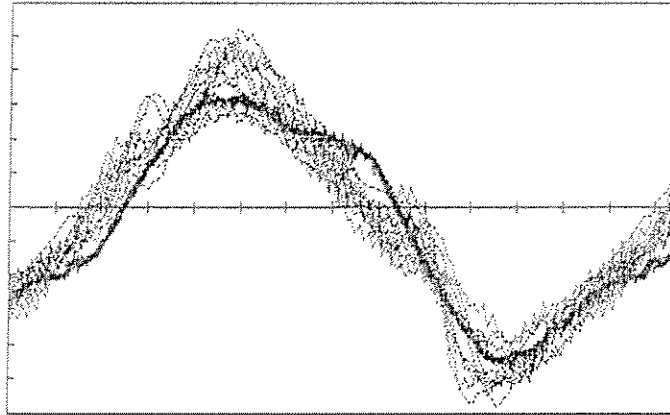
Level I
Prediction

FORCE PREDICTIONS WITH LEVEL II

Periodic KC-Number= 6.3 or $A_x/D = 1$ with $U_s/U_p = 0.1$

B-2

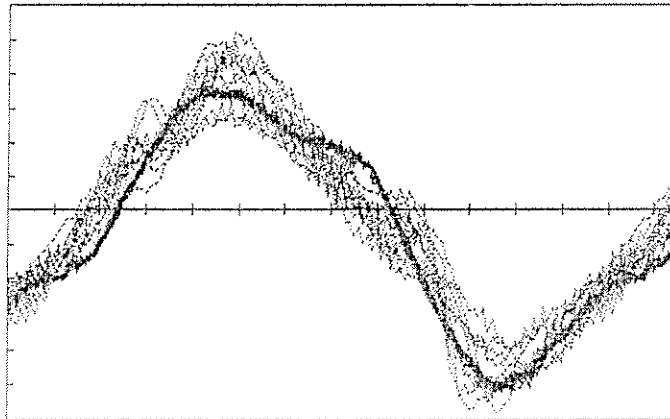
365 $C_d = .7$ $Ca' = .52$



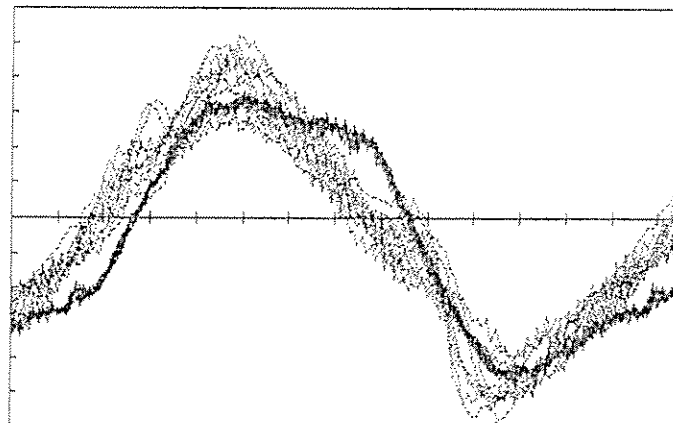
High Velocity
Prediction

365 $C_d = .8$ $Ca' = .5$

Low Velocity
Prediction



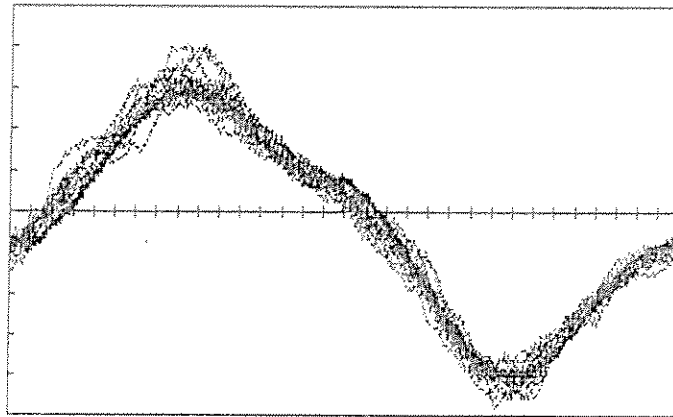
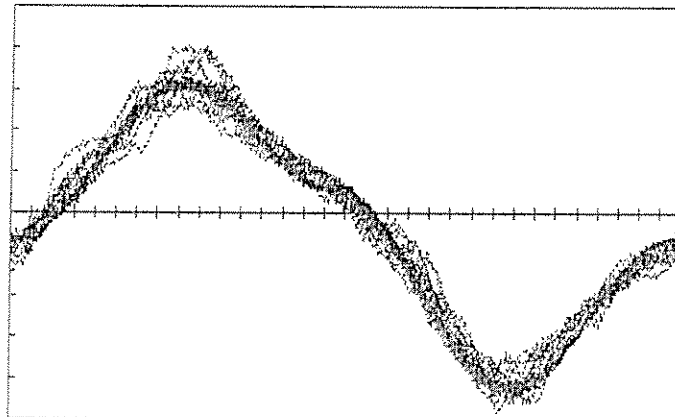
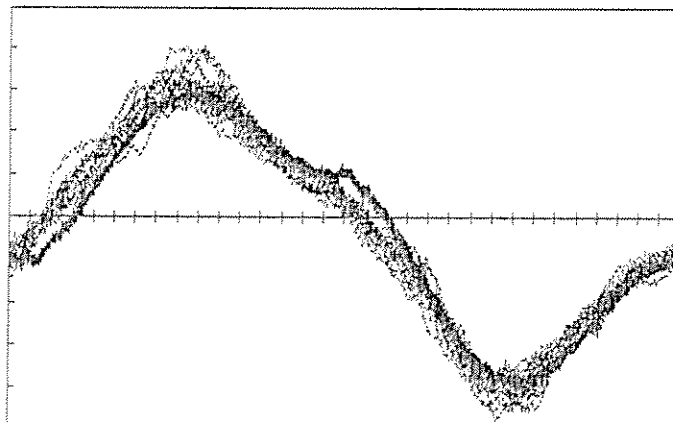
365 $C_d = .67$ $Ca' = .67$



Level I
Prediction

FORCE PREDICTIONS WITH LEVEL II

Periodic KC-Number=12.6 or $A_x/D = 2$ with $U_s/U_p = 0.1$

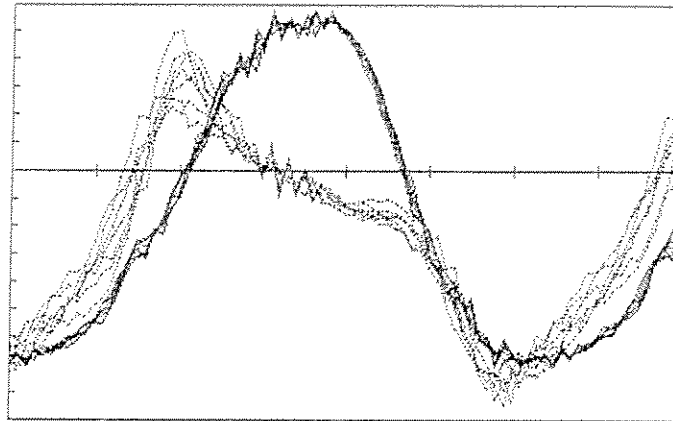
366 $C_d = .69$ $Ca' = .5$ High Velocity
Prediction366 $C_d = .75$ $Ca' = .4$ Low Velocity
Prediction366 $C_d = .67$ $Ca' = .67$ Level I
Prediction

FORCE PREDICTIONS WITH LEVEL II

Periodic KC-Number=31.4 or $A_x/D = 5$ with $U_s/U_p = 0.1$

B-4

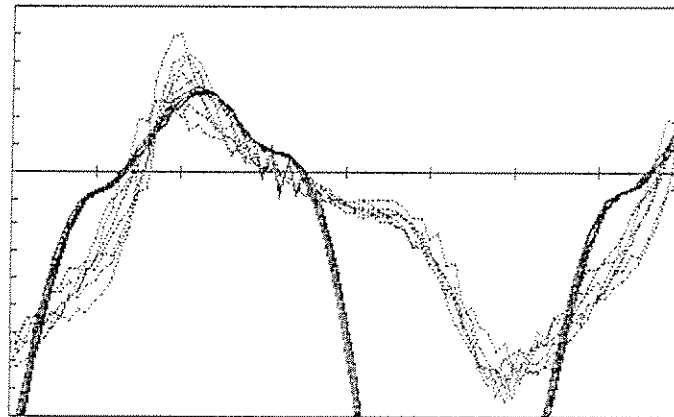
368 $C_d = .35$ $Ca' = .75$



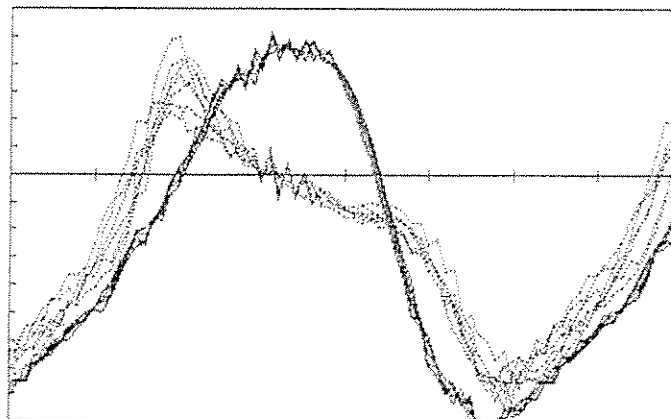
High Velocity
Prediction

368 $C_d = 2.1$ $Ca' = .1$

Low Velocity
Prediction



368 $C_d = .67$ $Ca' = .67$



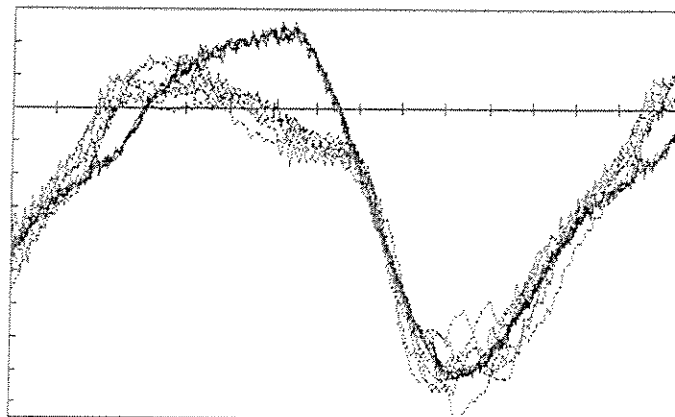
Level I
Prediction

FORCE PREDICTIONS WITH LEVEL II

Periodic KC-Number= 6.3 or $A_x/D = 1$ with $U_s/U_p = 0.5$

B-5

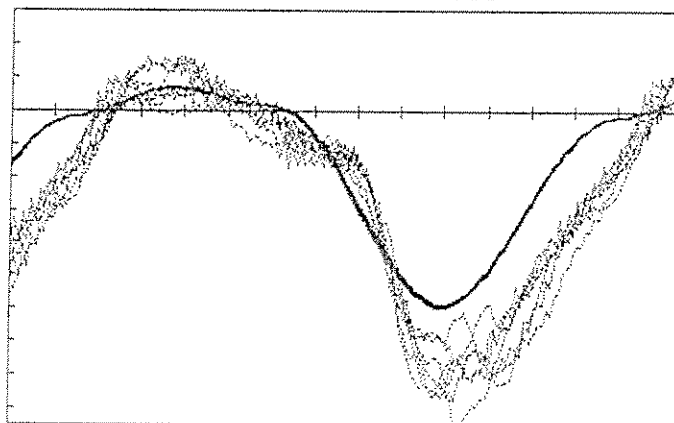
370 $C_d = .69$ $Ca' = .67$



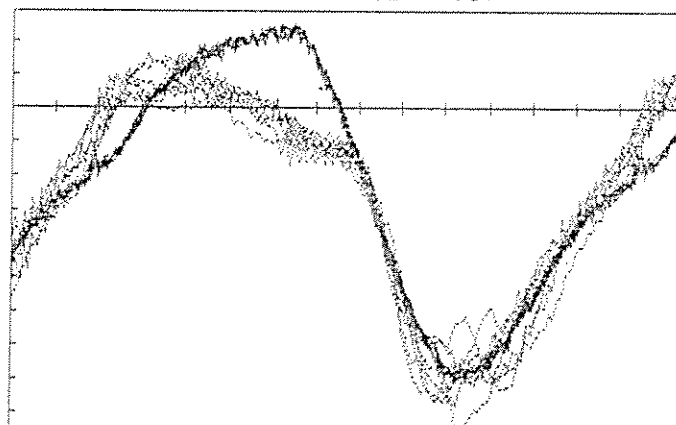
High Velocity
Prediction

370 $C_d = .53$ $Ca' = .05$

Low Velocity
Prediction



370 $C_d = .67$ $Ca' = .67$



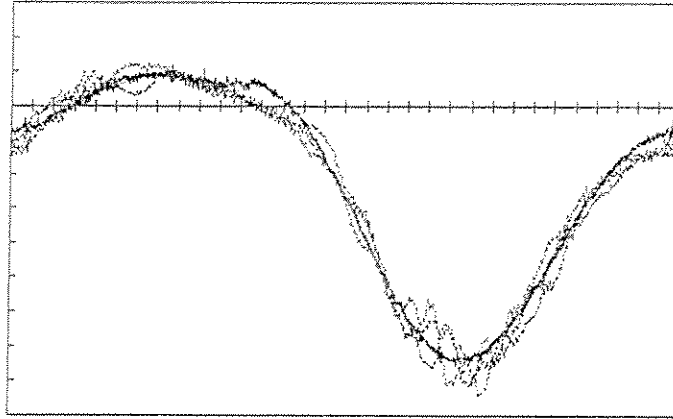
Level I
Prediction

FORCE PREDICTIONS WITH LEVEL II

Periodic KC-Number=12.6 or $A_x/D = 2$ with $U_s/U_p = 0.5$

B-6

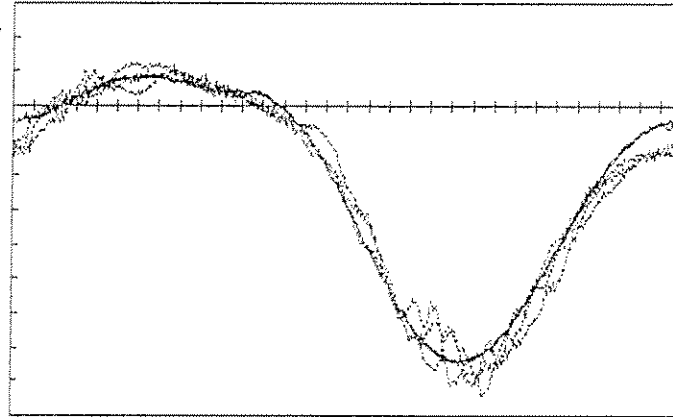
372 $C_d = .67$ $Ca' = .5$



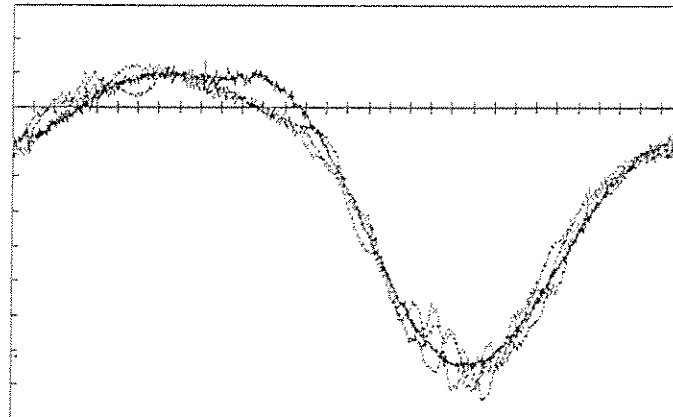
High Velocity
Prediction

372 $C_d = .67$ $Ca' = .3$

Low Velocity
Prediction



372 $C_d = .67$ $Ca' = .67$



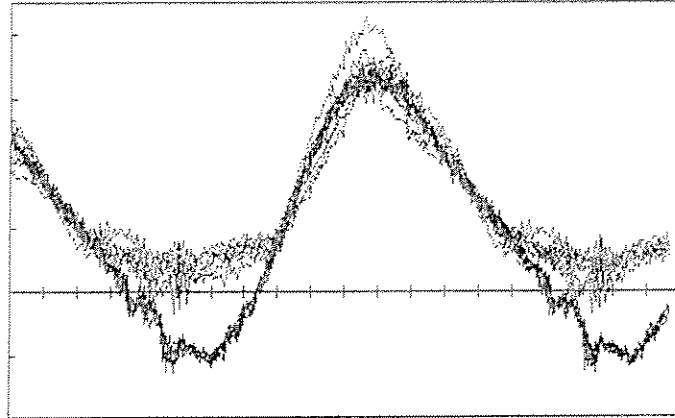
Level I
Prediction

FORCE PREDICTIONS WITH LEVEL II

Periodic KC-Number=31.4 or $A_x/D = 5$ with $U_s/U_p = 0.5$

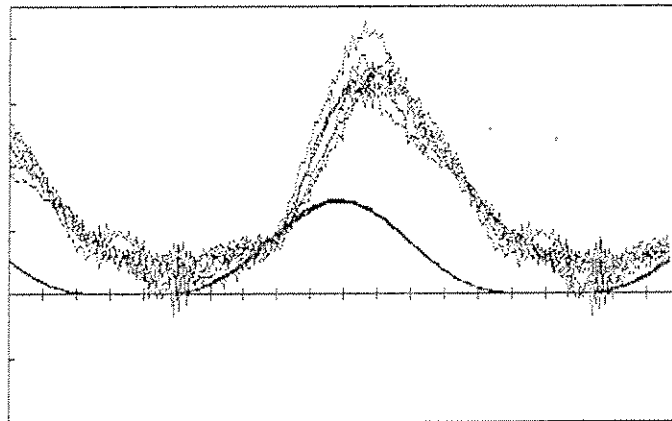
B-7

375 $C_d = .61$ $Ca' = .7$



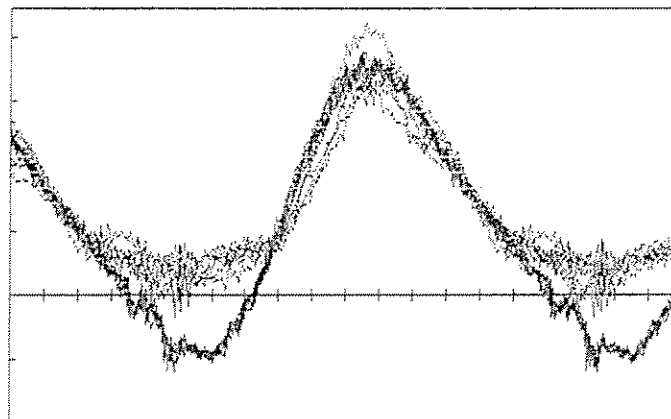
High Velocity
Prediction

375 $C_d = .3$ $Ca' = 0$



Low Velocity
Prediction

375 $C_d = .67$ $Ca' = .67$



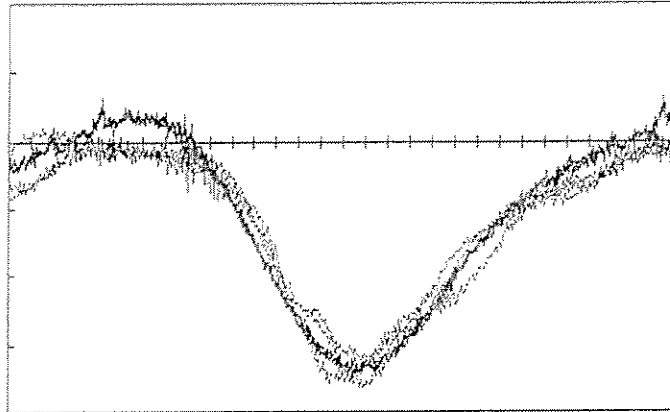
Level I
Prediction

FORCE PREDICTIONS WITH LEVEL II

Periodic KC-Number= 6.3 or $A_x/D = 1$ with $U_s/U_p = 1.0$

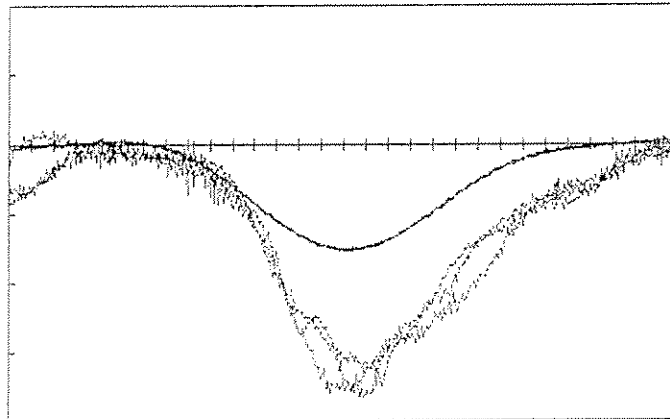
B-8

376 Cd = .65 Ca' .65



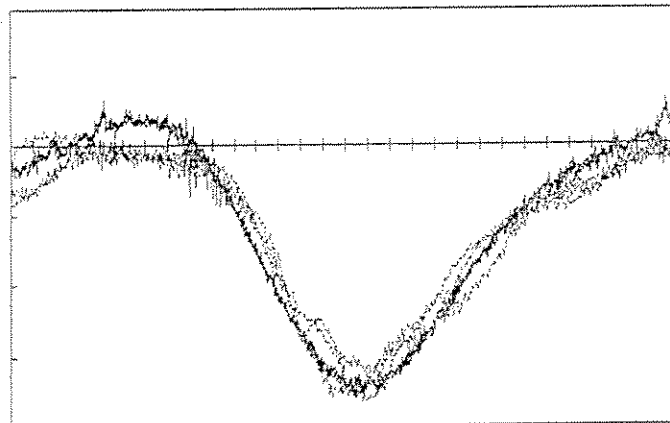
High Velocity
Prediction

376 Cd = .3 Ca' .1



Low Velocity
Prediction

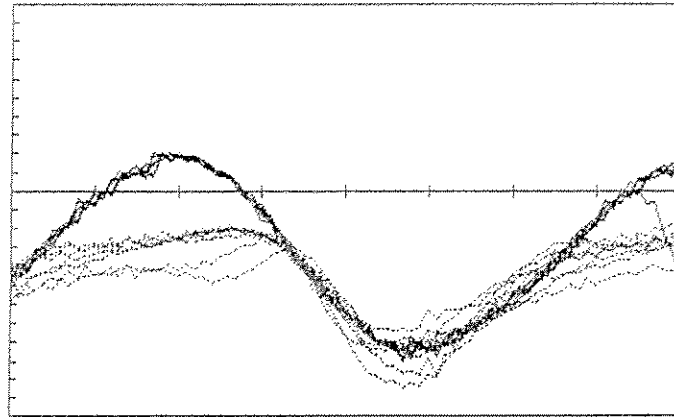
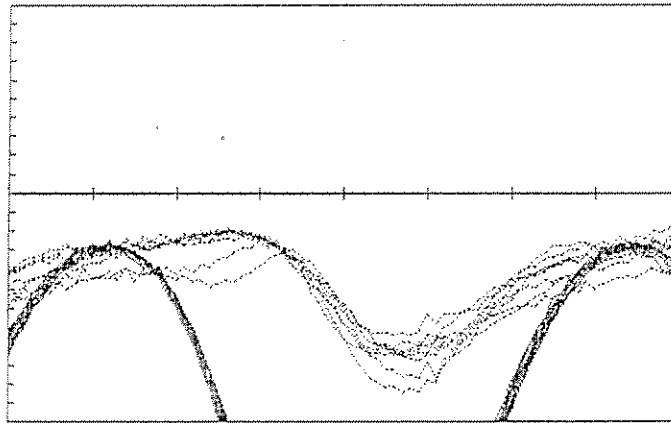
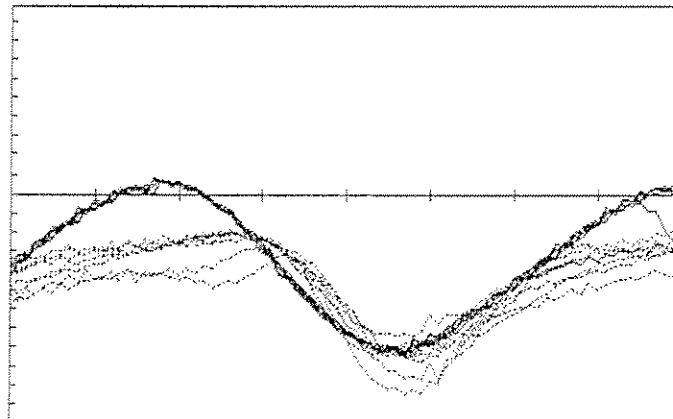
376 Cd = .67 Ca' .67



Level I
Prediction

FORCE PREDICTIONS WITH LEVEL II

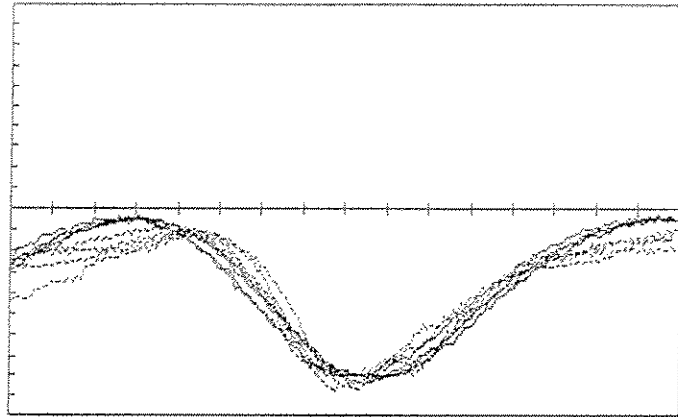
Periodic KC-Number=12.6 or $A_x/D = 2$ with $U_s/U_p = 1.0$

378 $C_d = .61$ $Ca' = 1$ High Velocity
Prediction378 $C_d = 2.67$ $Ca' = .5$ Low Velocity
Prediction378 $C_d = .67$ $Ca' = .67$ Level I
Prediction

FORCE PREDICTIONS WITH LEVEL II

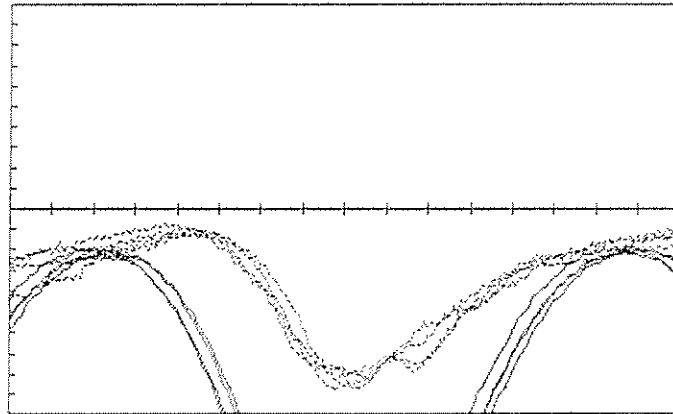
Periodic KC-Number= 3.1 or $A_x/D=0.5$ with $U_s/U_p = 2.0$

380 $C_d = .75$ $Ca' = .8$



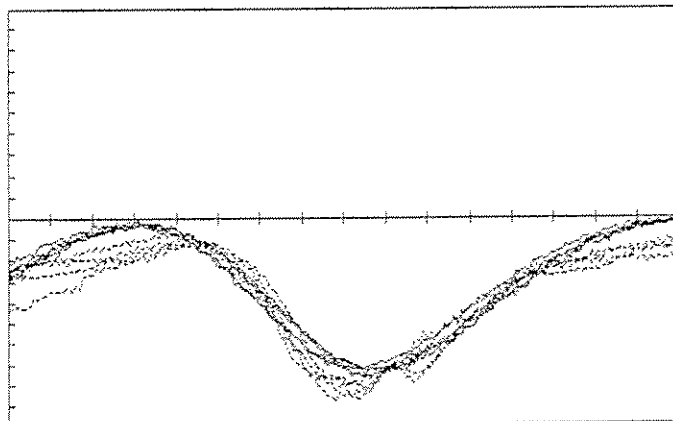
High Velocity
Prediction

380 $C_d = 2$ $Ca' = .5$



Low Velocity
Prediction

380 $C_d = .67$ $Ca' = .67$



Level I
Prediction

FORCE PREDICTIONS WITH LEVEL II

Periodic KC-Number= 6.3 or $A_x/D = 1$ with $U_s/U_p = 2.0$